Dissertation

Multi-Level and Time-Parallel Solution of Time-Periodic Problems

University of Wuppertal

Faculty of Mathematics and Natural Sciences

submitted by

Sergiy Bogdanov, M. Sc.

in partial fulfillment of the requirements for the degree of Doctor of Natural Sciences

Scientifically Advised by Dr. Stephanie Friedhoff

Supervised by Prof. Dr. Matthias Bolten

April 13, 2025, Wuppertal

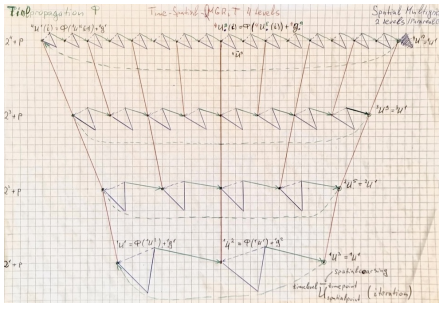

Abstract

The Quotient Multi-Grid Reduction in Time (QMGRIT) algorithm is developed and applied in this dissertation, showing its potential to solve intricate scientific and engineering problems like electric motor modelling. We investigate the efficacy of the QMGRIT algorithm in solving periodic time-dependent partial differential equations (PDEs), with particular attention to the heat and wave equations, aiming to scope both kinds of PDEs: the parabolic and hyperbolic PDEs. We validate the QMGRIT algorithm by constructing its mathematical foundations and presenting empirical analysis, demonstrating its advancement in computational mathematics. Compared to conventional multi-grid and parallel computing techniques, we assess QMGRIT's computing capabilities and efficiency; e.g., on QMGRIT's forerunner algorithm, MGRIT, we find a notable improvement with QMGRIT. This thesis also presents a parallelization paradigm for computing performance improvement and time-energy-saving in high-performance computing (HPC) environments: ghosted QMGRIT (gQMGRIT). To improve convergence rates and resource allocation by a range of scenarios, we evaluate the gQMGRIT and show the effectiveness of the paradigm for QMGRIT solutions. In general, the work seeks to benefit the scientific computing community by offering insight into the design of an innovative combination of two: a parallel-in-time multi-grid algorithm that supplies the *ghosted* approach of parallelization for the periodic problems; and the objective is to facilitate the more effective treatment of challenging, time-periodic PDEs with impacts that go beyond academia and encompass diverse scientific and engineering fields.

Acknowledgements

I wish to express my profound thanks to several people, especially Dr. Stephanie Friedhoff[1] and Prof. Dr. Matthias Bolten[2], for shaping my research and elaborating on some of the complexities in the academic world. Furthermore, I thank Gabi, Jens, Lisa, Marcel, Isa, and other great People from our gorgeous team for collaborative environment. I wish to express my greatest appreciation to my wonderful parents, my Mom and my Dad, for their incredible support during my lifetime, and this journey — their unwavering support and encouragement have been the catalyst for the acquisition of my goals. I am grateful to my dear sister and my dearest nephew Max for being my great companions, brightening my life with their joy, and reminding me of the importance of family. To my beloved Oleksandra — I will never truly articulate the value of your love, kindness, and unyielding support —, the inspiration, strength, and safe space you provided me have been irreplaceable since we met. For all that, I am grateful beyond words. Lastly, without the financial base of the grants 05M18PXB (PASIROM) and 955701 (TIME X), this work would not have been conducted — and thus, I am sincerely thankful for this support; all together have afforded me opportunities to explore my research interests and grow as a contributor to the wider academic community.

[1] Stephanie Friedhoff is a German mathematician and computer scientist with contributions to numerical analysis and scientific computing. Her research includes the advanced development of numerical methods for PDEs and the application of HPC techniques, e.g., MGRIT and SAMA. These efforts address complex challenges in physics, engineering, and beyond. Dr. Friedhoff's work is recognized for its impact on these disciplines.

[2] Matthias Bolten is a contemporary German mathematician who has contributed to the fields of numerical analysis and applied mathematics. His work primarily focuses on iterative methods and multi-grid techniques. Prof. Bolten has been involved in the development and analysis of algorithms aimed at solving large-scale linear and nonlinear problems, a key area within scientific computing.

Declaration

I declare the following.

1. This thesis is a result of my own original research and has not been submitted for any other degree or professional qualification. The work was conducted under the guidance of my supervisor, Prof. Dr. Matthias Bolten, and scientific adviser, Dr. Stephanie Friedhoff, at the Scientific Computing and High Performance Computing group, University of Wuppertal.

2. To the best of my knowledge, all sources of information, data, and ideas have been properly cited and referenced throughout the thesis.

3. Certain parts of the writing during April 2023 - April 2024 were conducted extensively with the employment of various services and technologies as helpful writing assistance and for the further development of individual writing skills, including IT-/AI-supported tools:

    - As DeepL SE Translator[3] and Grammarly Grammar Checker[4], for language translation, sentence structuring, grammar, and spelling checks which affected the text-parts of the entire thesis;

    - As OpenAI's ChatGPT-4[5], for general assistance (i.e., transferring CSV data to and layouting of LaTeX tables, collecting — and verifying afterwards — into the footnotes through the entire manuscript public biographical data on known scientists), proofreading (i.e., assistance with suggestions on grammatical or stylistic improvements for provided own texts iteratively), and discussing ideas (i.e., chapters structuring, and structure suggestions on a bullet list to text expansions, particularly in Chapters 1-2, especially in Sections 1.1-1.2

[3] DeepL Translator, DeepL SE (online standalone version as of April 2024): https://www.deepl.com/translator
[4] Grammarly (online standalone version as of April 2024): https://www.grammarly.com
[5] ChatGPT-4, OpenAI (online standalone version as of April 2024): https://www.openai.com/chatgpt

and 2.1-2.2.) which affected the table's layouts and text-parts of the entire thesis, excluding Chapter 5 and every part of mathematical analysis through the whole manuscript.

I confirm that the tools listed have been disclosed in full, including their names, functions, and total scope of use. During the preparation of this thesis, I worked independently throughout and exercised control when using IT-/AI-supported tools under my direction — at the same time, these services provided broad support in improving text-readability, text-formatting, and text-structure, and I maintained complete intellectual control over the research and thesis's development, full responsibility for the content and the essence of the work, which is a product of my original mathematical thinking. All ideas, mathematical analyses, and substantive content reflect my original contributions and critical oversight. This declaration adheres to principles of transparency and academic integrity. Since the BUW *Leitfaden*[6] recommending detailed procedural documentation became available in September 2024 after a primary use of these tools, certain retrospective records, such as the detailed time or prompts logs, were not maintained[7] — however, this declaration faithfully outlines the scope and nature of the tools' use to the best of my ability.

4. Certain parts of the thesis have been previously presented at conferences:

   - Section 3.1.3 was presented at the 8th Workshop on Parallel-in-Time Integration, Bielefeld, Germany, 22.05.2019;
   - Section 3.2.3 was presented at the GAMM Annual Meeting, Aachen, Germany, 17.08.2022;
   - Section 4.3.1 was presented at the Time X Hackathon, Lugano, Switzerland, 09.02.2023.

5. I understand that the copyright of this thesis rests with the author. This copy has been supplied on the understanding that it is copyrighted material and that no quotation from the thesis may be published without proper acknowledgement.

Sergiy Bogdanov

April 13, 2025

[6] KI-Handreichungen (accessed on November 27, 2024): https://uniservice-dl.uni-wuppertal.de/de/faq-zur-digitalen-lehre/direktlink-ki-handreichungen/

[7] As the focus of tools usage was on iterative improvement by proofreading across text-parts rather than singular generated outputs.

Dedication

Toward self-development and self-reflection;
in memory of my grandmother Tamara,
and for my grandmother Maria.

I am fine, post tenebras lux. Now, everything is here inspired by the Ukrainian people's determination, who demonstrate incredible Resilience and Courage in battling unwarranted military aggression from Russia. As a person from Kyiv, the ongoing invasion shocks and shakes me highly intensely. I hold Ukraine close to my heart and my consciousness near to Ukraine — now, though I am so far away in Germany —, I have been volunteering in the refugee sector and trying to help those who are without homes; I am organizing rallies against the injustice and sometimes trying to understand the depression episodes that I have lived through since 24.02.2022; now, it is a deep inner conflict that is potentially necessary to live through this. It is within the work; it is a commitment that has come from all this Resilience, and it is also our energy — may this energy, divining that there is still work to be done, be present in all forthcoming completions and victories for Peace, Freedom, and Dignity for those of majestic people. In Remembrance of the Defenders of Ukraine fallen in the struggle for independence, sovereignty and territorial integrity of Ukraine. Слава Україні!

Contents

List of Abbreviations

Algorithms and Methods

BE : Backward Euler method: an implicit, first-order finite difference method [67, 68]

EW : Eternal Wanderlust scheme, a basic iterative method provides time-stepping on the factor space of time domain, i.e., time-stepping on the time domain modulo its endpoints [conceptualized in this document]

FAS : Full Approximation Storage scheme [10]

FDM : Finite Difference Method [29, 52, 74, 79]

FEM : Finite Element Method [16, 71]

GMRES : Generalized Minimal Residual method [104]

LFA : Local Fourier Analysis [10]

MGRIT : Multi-grid Reduction In Time method [30]

Parareal : Two-grid time-parallel time-integration method [83]

QMGRIT and QMGRIT FAS, gQMGRIT : Quotient Multi-grid Reduction In Time method and its FAS formulation, ghosted QMGRIT paradigm [unveiled in the scope of this work]

SAMA : Semi-Algebraic Mode Analysis [42]

QMGRIT (and partly MGRIT) Components

C-Point : Coarse Point

CF : Coarse-Fine (relaxation, i.e., updating all F-Points, then all C-Points)

F-Point : Fine Point

FCF : Fine-Coarse-Fine (smoothing, i.e., updating all F-Points, then all C-Points, then all F-Points)

γ : Number of EW iterations on the coarsest grid

L : Number of grids

m : Coarsening factor (also $m_0,\ m_1$), usually $m = 2^{\alpha_m}$, where $\alpha_m \in \mathbb{N}$

M : Discretization matrix leading via $M^{-1} = \Phi$ to the time-stepping operator

N_t**,** N_c **and** N_x : Number of temporal sub-intervals, coarse grid sub-intervals and spatial grid sub-intervals, usually $N_t = 2^{\alpha_{N_t}}$, $N_c = 2^{\alpha_{N_t} - \alpha_m}$ and $N_x = 2^{\alpha_{N_x}}$, where $\alpha_{N_t}, \alpha_{N_x} \in \mathbb{N}$

ν : Number of CF-relaxations

P : Prolongation operator (also P_1, P_2 for gQMGRIT)

Φ : Time-stepping operator

Φ_c : Coarse grid time-stepping operator

Ψ : 2x2 block time-stepping operator for a two-step integration method

Q : EW iteration operator

$Q(\gamma, \nu, \kappa)$: two-grid iteration operator of κ QMGRIT cycles with γ EW iterations and ν CF-relaxations

$R,\ R_I$: Restriction operator (also R_1, R_2 for gQMGRIT)

T_{MGRIT} : two-grid iteration operator of MGRIT

$T_{gQMGRIT}$: two-grid iteration operator of gQMGRIT

Mathematical Notations

A, B, L : Matrices in linear systems

A_{Δ}^{iv} : Schur Complement of initial value system A

$A_{\Delta,p}$: Schur Complement of periodic boundary system A_p

A_{cc} : Matrix for coarse-to-coarse grid points

A_{cf} : Matrix for coarse-to-fine grid points

A_{fc} : Matrix for fine-to-coarse grid points

A_{ff} : Matrix for fine-to-fine grid points

A_p : System matrix of periodic linear system

b : Vector notation for linear system's right hand side incorporating source term of governing inhomogeneous differential equation

$C(I, \mathbb{R}^n \times \mathbb{R}^n)$: Continuous functions over interval I with values in $\mathbb{R}^n \times \mathbb{R}^n$

Δx **and** Δt : Discretization step in space and discretization step in time

d : Vector notation for iteration's defects

∇ : Gradient operator

∇^2 **or** Δ : Laplacian operator

$g(\cdot)$: Source term of governing differential equation, general function notation

$\lambda_\cdot$: Placeholder for specific eigenvalues

$\partial\Omega$: Boundaries of the domain Ω

$\rho(\cdot)$: Spectral radius

$\rho_{SAMA}(\cdot)$: Spectral radius in SAMA context

$\Pi\,(t, s)$: Monodromy matrix

$\mathbb{N}$: Set of natural numbers

$\mathbb{R}$: Set of real numbers

t : Variable in time dimension

$\mathbf{u}, \mathbf{U}$: Vector notations for unknown function

$\mathbf{u_p}$: Vector notation for periodic unknown function

(x_j, t_i) : Discrete spatial and temporal points

$u(x_j, t_i)$**,** $u_{j,i}$: Evaluation of the unknown function and its approximation in (x_j, t_i)

$\mathbf{v}$: Vector notation for iteration's errors

x : Variable in spatial dimension

$\frac{\partial u(x,t)}{\partial t}$ **or** $\dot{u}$: Partial derivative of u with respect to time

$\frac{\partial^2 u(x,t)}{\partial x^2}$ **or** Δu : Laplacian of u with respect to spatial dimension

$\frac{\partial^2 u(x,t)}{\partial t^2}$: Second partial derivative of u with respect to time

$\|.\|$**,** $\|.\|_1$**,** $\|.\|_2$**,** $\|.\|_{\max}$: Norms (Euclidean, 1-norm, 2-norm, max norm)

Heat Equation

a : Thermal diffusivity coefficient

Convection-Diffusion-Decay Equation

D : Dispersion magnitude, $D > 0$

ν : Drift velocity, where $\nu > 0$

λ : Decay magnitude, where $\lambda > 0$

Wave Equation

c : Wave speed

F_u, F_v, A, D : Discretization matrices for two-variable system

Coaxial Cable

A : Magnetic vector potential

B : Magnetic flux density

D : Electric flux density

E : Electric field strength

ϵ : Permittivity of the wire material or surrounding medium

f : Frequency of the external source

H : Magnetic field strength

I_d, K_d : Modified Bessel functions of the first and second kind

J : Electric current density

J_s : Electric source current density

C_0**,...,**C_5 : Constants

μ : Permeability of the wire

ν : Reluctivity of the wire

ρ : Charge density

σ : Conductivity of the wire

δ : Skin depth

ω : Angular frequency

ξ : Helmholtz Constant

Electrical Machine

C : Friction coefficient

I : Moment of inertia

κ : Torsion coefficient

T : Mechanical excitation given by the magnetic field

θ : Rotor angular displacement (rotor angle)

$\mathbf{u}$: Vector of (line-integrated) magnetic vector potentials

ν : Rotor angular velocity

Miscellaneous

1D : One-dimensional

2D : Two-dimensional

3D : Three-dimensional

HPC : High-performance Computing

ODE : Ordinary Differential Equation [11, 100]

PDE : Partial Differential Equation [97, 120]

PinT : Parallel-in-Time, methods and software in the field of parallel-in-time integration methods [94]

Programming Languages and Software

GetDP : A General Environment for the Treatment of Discrete Problems [24, 25, 54]

MATLAB : Matrix Laboratory, a programming and numeric computing platform used for algorithm development, data analysis, visualization, and numerical computation [86]

pyMGRIT : A Python implementation of MGRIT [63]

Python : A high-level, interpreted programming language known for its readability, versatility, and wide range of libraries for scientific computing and data analysis [95]

Qmgrit : A MATLAB implementation of QMGRIT function solving the linear grounded heat equation [5]

xBraid : A PinT software package providing a non-intrusive, optimal-scaling time-parallel MGRIT method [124]

Chapter 1

Introduction

> *'Distances are not gauged, ellipses not measured, velocities not ascertained, times not known. Nevertheless, the recurrence is sure. What the mind suffered last week, or last year, it does not suffer now; but it will suffer again next week or next year.'*
>
> — *Alice Meynell*[a]

[a] Alice Christiana Gertrude Meynell (*22 September 1847 in Barnes, London, England; †27 November 1922 in London, England) was an English poet, essayist, and suffragist.

The fields of natural sciences, where the development of software, models, and algorithms is of utmost importance, have recognized the significance of scientific computing and high-performance computing (HPC) as essential components [45, 92]. HPC facilitates significant insights into practical problems and reduces the need for costly physical experiments — thus, scientific computing, particularly high-performance numerical simulation, has become an indispensable supplement to both experimental and theoretical approaches when dealing with challenges and riddles in the natural sciences [30, 33]. It is pivotal in this field to have simulations that are accurate, and efficient in terms of memory, time-to-solution, and, when possible, energy consumption. Efforts should be made to optimize resource utilization and minimize energy consumption while employing parallelization techniques. This is particularly true when dealing with the complexities of time-dependent PDEs. We will examine the development of iterative methods, which have been extremely helpful in overcoming the challenges associated with scientific computing and HPC, as the complexity of these challenges is growing at an increasing rate.

1.1 Evolution of Iterative Methods in Computational Mathematics

The journey of solving linear systems has seen significant evolution, starting from the foundational contributions of C.F. Gauss[1] [52] and moving through a series of substantial advancements [29, 74, 79]. This path marks a transition from early direct elimination techniques, effective for small-scale problems, to sophisticated iterative methods more suited for large, complex systems modelling, e.g. vibrations or elasticity [16, 61, 71, 103]. The shift from Gauss's direct methods to iterative strategies signifies a pivotal transition in numerical methods, catering to the increasing complexity and scale of computational challenges — iterative methods have become prominent, particularly for their efficiency in coping with large and sparse matrix systems, often resulting from discretizing PDEs across various scientific and engineering applications. Iterative methods, including Gauss-Seidel[2]and SOR iterations [61, 103], have shown immense practical value, excelling in managing large, sparse systems — this capability is especially relevant in discretizing time-dependent PDEs, as commonly encountered in dynamic simulations and complex geometrical computations. A comparative analysis reveals that iterative methods offer significant computational benefits over direct methods like Gaussian elimination, predominantly evident in their adeptness at efficiently dealing with sparse matrices, a frequent necessity in contemporary computational tasks. The advent of multi-grid methods marks a notable advancement in iterative techniques [60, 101, 114], they are essential for accelerating the convergence of solutions in large-scale linear systems, particularly those stemming from the discretization of PDEs in computational applied mathematics and physics — multi-grid methods have demonstrated remarkable versatility and efficiency in practical applications, such as solving flow equations over complex geometries in fluid dynamics and efficiently solving Maxwell's[3] equations [75, 87, 96] in electromagnetism. Integrating iterative methods into HPC, including the application of time-parallel time integration methods [30, 92], has been a significant leap forward as well, especially given the limitations in processor clock speeds — this has made parallelization in the time direction an increasingly essen-

[1] Johann Carl Friedrich Gauss (*30 April 1777 in Braunschweig, Principality of Braunschweig-Wolfenbüttel; †23 February 1855 in Göttingen, Kingdom of Hanover) was a German mathematician and physicist. His contributions to the fields of number theory, statistics, differential geometry, and astronomy laid foundational principles that have influenced many areas of mathematics and science.

[2] Philipp Ludwig von Seidel (*24 October 1821 in Zweibrücken, Kingdom of Bavaria; †13 August 1896 in Munich, Kingdom of Bavaria) was a German mathematician and physicist renowned for his work in optics, particularly in the calculation of lens systems. He identified the Seidel aberrations, critical in optical design and theory.

[3] James Clerk Maxwell FRSE FRS (*13 June 1831 in Edinburgh, Scotland; †5 November 1879 in Cambridge, England) was a Scottish physicist and mathematician. His formulation of the classical theory of electromagnetic radiation, bringing together for the first time electricity, magnetism, and light as different manifestations of the same phenomenon, Maxwell's equations, demonstrated the unity of electromagnetism.

tial aspect of solving time-dependent PDEs [45]. The iterative approach to solving linear systems has continually been adapted and refined to meet the challenges of modern scientific computation. This trajectory, from its origins to its integration with cutting-edge computing techniques like parallel-in-time (PinT) algorithms [45, 83, 90], underlines the dynamic nature of the field and its critical role in advancing computational mathematics, and related disciplines — building on the foundational work of Gauss and others, we now turn our focus to modern iterative and multi-grid methods [61, 113], which represent the culmination of this evolution.

1.2 The Evolution and Importance of Multi-grid Methods

Multi-grid methods stand at the limelight of scientific computing and represent a sophisticated class of iterative techniques essential for precipitate the convergence of solutions in large-scale linear systems [60, 114]. These systems frequently arise from the discretization of PDEs — a standard practice in computational applied mathematics and, e.g., physics, where continuous functions, models, variables, and equations are transformed into their discrete counterparts [105]. The cornerstone of multi-grid methods lies in their use of multiple discretization levels, or 'grids' [10]. This hierarchical approach deal with various frequency components of error terms effectively during the solution process [7] — in this manner, multi-grid methods efficiently reduce error by coping with high-frequency components on finer grids, while resolving low-frequency components on coarser grids through recursive coarse-grid correction [62]. The mutual influence between smoothing and coarse-grid correction across multiple grid levels allows multi-grid methods to effectively deal with errors at different scales, leading to fast convergence [60] — this optimizes computational resources by possibly tackling each error level with the most appropriate resolution. A key attribute of multi-grid methods is their exceptional computational efficiency, indispensable for managing complex systems in contemporary scientific calculations [113]. This efficiency arises from their multilevel approach, and the algorithm's inherent ability, in the case of successful design, to maintain an optimal convergence rate independent of grid size [34]. The broad applicability of multi-grid methods across various scientific and engineering disciplines showcases their versatility, as demonstrated by their instrumental role in treating problems of fluid dynamics [112] and resolving Maxwell's equations in electromagnetism [2, 3, 6]. In addition, integrating multi-grid methods into HPC represents a significant advancement in computational mathematics again — their capability in navigating complex, large-scale systems aligns with the demands of modern sci-

entific research, making them integral in computational strategies and significantly contributing to advanced research and academic pursuits in this dynamic field [34]. Notable examples of multi-grid methods' application in HPC include NVIDIA's AmgX [91] and the HYPRE library [73], which improve efficiency and scalability in challenging Finite Element Method (FEM) models, particularly in computational fluid dynamics.

1.2.1 Parallel-in-Time Methods

In applications with a *small* number of degrees of freedom (DOF), such as robotics, multi-body dynamics, or protein folding, the opportunity for parallel resolving within each time step is minimal; effectively harnessing the capabilities of numerous processors becomes challenging, resulting in scalability issues — so, these issues become particularly pronounced when the spatial domain is thoroughly resolved, and there is still access to vast parallel computing resources aimed at reducing the time required to reach a solution. The necessity for real-time responses further amplifies the need for parallel solving across time, despite potential reductions in parallel efficiency. However, the inherently sequential nature of time-stepping processes makes distributing computations across the temporal dimension a significant technical obstacle [30, 45]. Time-parallel methods have evolved as significant advancements in computational mathematics, resolving stiff differential equations, large-scale dynamical systems, and boundary value problems — the development of PinT methods dates back at least 60 years [90], with the majority being multi-level and iterative. Examples include Parareal [83], the parallel full approximation scheme in space and time (PFASST) [27], and Multi-grid Reduction in Time (MGRIT) [30]. Parareal, probably the most studied PinT method — it can be interpreted as a multiple-shooting method or a multi-grid method in time. PFASST is based on spectral deferred correction (SDC) [26] and allows space-time parallelization using SDC on a space-time hierarchy. MGRIT applies the principles of multi-grid reduction in the time domain. Other PinT methods include waveform relaxation [119], space-time multi-grid [50], and revisionist integral deferred correction [14]. For a comprehensive overview, refer to [45, 92]. MGRIT, the method we focus on in this thesis, has been theoretically studied [19, 34, 44, 69] and successfully applied to various problems, including linear and nonlinear parabolic problems [30, 34], compressible fluid dynamics [32], power systems [81, 115, 116], linear advection [19, 70], and machine learning [58, 89, 108]. Spatial coarsening in MGRIT was in-

vestigated for the p-Laplacian[4] [34] and the Burgers[5] equation [70]. Motivated by the limitations of the temporal grid hierarchy in two-grid Parareal when applied to, e.g., the induction machine model, or processor-local multi-grid hierarchies in geometric and algebraic multi-grid for elliptic or parabolic problems [30, 119], the structure of the multi-level hierarchy within MGRIT is both critical and challenging. The typical choice of the coarse grid in the two-level setting is based on the number of processes [83], but for a large number of processes, the serial work on the coarsest level may dominate the runtime. Using more than two grid levels can reduce the serial work, but the resulting large time steps can be ineffective or infeasible for some applications [112] and may affect the convergence [18]. In [65], a new way to define the coarsest level in MGRIT was introduced (AT-MGRIT), with emphasis on reducing the serial work while avoiding large time steps. In general, domain decomposition techniques excel in multi-dimensional problems like fluid dynamics or structural analysis, breaking the problem space into smaller sections for simultaneous solving, and improving efficiency in large-scale, complex tasks [15]. Waveform relaxation, commonly used in circuit simulation, iteratively solves these sub-problems, improving overall solution accuracy [40, 72]. Direct time parallel methods utilize HPC to distribute computational tasks across multiple processors, optimizing resource use and ensuring scalability [44]. These all aspects are particularly essential in high-resolution modelling or real-time data analysis. In conclusion, time-parallel methods represent a significant stride in computational mathematics, illustrating the critical relationship between theory and practical application — their evolution mirrors technological advancements and indicates future possibilities in HPC.

1.3 Research Gap and Objectives

This research introduces the novel Quotient Multi-grid Reduction in Time (QMGRIT) algorithm, an advancement in the field of PinT multi-grid methods — this algorithm extends the capabilities of existing two-grid approaches, offering a generalized framework for resolving periodic problems in HPC. The primary four objectives of this dissertation are the following.

1. To present the development and theoretical foundation of the QMGRIT algorithm, including a

[4] Pierre-Simon Laplace (*23 March 1749 in Beaumont-en-Auge, France; †5 March 1827 in Paris, France) was a French mathematician and astronomer notable for his developments in celestial mechanics, statistics, and the formulation of Laplace's equation. His work laid key foundations in mathematical physics and statistics.

[5] Johannes Martinus Burgers (*13 January 1895 in Arnhem, Netherlands; †7 June 1981 in Maryland, USA) was a Dutch physicist and mathematician known for his foundational work in fluid dynamics. Burgers contributed significantly to the theory of turbulence and the development of what is now known as the Burgers equation, a fundamental nonlinear partial differential equation used in various areas of applied mathematics and physics.

detailed exposition of its generalization capabilities over traditional two-grid methods, emphasizing its application in parallel computing (assessed in 3.2).

2. To apply the QMGRIT algorithm to a variety of periodic problems, demonstrating its broad applicability and effectiveness through specific case studies showcasing the algorithm's practical utility in solving complex periodic problems in computational science (emphasized in 4).

3. To analyze the computational efficiency and accuracy of the QMGRIT method, comparing its performance against existing methods in terms of computation time and accuracy, particularly in parallel computing environments (illustrated in 4.2).

4. To explore strategies for integrating QMGRIT with contemporary HPC frameworks, proposing and evaluating techniques to improve the algorithm's scalability and performance in various distributed computing environments (investigated in 3.2.3 and in 4.5).

1.3.1 Quotient Multi-grid Reduction in Time

The importance, significance, and relevance to evolve the parallel iterative multi-grid approaches align with how the QMGRIT algorithm represents a modern key methodologies that confront the challenges when solving time-periodic problems — QMGRIT is a notable development beyond MGRIT because it can better deal with and solve time-periodic problems. It is crucial to know why and how it differs from and improves upon the standard MGRIT to advance computational toolsets. Within the field of computational mathematics, specifically concerning solving time-periodic problems, it is commonplace that, to start the steady-state solution process from an initial value and proceed with the simulation till the steady-state appearance. So, the existing methodologies may require extensive work, i.e., computationally extensive. While traditional two-grid methods are effective in many ways, they can become limited in terms of scalability, particularly parallel scalability, making it hard to continue to use the approaches with more and more processors, which is stagnating and restrictive. Specifically, QMGRIT works to solve these challenges in parallel environments and utilizes a multi-level approach, improving parallel scalability and total efficiency in logical matters of these types of computations — QMGRIT makes the computation for time-periodic problems much simpler by focusing on the period and intrinsically pushes past what the traditional two-grid did with parallel stagnation, which results in using a potentially much more powerful and effective array of computational resources. QMGRIT advances previous multi-grid methodologies in navigating the challenges of introducing periodicity specifically

in the temporal domain, and by taking advantage of the natural structure within time-periodic problems, QMGRIT is aiming to improve convergence and parallel efficiency over the standard MGRIT — this is done through a periodic multi-level procedure that allows information to be seamlessly passed between different domains across periodic boundaries, eventually converging to the desired solution —, allowing for a more scalable, and robust solution methodology.

1.4 Practical Relevance of the Research

The QMGRIT algorithm is a further development concerning the theoretical and practical sides of numerical solutions to periodic time-dependent PDEs. The application area covers broad scientific disciplines, such as physics, engineering and environmental science, where efficient and accurate simulation of periodic problems is essential. QMGRIT has the potential to deal with challenging time-dependent simulations efficiently, and may lead to improvements in computer algorithms within these fields — this research represents an improvement of computational methodologies leading to more efficient computational techniques, and can therefore be seen as a contribution towards scientific modelling and problem solving across different contexts.

1.5 Structure of the Thesis

This dissertation is devoted to a thorough examination of QMGRIT algorithm, which is constructed in a systematic manner to disentangle all the chapters of the subject comprehensively.

The thesis initiates with a Chapter 1 in the form of an introduction — the focus and background of QMGRIT is established in this chapter, which includes the historical development of iterative methods and the importance of multi-grid methods while concentrating particularly on the development and application of QMGRIT.

A detailed literature review follows in Chapter 2, examining the historical evolution of multi-grid methods and the progression to MGRIT and QMGRIT — this chapter also focuses on the analysis and the limitations of the existing results, especially when considering the challenging problems, especially when appreciating the tasks we aim for in this development.

The succeeding chapter cover the theoretical structure for a thorough understanding of QMGRIT, addressed in Chapter 3, discussing time-dependent PDEs and numerical schemes for their solution — including a prolonged discussion on the theoretical foundation of QMGRIT and the mathematical

foundation of the algorithm's construction, and the analytical technique behind the design of QMGRIT, which includes the algorithm, methodologies such as gQMGRIT, and other analytical basis for the algorithm's construction. Several applications of QMGRIT for periodic problems — especially, heat equation — include a complete formulation, summary, and example descriptions, examining the issue of computational efficiency and accuracy.

An extensive context of numerical experiments and results is the significant tribute of this dissertation, presented in Chapter 4, and provides an application of QMGRIT on various problems on the top of the heat equation, including coaxial cable problem, electrical machine, and wave equation. The performance analysis includes an additional portion, which provides a focus on the experimental setups — a discussion of scalability analysis, and a fair amount of discussion of the performance analysis applied as compared to the literature and findings in the field.

The thesis concludes with Chapter 5, which summarizes the observation and assertion of what we have discovered and the theoretical implications or practical implications, general analysis, identifications of the challenges, and the limitations. Further, we posit areas for future development in this context for more efficient and extended applicability of the algorithm to a much broader problem class.

Chapter 2

Literature Review

The literature review aims to contextualize the significance of multi-grid methods in computational mathematics, specifically focusing on MGRIT and the emerging QMGRIT.

2.1 Historical Development of Multi-grid Methods

Extending the historical trajectory of multi-grid methods in computational mathematics, we witness a story of significant theoretical advancement and remarkable innovation. These methods were a paradigm shift, first developed to overcome the shortcomings of classical iterative techniques for large-scale linear systems — they revolutionized computational efficiency by introducing a multi-level framework capable of controlling and eliminating errors at different scales. A. Brandt's[1] [10] groundbreaking contributions, who cleverly proposed operating across multiple grid resolutions for non-linear problems to speedup convergence, marked the beginning of modern multi-grid methods. The foundational ideas of multi-grid methods can be traced back to the pioneering works of R.P. Fedorenko[2] [37] and N.S. Bakhvalov[3] [1] in the 1960s. Fedorenko introduced the concept of using a hierarchy of grids to accelerate the convergence of iterative methods for solving elliptic PDEs, while Bakhvalov further

[1] Achiezer Brandt (*1938 in Givat Brenner, today in Israel) is an Israeli mathematician and computer scientist. He revolutionized computational mathematics with the introduction of the multi-grid method, significantly improving the efficiency of solving large-scale differential equations. His interdisciplinary approach has also impacted numerical linear algebra and optimization problems.

[2] Rafail Petrovich Fedorenko (*1929 in Saratov, Soviet Union; †2011 in Moscow, Russia) was a Soviet mathematician and economist known for his pioneering work in the development of the multi-grid method. His research laid the groundwork for numerical solutions to PDEs, particularly in improving computational efficiency..

[3] Nikolai Sergeevich Bakhvalov (*29 May 1934 in Moscow, Soviet Union; †29 August 2005 in Moscow, Russia) was a Soviet mathematician distinguished for his pioneering work in numerical methods in computational physics. His seminal contributions extend to the theory of optimization and the rigorous analysis of algorithmic complexity, making critical advancements in the efficiency of numerical integration techniques.

developed these ideas and provided a rigorous mathematical foundation for the convergence of multi-grid methods. Building upon these early contributions, Brandt's work in the 1970s [10] significantly advanced the field by introducing the key concepts of error smoothing and recursive application over multiple grid levels, demonstrating the asymptotic optimality of multi-grid methods and their ability to solve elliptic PDEs with a computational complexity proportional to the number of unknowns. A further notable step in the adaptation of multi-grid methods to broader contexts was the development of Algebraic Multi-Grid (AMG) methods. Pioneered in [101], AMG methods offered a revolutionary approach to dealing with large-scale linear algebraic systems that arise from the discretization of partial differential equations — unlike traditional multi-grid techniques, AMG methods do not rely on geometric information but on the algebraic properties of the matrix itself, enabling effective application to problems lacking a clear geometric interpretation. This innovation has significantly expanded the applicability of multi-grid methods, making them a versatile tool for a wide range of computational challenges [35, 101, 113]. In the following decades, W. Hackbusch[4] [60, 62, 61] and others made significant contributions to the theoretical comprehending and practical implementation of multi-grid methods, building the understanding of all essential elements like smoothing and coarse-grid correction together, which improved the robustness and efficiency of the multi-grid framework. One notable development in the evolution of multi-grid methods was the introduction of the Multi-grid Reduction (MGR) approach by Ries[5] et al. [98], extending the multi-grid concepts to more general classes of problems beyond elliptic PDEs. It introduced intermediate grids and specialized transfer operators to effectively deal with anisotropic and non-symmetric problems. The MGR ideas laid the foundation for the development of the Multi-grid Reduction in Time (MGRIT) method by Falgout[6] et al. [30], which creatively adapted the MGR principles to the time domain, enabling the efficient PinT solution of time-dependent problems by introducing a hierarchy of time grids and a parallel coarse-grid correction scheme. Concurrently, theoretical and analytical advancements such as Local Fourier[7] Analysis

[4] Wolfgang Hackbusch (*October 24, 1948 in Westerstede, Lower Saxony, Germany) is a German mathematician acclaimed for his pioneering research in numerical linear algebra and scientific computing, particularly the development of the multi-grid method and hierarchical matrices. His distinguished work has been recognized by the prestigious Leibniz Prize, among other honours, highlighting his influential role in the field.

[5] Manfred Ries (*10 July 1954 in Koblenz, Germany) is a German mathematician renowned for his significant contributions to the development of scalable linear and nonlinear solvers for HPC. His work, particularly in the design and analysis of multi-grid algorithms, plays a pivotal role in advancing computational efficiency and solving large-scale scientific problems.

[6] Robert D. Falgout is an American mathematician and computer scientist, best known for his work in the development of multi-grid methods and their application to large-scale parallel computing. As a key figure in scientific computing, his contributions include the co-creation of the HYPRE library, a highly regarded toolkit for solving large, sparse linear systems of equations on massively parallel computers.

[7] Jean-Baptiste Joseph Fourier (*21 March 1768 in Auxerre, Kingdom of France; †16 May 1830 in Paris, Kingdom of France) was a French mathematician and physicist best known for initiating the investigation of Fourier series and their applications to problems of heat transfer and vibrations. The "Fourier transform" and "Fourier's law of heat conduction" are named in his honour, profoundly influencing many branches of mathematics, physics, and engineering.

(LFA) [7, 51, 77, 99] and Semi-Algebraic Mode Analysis (SAMA) [42] provided deeper insights into the convergence behaviour and optimal design of multi-grid methods, instrumental in understanding the performance characteristics of multi-grid algorithms and guiding their further development. Recent research has focused on extending multi-grid methods to a wider range of applications beyond their original scope, successfully applying them to solve challenging multi-physics problems, to optimize PDE-constrained systems, and to navigate challenges in scientific computing and engineering simulations [31, 80, 92]. The development of multi-grid techniques, from the early works of Fedorenko to the latest advancements in PinT methods like MGRIT, showcases the power of combining theoretical insights with practical application, pointing out the importance of multi-grid methods as an essential tool for efficient and scalable solutions to challenging computational problems.

2.2 Review of Applications and Case Studies

The effectiveness of PinT methods, including MGRIT and its variants, has been demonstrated across a wide range of applications and case studies — these methods have been successfully applied to solve challenging problems in various domains, such as fluid dynamics, structural analysis, and electromagnetic simulations. In the field of fluid dynamics, PinT methods have been used to approach the acceleration of the simulation of unsteady flows [112, 118]. These studies have shown a speedup and improved scalability compared to traditional time-stepping approaches — the ability to parallelize in time has proven particularly beneficial for long-time integration of challenging problems, where the sequential nature of time-stepping can be a bottleneck. Structural mechanics is another area where PinT methods have found success. The simulation of dynamic behaviour of structures, such as vibration analysis and transient response, often involves time-dependent PDEs. MGRIT and its variants have been applied to efficiently solve these problems, enabling faster and more accurate predictions of structural performance [6, 15]. Electromagnetic simulations, particularly those involving eddy currents and time-varying fields, also have benefited from PinT approaches. Studies have demonstrated the effectiveness of MGRIT in reducing the computational time and memory requirements for these simulations [47, 76, 107]. The ability to parallelize in time has opened up new possibilities for the efficient modelling and design of electromagnetic devices. In addition to these specific domains, PinT methods have been applied to a broader range of problems, including optimization [92], uncertainty quantification [125] and multi-scale simulations. These studies have consistently demonstrated the po-

tential of PinT approaches to accelerate computations and enable the solution of previously intractable problems. As the field of PinT methods continues to evolve, it is expected that new applications and case studies will arise, further showcasing the versatility and effectiveness of these techniques — the ongoing development of specialized algorithms, such as QMGRIT for time-periodic problems, will likely expand the range of problems that can benefit from PinT approaches.

2.3 Emergence of QMGRIT

Building upon the accomplishments of the MGRIT algorithm, the QMGRIT algorithm provide a new approach for solving time-periodic problems. Although QMGRIT is a new method, it was inspired by PinT methods like the Parareal [83] and its extensions to time-periodic problems [46, 76] and extends its scope to a multi-grid framework. QMGRIT also extends the MGRIT method by introducing a quotient space formulation, which *glues* the endpoints of the time interval, in order to deal with the time-periodicity by using the inherent structure of time-periodic problems. The intent of QMGRIT is to achieve faster convergence and better parallel performance than the standard MGRIT, by reformulating the problem of time-periodicity in a quotient space, where impositions of the periodicity condition are immanent [78, 119, 120, 121]. Reformulating the problem in the quotient space allows the usage of multiple coarser temporal grids and permits the propagation of information across periodic boundaries efficiently. The QMGRIT algorithm utilizes a multi-level approach, similar to MGRIT, with specialized prolongation and restriction operators that honour the periodic structure. QMGRIT is at an early stage of its development, but due inheriting from MGRIT, it promises to be able to solve a broad range of fields, such as fluid dynamics [112], electromagnetism [76], and structural mechanics [36]. The potential benefits of QMGRIT include accelerated convergence rates, reduced computational cost, and improved scalability on parallel architectures. As QMGRIT continues to evolve, it is important to deepen the theoretical analysis and numerical experiments to understand its performance and robustness across a broader range of different problem classes — in this dissertation, compared with the existing PinT methods and traditional time-stepping techniques, there are results to suggest advantages and limitations. QMGRIT represents a new and engaging direction for PinT methods, primarily[8] for time-periodic problems. By combining the successful aspects of MGRIT and working with a deep history of multi-grid methods, QMGRIT stands to make a significant contribution to efficiently and

[8]Straightforwardly, not all the functions u with $u(\cdot, t_1) = u(\cdot, t_2)$ for some points t_1, t_2 in time are time-periodic — still, we may use efficient time-periodic algorithms on the interval $[t_1, t_2]$.

scalable solving time-periodic PDEs.

2.4 Critical Analysis of Current Literature

Notwithstanding the advancements in PinT methods documented in the literature, certain obstacles persist that necessitate additional research. Scalability and efficiency on massively parallel architectures are among the largest challenges — as we increase the number of processors, load balancing and communication overhead may have an impact on the speedup that performance will see. Particularly, the study [44] presents a performance model for a multi-grid-in-time solver, which helps in deciding the optimal amount of parallelism to devote to space versus time — the model selects the best parallel configuration in most test cases, bringing to the forefront the importance of balancing communication and computation to achieve optimal performance. In order to deal with this obstacle, there are several solutions can be considered: adaptive load balancing methods, where we can optimize the communications patterns, asynchronous communication techniques, the use of hierarchical parallelization, etc.

The robustness and stability of PinT methods across a broad range of problems also need attention. While PinT methods can be successful on a case-by-case basis, the performance can vary based on the underlying physics, discretization schemes of the problem, and the parameters of the problem. A better understanding of the convergence and numerical properties of PinT methods will be essential to using these methods successfully and efficiently [50, 123], e.g., [123] demonstrated that the convergence of MGRIT for advection-diffusion equations with uncertain coefficients can be significantly improved by using the 2nd-order Lobatto IIIC (LIIIC-2) method as the coarse propagator instead of the backward Euler[9] (BE) method — they observed that the LIIIC-2 method resulted in approximately **50%** reduction in the number of iterations required for convergence. Thus, developing adaptive algorithms that can automatically adjust their parameters based on the problem characteristics could improve robustness — additionally, incorporating problem-specific knowledge into the coarse-grid operators might enhance stability for challenging problem classes.

The community faces both unique opportunities and challenges in integrating PinT methods with advanced computational techniques such as adaptive mesh refinement, multi-scale modeling, and un-

[9] Leonhard Euler (*15 April 1707 in Basel, Switzerland; †18 September 1783 in Saint Petersburg, Russian Empire) was a Swiss mathematician and physicist, one of the most prolific mathematicians in history. His work in mathematics and physics is vast, covering areas such as infinitesimal calculus, graph theory, and introducing much of the modern mathematical terminology and notation.

certainty quantification. This integration could yield efficient and powerful solution strategies for complex multi-physics problems. Notably, [125] developed a MGRIT algorithm tailored for unsteady fractional Laplacian problems, introducing a generalized two-level convergence theory that expands the applicability of the MGRIT method — their numerical experiments validated the theoretical predictions regarding the algorithm's robustness and scalability —, the study also identified promising future research directions, including multilevel convergence analysis and extensions to time-fractional problems and adaptive time-stepping scenarios. Thus, creating unified frameworks that seamlessly integrate PinT methods with these advanced techniques may lead to more effective solution strategies, potentially involving adaptive algorithms that dynamically allocate resources based on specific problem requirements.

In addition to these considerations, there are specific developments required to enable the application of, and accelerate the adoption of PinT methods in practice. Notably, the development of software frameworks and libraries that encapsulate and enable the application of PinT methods in practice is necessary for the community to move forward. Progress has been made in this area with, e.g., the introduction of XBraid [124] and PyMGRIT [63]; yet, further development is needed to create more complete and flexible tools that can be used with simulation codes in practice — it may be noted, e.g., that while PyMGRIT provides a Python implementation of MGRIT, integrating it with large-scale simulation codes written in other languages can be challenging due to language barriers and performance considerations. Developing more versatile software frameworks with robust APIs and language bindings could facilitate easier integration with existing codes. Additionally, creating user-friendly interfaces and comprehensive documentation could help broaden the adoption of PinT methods in various scientific and engineering disciplines.

Moreover, the theoretical foundations of PinT methods, particularly in the context of non-linear and coupled problems, also need to be refined. A careful mathematical investigation of the properties of convergence, stability, and error propagation of PinT methods will continue to be necessary to understand the conditions that make them optimal and the theory of correctly deploying these methods, e.g., [31] studied the application of MGRIT to linear parabolic problems. They compared MGRIT with other multi-grid methods such as space-time multi-grid and waveform relaxation multi-grid with cyclic reduction — their results showed that MGRIT can provide significant speedup compared to sequential time stepping when sufficient parallel resources are available, though it may require more processors than other methods to achieve optimal performance. Thus, performing thorough mathe-

matical analysis of the convergence, stability, and error propagation properties of PinT methods for non-linear problems and/or coupled problems has the potential to guide the developments of more robust algorithms — this may involve the extension of existing linear techniques to the non-linear setting or the invention of new theoretical frameworks. Further research is needed to understand how MGRIT and other PinT methods perform for non-linear problems, and how their convergence behavior might be affected by problem-specific parameters.

The gap existing between established methods such as the periodic versions of Parareal [46] and MGRIT [30] is evident, especially when dealing with periodic problems efficiently — periodic Parareal can be effective for time-periodic problems, but is lacking in the scalability of multi-level methods, while MGRIT, though powerful, may not manage periodic boundary condition as effectively. This research aims to bridge this gap by introducing the QMGRIT algorithm, which extends the capabilities of existing two-grid approaches to deal with periodic problems in HPC more efficiently.

Resolving the shortcomings of PinT methods, in this light, is a requisite for progress in the field of PinT methods. For PinT methods to be useful in scientific computation and application in the engineering sciences, navigating and advancing PinT methods beyond the issues that are known is necessary.

2.5 Summary Overview and Research Initiation

The current literature overview provides a historical account of multi-grid methods from their origins to the development of PinT techniques exemplified by MGRIT and QMGRIT. In addition, the current review accentuates successful applications of these techniques across several domains, demonstrating how and why these methods can be used to speedup simulations and solve difficult time-dependent problems. The review of the literature also identified a number of areas where more work or research needs to be done — these include but are not limited to the scalability and efficiency of PinT across massively parallel architectures, robustness and stability for different problem classes, combining with other advanced computational techniques, making these techniques usable offline dynamically so that experts in different domain areas can easily use them, establishing a theoretical foundation for these new techniques and algorithms, etc. Building upon this literature review, the research presented in this manuscript will strive to deal with some of these open research areas and add to the advancement of PinT methods, principally QMGRIT, for time-periodic problems. The following chapters will develop the theory, implementation, and numerical experiments for QMGRIT, showing its potential for

efficient and scalable PinT solvers for challenging time-periodic PDEs.

Inspired by the historical progression of multi-grid techniques and the most recent advancements in PinT techniques, this research will guide the way aiming to push the limits of computation in scientific computing and engineering simulations. The idea is to offer neophytes and experts in the area a new tool and algorithm that will allow them to more easily navigate the rapidly changing and growing complexity of problems, particularly the periodic problems, in the real-world — and be more of a driver in cutting edge research in many different application areas.

2.5.1 Details of MGRIT

Introduced in 2014, the non-invasive $O(N)$ solver, MGRIT, is one of the well known PinT integration methods [6, 20, 22, 30, 43, 69, 92, 111]. The MGRIT algorithm, inspired by the Parareal algorithm, adopts an algebraic multi-grid approach for temporal multi-grid computations. It uses a hierarchy of time grids and a parallel, iterative coarse-grid correction scheme based on multi-grid reduction principles [98]. Within the algebraic framework, discretization points are categorized as either F-Points (fine) or C-Points (coarse), with corresponding smoothing processes termed F-relaxation and C-relaxation, respectively. So the relaxation relies on two relaxation schemes and their combinations. F-relaxation focuses on updating the solution at all F-Points by propagating it from a C-Point to the subsequent F-Points until the next C-Point is reached. This process can be carried out in parallel for each interval of F-Points, involving $(m-1)$ sequential applications of the time integrator, where m denotes the coarsening factor. Conversely, C-relaxation updates the solution at all C-Points by propagating it from the preceding F-Point to a C-Point, with all C-Point intervals being able to be updated in parallel. The standard approach in the MGRIT algorithm is to employ the FCF-relaxation, which consists of an F-relaxation, followed by a C-relaxation, and then another F-relaxation. Other combinations of these relaxations are also feasible. Time-dependent initial value problems are commonly treated using time-stepping, MGRIT or other similar PinT approaches. Given an initial value $u(t_1) = u_1$ and a coefficient matrix O in the linear case, when solving an ODE's initial value problem

$$u'(t) = Ou(t) + g(t), \tag{2.1}$$

$$u(t_1) = u_1, \tag{2.2}$$

using time-stepping, where b_i incorporates the modified ODE's right-hand side, we write

$$u_1 = b_1 \quad \wedge \quad \forall i \geq 2 : u_i = \Phi u_{i-1} + b_i \in \mathbb{R}^{N_x+1}, \tag{2.3}$$

which is equivalent to a linear system of equations,

$$A\mathbf{u} \equiv \begin{pmatrix} \mathbb{I} & & & \\ -\Phi & \mathbb{I} & & \\ & \ddots & \ddots & \\ & & -\Phi & \mathbb{I} \end{pmatrix} \cdot \begin{pmatrix} u_1 \\ u_2 \\ \vdots \\ u_{N_t+1} \end{pmatrix} = \begin{pmatrix} b_1 \\ b_2 \\ \vdots \\ b_{N_t+1} \end{pmatrix} \equiv \mathbf{b} \in \mathbb{R}^{(N_x+1)(N_t+1)}, \tag{2.4}$$

where $\Phi \in \mathbb{R}^{(N_x+1)\times(N_x+1)}$ is a constant[10] square matrix representing an integrator application or a so-called time-stepping function, where $N_x + 1$ and $N_t + 1$ denote number of spatial and temporal DOF, respectively. The procedure of categorizing the discretization points as either F-Points or C-Points effectively reorganizes the system matrix of a generic linear equation $A\mathbf{u} = \mathbf{b}$ into block-form $A \begin{pmatrix} \mathbf{u}_f \\ \mathbf{u}_c \end{pmatrix} = \begin{pmatrix} \mathbf{b}_f \\ \mathbf{b}_c \end{pmatrix}$, where

$$A = \begin{pmatrix} A_{ff} & A_{fc} \\ A_{cf} & A_{cc} \end{pmatrix} \in \mathbb{R}^{(N_x+1)(N_t+1)\times(N_x+1)(N_t+1)}. \tag{2.5}$$

Defining the $(m-1) \times (m-1)$ block matrix A_m, we write

$$A_m = \begin{pmatrix} \mathbb{I} & & & \\ -\Phi & \mathbb{I} & & \\ & \ddots & \ddots & \\ & & -\Phi & \mathbb{I} \end{pmatrix}, \qquad A_{ff} = \begin{pmatrix} A_m & & & \\ & A_m & & \\ & & \ddots & \\ & & & A_m \end{pmatrix}. \tag{2.6}$$

[10] For simplicity, we assume $\Phi(t)$ to be constant, a purely analytical convenience. However, our framework can be generalized to scenarios where $\Phi(t)$ varies over time (see 3.4). While Fast Fourier Transformation techniques are effective for periodic problems with constant Φ, our research allows for parallelization even when $\Phi(t)$ is not constant, ensuring applicability to a wide range of real-world scenarios.

The block matrices A_{fc} and A_{cf} are defined as follows

$$A_{fc} = \begin{pmatrix} -\Phi & & \\ 0 & & \\ \vdots & & \\ 0 & & \\ & \ddots & \\ & & -\Phi \\ & & 0 \\ & & \vdots \\ & & 0 \end{pmatrix}, \tag{2.7}$$

and

$$A_{cf} = \begin{pmatrix} 0 & \dots & 0 & -\Phi & & & & & & & & \\ & & & & 0 & \dots & 0 & -\Phi & & & & \\ & & & & & & & & \ddots & & & \\ & & & & & & & & & 0 & \dots & 0 & -\Phi \end{pmatrix}. \tag{2.8}$$

Here, A_{fc} and A_{cf} are composed of $(m-1) \times 1$ and $1 \times (m-1)$ sub-block matrices, respectively. In addition, $A_{cc} = \mathbb{I}_c$. It follows

$$A = \begin{pmatrix} \mathbb{I}_f & 0 \\ A_{cf}A_{ff}^{-1} & \mathbb{I}_c \end{pmatrix} \begin{pmatrix} A_{ff} & 0 \\ 0 & A_{cc} - A_{cf}A_{ff}^{-1}A_{fc} \end{pmatrix} \begin{pmatrix} \mathbb{I}_f & A_{ff}^{-1}A_{fc} \\ 0 & \mathbb{I}_c \end{pmatrix} \tag{2.9}$$

and

$$A^{-1} = \begin{pmatrix} \mathbb{I}_f & -A_{ff}^{-1}A_{fc} \\ 0 & \mathbb{I}_c \end{pmatrix} \begin{pmatrix} A_{ff}^{-1} & 0 \\ 0 & \left(A_{\Delta}^{iv}\right)^{-1} \end{pmatrix} \begin{pmatrix} \mathbb{I}_f & 0 \\ -A_{cf}A_{ff}^{-1} & \mathbb{I}_c \end{pmatrix}, \tag{2.10}$$

with

$$A_{\Delta}^{iv} \coloneqq A_{cc} - A_{cf}A_{ff}^{-1}A_{fc} = \begin{pmatrix} \mathbb{I} & & & \\ -\Phi^m & \mathbb{I} & & \\ & \ddots & \ddots & \\ & & -\Phi^m & \mathbb{I} \end{pmatrix}, \tag{2.11}$$

whereas A_{Δ}^{iv} is the Schur[11] complement of matrix A. The method draws its inspiration from the goal of mimicking a direct solver approach, utilizing a Schur complement factorization technique — this technique involves eliminating all F-Points initially, resolving the Schur complement system at the C-Points, and subsequently determining the F-Point values based on these coarse resolutions[12]. We define the restriction operator for the MGRIT algorithm[13]

$$R_I \coloneqq \begin{pmatrix} 0 & \mathbb{I}_c \end{pmatrix} \in \mathbb{R}^{(N_x+1)(N_t/m+1)\times(N_x+1)(N_t+1)}, \tag{2.12}$$

and the 'ideal' prolongation operator

$$P \coloneqq \begin{pmatrix} -A_{ff}^{-1}A_{fc} \\ \mathbb{I}_c \end{pmatrix} = \left(\begin{array}{ccc} \Phi & & \\ \vdots & & \\ \Phi^{m-1} & & \\ & \ddots & \\ & & \Phi \\ & & \vdots \\ & & \Phi^{m-1} \\ \hline & & \\ & \mathbb{I}_c & \\ & & \end{array}\right) \in \mathbb{R}^{(N_x+1)(N_t+1)\times(N_x+1)(N_t/m+1)}. \tag{2.13}$$

Then, the iteration operator of the two-grid MGRIT with an an F-relaxation followed by CF-relaxation

[11] Issai Schur (*10 January 1875 in Mogilev, Russian Empire (now in Belarus); †10 January 1941 in Tel Aviv, Mandatory Palestine) was a German mathematician, known for his work in the theory of algebraic equations, group theory, and for the development of Schur decomposition and Schur complements in linear algebra.

[12] In the context of this technique, the term 'ideal' is used to describe the restriction and prolongation operators.

[13] As the 'ideal' restriction operator, one would have $R \coloneqq \begin{pmatrix} -A_{\mathrm{cf}}A_{\mathrm{ff}}^{-1} & \mathbb{I}_c \end{pmatrix}$

— or simply the two-grid MGRIT algorithm — is given by

$$T_{\text{MGRIT}}^{(1,2)} \coloneqq P\left(\mathbb{I}_c - A_c^{-1} A_\Delta^{iv}\right)\left(\mathbb{I}_c - A_\Delta^{iv}\right) R_I, \tag{2.14}$$

where A_c is the *initial value system* re-discretization, i.e., is an $(N_c+1)\times(N_c+1)$ block matrix, given by

$$A_c = \begin{pmatrix} I & & & \\ -\Phi_c & I & & \\ & \ddots & \ddots & \\ & & -\Phi_c & I \end{pmatrix}, \tag{2.15}$$

where Φ_c denote the coarse time propagator and $N_c = {}^{N_t}/_{m}$ is the number of coarse time intervals.

Chapter 3

QMGRIT Algorithm Development

The evolution of the QMGRIT algorithm is the subject of this chapter. First we discuss the existence of solutions to the time-periodic problems and their uniqueness in Section 3.1.1. Going forward, we will present the stationary basic iterative methods in Section 3.1.2 and the idea of Eternal Wanderlust (EW) in Section 3.1.3. Afterwards, we consider three test equations: the heat equation in Section 3.1.4, the Fourier-Poisson-Kelvin problem in Section 3.1.5, which incorporates diffusion, convection, and decay, and the wave equation in Section 3.1.6. The latter equations will be used as test cases for our algorithm. Next, we present the QMGRIT method, a multi-grid time-parallel approach, which is central to our research in Section 3.2. The convergence properties of QMGRIT will be better understood by delving into its spectral analysis in Section 3.2.1. We will also present the gQMGRIT parallelization paradigm in Section 3.2.3, which is designed to improve the algorithm's efficiency. By applying QMGRIT to the heat equation in Section 3.2.2, we will validate the results of the spectral analysis. By analyzing the method for this application using the SAMA methodology in Section 3.2.4, we will demonstrate the convenience of gQMGRIT algorithm with respect to QMGRIT numerically and analytically. As a final step, in Section 3.2.5, we will compare the QMGRIT method with the periodic Parareal ones theoretically in order to emphasize the benefits and distinctions of these two time-parallel techniques.

3.1 Excursus on Eternal Wanderlust and Test Equations

3.1.1 Existence and Uniqueness of the Solution

We consider a periodic ODE in the form

$$u'(t) = Ou(t) + g(t), \tag{3.1}$$

$$u(t+\omega) = u(t), \tag{3.2}$$

with $O \equiv O(t) \in C(I, \mathbb{R}^n \times \mathbb{R}^n)$ and $g \in C(I, \mathbb{R}^n)$. It is well known, e.g., [117], that for given[1] $u(0) = u_0$ the unique solution to Equation (3.1) reads

$$u(t) = \Pi(t,0)\, u_0 + \Pi(t,0) \int_0^t \Pi(s,0)^{-1} g(s) ds, \tag{3.3}$$

where $\Pi(t,s) \coloneqq e^{(t-s)O}$ is invertible *monodromy* matrix. By uniqueness and periodicity from Equation (3.2), $u(t)$ in Equation (3.3) is ω-periodic if and only if $u(\omega) = u(0) = u_0$, which is then equivalent to

$$(\mathbb{I} - \Pi(\omega,0))\, u(\omega) = \Pi(\omega,0) \int_0^\omega \Pi(s,0)^{-1} g(s) ds, \tag{3.4}$$

where $\mathbb{I}$ denotes the identity matrix of corresponding size. Rearranging, Equation (3.4) is equivalent to the following linear system of equations

$$\left(\Pi(\omega,0)^{-1} - \mathbb{I}\right) u(\omega) = \int_0^\omega \Pi(s,0)^{-1} g(s) ds. \tag{3.5}$$

These observations, together with the exercise [117, Chapter 3, Problem 3.43.], lead to the following.

Theorem 3.1. *The inhomogeneous equation*

$$u'(t) = Ou(t) + g(t), \tag{3.6}$$

where $g(t)$ is periodic with period ω, has a unique periodic solution with period ω if and only if $\lambda = 1$ is not an eigenvalue of the monodromy matrix $\Pi(\omega,0)$.

Proof. If and only if the matrix

$$\Pi(\omega,0)^{-1} - \mathbb{I} = e^{-\omega O} - \mathbb{I} \tag{3.7}$$

[1] Without loss of generality $t_0 = 0$.

has full rank, so it is invertible and has a non-zero determinant, the linear system of equations in (3.5) has the unique solution — i.e., the unique solution to this linear system reads

$$u(\omega) = \left(\Pi\left(\omega, 0\right)^{-1} - \mathbb{I}\right)^{-1} \int_0^{\omega} \Pi(s,0)^{-1} g(s) ds, \tag{3.8}$$

if and only if $\lambda = 1$ is not an eigenvalue of the monodromy matrix $\Pi\left(\omega, 0\right)$. This is because on contrary, if the determinant is zero, we have

$$\det\left(\Pi(\omega,0)^{-1} - \mathbb{I}\right) = 0 \tag{3.9}$$

$$\Leftrightarrow \exists v \neq 0 : \left(\Pi(\omega,0)^{-1} - \mathbb{I}\right) v = 0 \tag{3.10}$$

$$\Leftrightarrow \Pi(\omega,0)^{-1} v = v \tag{3.11}$$

$$\Leftrightarrow \Pi(\omega,0) v = v \tag{3.12}$$

and this last Equation (3.12) is precisely the definition of $\lambda = 1$ being an eigenvalue of $\Pi(\omega, 0)$. Thus, with Equations (3.3) and (3.8) the unique periodic solution to Equation (3.6) reads

$$u(t) = \Pi\left(t, 0\right) \left(\Pi\left(\omega, 0\right)^{-1} - \mathbb{I}\right)^{-1} \int_0^{\omega} \Pi(s,0)^{-1} g(s) ds + \Pi\left(t, 0\right) \int_0^{t} \Pi(s,0)^{-1} g(s) ds, \tag{3.13}$$

if and only if $\lambda = 1$ is not an eigenvalue of $\Pi\left(\omega, 0\right)$. □

For further existence and uniqueness results on periodic problems refer to [8, 78, 85, 109, 121], and especially [120], which covers an overview spanning about 500 publications. The above Theorem's 3.1 statement is sufficient for the purpose and the setting of this work.

3.1.2 Basic Iterative Method

Let $\mathbf{u}^j$ be any approximation of a solution $\mathbf{u}^*$ of some linear *problem equation*, whereas L is a square matrix,

$$L\mathbf{u} = \mathbf{b}. \tag{3.14}$$

Then, denoting

$$\mathbf{v}^j := \mathbf{u}^* - \mathbf{u}^j \tag{3.15}$$

the *error* of $\mathbf{u}^j$, and

$$\mathbf{d}^j := \mathbf{b} - L\mathbf{u}^j \tag{3.16}$$

the *residual* of $\mathbf{u}^j$, the corresponding residual operator is $\mathbb{I} - LB$. The *residual equation*

$$L\mathbf{v}^j = \mathbf{d}^j \tag{3.17}$$

is equivalent to the original problem equation, yielding

$$\mathbf{u}^* = \mathbf{u}^j + \mathbf{v}^j. \tag{3.18}$$

We note that if in Equation (3.17) L is replaced by any 'simpler' operator $\hat{L}$ such that action of inverse $\hat{L}^{-1}$ is known, i.e., can be computed efficiently, the solution $\hat{\mathbf{v}}^j$ of

$$\hat{L}\hat{\mathbf{v}}^j = \mathbf{d}^j \tag{3.19}$$

gives a new approximation

$$\mathbf{u}^{j+1} = \mathbf{u}^j + \hat{\mathbf{v}}^j. \tag{3.20}$$

Starting with a given[2] $\mathbf{u}^0$, the successive application of an iteration operator given by

$$Q := \mathbb{I} - BL, \tag{3.21}$$

where $B := \hat{L}^{-1}$ and $\mathbb{I}$ denotes the identity of corresponding size, defines the basic iterative method procedure [23, 61, 103, 114]. Then, it follows

$$\mathbf{v}^{j+1} = \mathbf{u}^* - \mathbf{u}^{j+1} = \mathbf{u}^* - (\mathbf{u}^j + \hat{\mathbf{v}}^j) \tag{3.22}$$

$$= \mathbf{v}^j - \hat{\mathbf{v}}^j = \mathbf{v}^j - \hat{L}^{-1}\mathbf{d}^j = \mathbf{v}^j - \hat{L}^{-1}L\mathbf{v}^j \tag{3.23}$$

$$= (\mathbb{I} - BL)\,\mathbf{v}^j = Q\mathbf{v}^j \quad (\mathrm{j} = 0, 1, 2, \ldots) \tag{3.24}$$

for the errors and

$$\mathbf{d}^{j+1} = (\mathbb{I} - LB)\,\mathbf{d}^j \quad (j = 0, 1, 2, \ldots) \tag{3.25}$$

[2]When applying the algorithms in the following sections and chapters for each run throughout the thesis, we use a random values initialization as the given solution approximation.

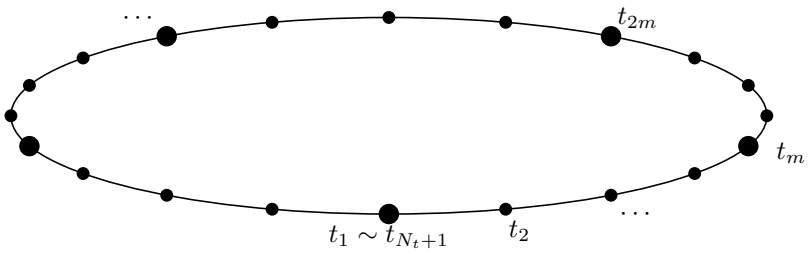

Figure 3.1: Quotient space ansatz representing the gluing of the endpoints of a time interval to deal with periodic problem in Equations (3.1)-(3.2) and Equation (3.26) according to the EW scheme

for the residuals. If some norm $\|.\|$ is defined, the corresponding operator norms

$$\|\mathbb{I} - BL\|, \quad \|\mathbb{I} - LB\|$$

give the *error reducing factor* and the *residual reducing factor*, respectively, per iteration step.

3.1.3 Eternal Wanderlust

Processing the periodic problem in Equations (3.1)-(3.2) numerically, we will use a time-stepping routine, i.e., we follow the ideas of the MGRIT algorithm, as in Section 2.5.1. We formulate the *Eternal Wanderlust* scheme to satisfy the time-periodic settings, thus rearrange the variables in Equation (2.4) and use the periodicity of $\mathbf{u}$, eliminating the last point in time $N_t + 1$, resulting

$$A_p \mathbf{u_p} \equiv \begin{pmatrix} \mathbb{I} & & & -\Phi \\ -\Phi & \mathbb{I} & & \\ & \ddots & \ddots & \\ & & -\Phi & \mathbb{I} \end{pmatrix} \cdot \begin{pmatrix} u_1 \\ u_2 \\ \vdots \\ u_{N_t} \end{pmatrix} = \begin{pmatrix} b_1 \\ b_2 \\ \vdots \\ b_{N_t} \end{pmatrix} \equiv \mathbf{b}_p \in \mathbb{R}^{(N_x+1)N_t}. \tag{3.26}$$

The above allows us to put together algebraic and topological points of view on periodic problems in time as we may observe from Figure 3.1 — in Equation (3.21) consider $L \coloneqq A_p$ and $\hat{L} \coloneqq \hat{A}$, where $\hat{A}$

is obtained from A (see Equation (2.4)) by removing the last row and column. Then, we get

$$Q = \begin{pmatrix} & & \Phi \\ & & \Phi^2 \\ & & \Phi^3 \\ & & \vdots \\ & & \Phi^{N_t} \end{pmatrix} \in \mathbb{R}^{(N_x+1)N_t \times (N_x+1)N_t} \tag{3.27}$$

and

$$\mathbb{I} - LB = \begin{pmatrix} \Phi^{N_t} & \dots & \Phi^3 & \Phi^2 & \Phi \\ & & & & \\ & & & & \\ & & & & \\ & & & & \end{pmatrix}. \tag{3.28}$$

Theorem 3.2. *If Φ is stable, i.e., $\rho(\Phi) < 1$, it follows*

$$\rho(Q) = \rho\left(\Phi^{N_t}\right) = \rho\left(\Phi\right)^{N_t} < 1, \tag{3.29}$$

where $\rho(\cdot)$ is the spectral radius.

Proof. Straightforward from Equation (3.27). □

Now, going through the EW iteration repetition, we conclude that EW is convergent in the following result — so, quoting Plato[3] in a post-ironic manner, 'there is no harm in repeating a good thing'.

Corollary 3.3. *For the linear iterative error system defined by $\mathbf{v}^{j+1} = Q\mathbf{v}^j$, where $\mathbf{u}^j$ serves as an approximation to the solution $\mathbf{u}^*$ and $\mathbf{v}^j = \mathbf{u}^* - \mathbf{u}^j$, the system exhibits an asymptotically stable zero solution, confirming the convergence of the error term $\mathbf{v}^j$ towards zero.*

Proof. Follows from Theorem 3.2. □

[3]Plato (*428/427 or 424/423 BCE in Athens, Greece; †348/347 BCE in Athens, Greece) was a Greek philosopher, a pivotal figure in the history of Western philosophy. The founder of the Academy in Athens, the first institution of higher learning in the Western world, Plato's work spans ethics, metaphysics, ontology, and epistemology. His dialogues, involving his teacher Socrates and his student Aristotle, have influenced thought for over two millennia.

Furthermore, we make use of the Löwner[4] partial order, which will be used for subsequent theoretical results, and show, as noted in Section 2.5.1, that imposing Φ constant is not a strict assumption. The Löwner partial order provides a framework for comparing the *magnitude* of positive semi-definite matrices of the same dimensions. Specifically, for two positive semi-definite matrices X and Y, we say that X is less than or equal to Y under the Löwner order (denoted $X \preceq Y$) if the matrix $Y - X$ is positive semi-definite (this means that for any non-zero vector z, the inequality $z^t(Y - X)z \geq 0$ holds, where z^t denotes the transpose of z). Now, for a varying time-stepping function, we conclude the following.

Corollary 3.4. *The following inequality applies*

$$Q_d = \begin{pmatrix} \Phi_{t_1} \\ \prod_{i=2,1} \Phi_{t_i} \\ \vdots \\ \prod_{i=N_t,\dots,2,1} \Phi_{t_i} \end{pmatrix} \preccurlyeq \begin{pmatrix} \Phi_\mu \\ \Phi_\mu^2 \\ \vdots \\ \Phi_\mu^{N_t} \end{pmatrix}, \tag{3.30}$$

whereas $\rho(\Phi_\mu) = \max\left\{\rho(\Phi_{t_i}) \;\middle|\; i = 1, 2, ..., N_t\right\}$ *applies, and*

$$\rho(Q_d) = \rho\left(\prod_{i=N_t,\dots,2,1} \Phi_{t_i}\right) \leq \rho(\Phi_\mu)^{N_t}. \tag{3.31}$$

Proof. Straightforward from properties of the spectral radius. □

After establishing the solution's existence and uniqueness in Theorem 3.1 and laying the theoretical foundation in Theorem 3.2, we present an algorithmic note on EW, as delineated in Algorithm 1.

3.1.4 Heat Equation

Joseph Fourier, in his groundbreaking work from 1822 [39], introduced the heat equation, a parabolic PDE. In his explanation, he modelled the heat equation using the Fourier transform for solving the equation, which has become a major mathematical foundation for describing heat transfer and diffusion processes since then [48, Section 1.4]. The heat equation is an important partial differential

[4] Karl Löwner (*19 May 1893 in Lány, Bohemia, Austro-Hungarian Empire; †22 January 1968 in Los Angeles, California, USA) was a Czech-German mathematician, renowned for his contributions to complex analysis, differential geometry, and the theory of real functions. Perhaps most famous for the Löwner equation in complex analysis, his work has had a lasting impact on the mathematical community, influencing both theoretical research and practical applications in various fields.

Algorithm 1 Eternal Wanderlust(Φ, $\mathbf{u}$, $\mathbf{b}_p$):

1. Let $\mathbf{u}^j$ be a given approximation of the solution.
2. Compute residual $\mathbf{d}^j \leftarrow \mathbf{b}_p - L\mathbf{u}^j = \mathbf{b}_p - \begin{pmatrix} -\Phi u^j_{N_t} + u^j_1 \\ -\Phi u^j_1 + u^j_2 \\ \vdots \\ -\Phi u^j_{N_t-1} + u^j_{N_t} \end{pmatrix}$.

while norm of residual is not small enough **do**

3. Perform periodic time-stepping $\Big(u^j_1 \leftarrow \Phi u^j_{N_t} + b^j_1,\ u^j_i \leftarrow \Phi u^j_{i-1} + b^j_i,\ i = 2, ..., N_t\Big)$.

end while

equation in mathematical physics — it describes how heat conducts in materials —, this PDE describes how the temperature in a given region changes over time, with the variations attributable to the internal heat conducting in the region. This is also why the study of it is important, because it provides insights about such kind of processes and makes it easier to transition to studying more difficult PDEs that are found across the many fields of science and engineering.

In this work, we only focus on a specific formulation of the heat equation. Denoted here as the grounded $1D$+$1D$ heat equation. This variant models how heat diffuses in a one-dimensional spatial domain over a time interval, giving us a simplified real-world problem for investigating methods to solve the heat equation analytically and numerically. We want to investigate how the heat equation behaves given periodic boundary conditions, employing finite difference (FD) method for discretizing in space and BE method for time discretizing — these methods are chosen for their simplicity, stability, and ease of implementation, making them ideal candidates for introducing and presenting numerical analysis.

Formulation

Consider the grounded $1D$+$1D$ heat equation defined on a square domain $[0,1]^2 \subset \mathbb{R}^2$, with spatial coordinate x and temporal coordinate t, given by

$$\frac{\partial u(x,t)}{\partial t} - a\frac{\partial^2 u(x,t)}{\partial x^2} = g(x,t), \qquad a > 0, \quad x \in [0,1], \quad t \in [0,1], \tag{3.32}$$

$$u(0,t) = u(1,t) = 0, \qquad t \in [0,1], \tag{3.33}$$

$$u(x,0) = u(x,1), \qquad x \in [0,1]. \tag{3.34}$$

The dD+1D equations for $d > 1$, with $d \in \mathbb{N}$, are analogously defined on $[0,1]^{d+1} \subset \mathbb{R}^{d+1}$, where $\mathbf{x} \in [0,1]^d \subset \mathbb{R}^d$. Here, $u(x,t)$ represents the temperature at point x and time t, a is the thermal diffusivity coefficient reflecting the material's ability to conduct heat, and $g(x,t)$ is a source term accounting for internal heat generation or absorption. The boundary conditions $u(0,t) = u(1,t) = 0$ signify that the ends of the domain are kept at a constant temperature (typically normalized to zero for simplicity). The periodic initial condition $u(x,0) = u(x,1)$ introduces a cyclical time-dependency, suggesting that the system's thermal state resets after each unit time interval, a setup that can model seasonal or diurnal temperature variations in simplified scenarios.

Exact Solution and Analysis

For the given problem setup, in Equations (3.32)-(3.34) with

$$g(x,t) = 2\pi x(x-1)cos(2\pi t) - 2a\sin(2\pi t), \tag{3.35}$$

the analytical solution is given by

$$u(x,t) = x(x-1)\sin(2\pi t). \tag{3.36}$$

This solution will serve as a benchmark for evaluating the accuracy and efficiency of our numerical methods. By comparing the numerical results to the analytical solution, we can assess the methods' performance and identify potential areas for refinement exactly.

The grounded $1D$+$1D$ heat equation presents a valuable model for studying fundamental aspects of heat diffusion and numerical solution strategies. Through analytical and numerical exploration, this work aims to deepen our understanding of the effectiveness of computational methods in simulating such phenomena — the interconnection between theory and computation underlines the broader significance of mathematical modelling in solving real-world problems (see Section 4.2). Building upon the Theorem 3.1, we conclude the following.

Corollary 3.5. *The induced by the grounded dD+1D heat equation semi-discrete inhomogeneous equation*

$$u'(t) = \mathcal{O}u(t) + g(t), \tag{3.37}$$

where $g(t)$ is a periodic function of period ω and $\mathcal{O}$ is an M-Matrix of the FD discretization method for the

dD-Laplacian operator, has unique periodic solution of period ω.

Proof. Using the Theorem 3.1, we provide a simple proof for $d = 2$. The proof for any other $d \in \mathbb{N} \setminus \{2\}$ is analogous. The Gershgorin[5] circle theorem [53] implies $\lambda_{\mathcal{O}} \in \left(0, \frac{8}{\Delta x^2}\right)$, where Δx is the equidistant spatial discretization parameter and $\lambda_{\mathcal{O}}$ denotes an eigenvalue of the matrix $\mathcal{O}$. It follows that $\lambda_{e^{\omega\mathcal{O}}} \in \left(1, e^{\frac{8\omega}{\Delta x^2}}\right)$ and, thus, one is not an eigenvalue of $e^{\omega\mathcal{O}}$. □

Discretization

The first step in numerically solving a differential equation is to convert the continuous problem to a discrete model. The usual approach for discretizing time-dependent PDEs is to first discretize the spatial dimensions and leave the time dimension continuous — this generally results in a system of ODEs in terms of time only and is referred to as a semi-discrete system. The semi-discrete system is then discretized in time by a time integration method, yielding a discretization of the complete set of algebraic equations. To numerically solve the heat equation, we use a spatial discretization method based on the FD method and a temporal integration method based on the BE — the FD method approximates derivatives by taking differences between values of a function at discrete points, while the BE is an implicit time-stepping scheme that is unconditionally stable, thereby providing an appropriate choice for stiff equations [67, 68]. The convergence of these numerical methods, and their ability to approximate the solution accurately as the resolution is increased, is a very fundamental part of our future analysis — it is crucial that we compare the order of convergence of the numerical solution against theoretical expectations. Furthermore, we will also examine the prediction outcomes of Theorem 3.2. On top, to provide a bit more insight into the process of possible discretization approaches, we offer a brief comment on the following

$$\dot{u} = \Delta u \overset{BE}{\Longrightarrow} -\Delta t \Delta u_i + u_i = u_{i-1}, \tag{3.38}$$

[5]Semyon Aronovich Gershgorin (*1901 in Pinsky, Russian Empire; †1933 in Leningrad, Soviet Union) was a Soviet mathematician known for the Gershgorin circle theorem, which provides a method to estimate the location of eigenvalues of a square matrix. His theorem has profound implications in numerical analysis, particularly in the study and computation of eigenvalues and eigenvectors.

FD: FEM:

$$
\begin{aligned}
(\Delta t O + I)u_i &= u_{i-1}, \\
\Leftrightarrow u_i &= (\Delta t O + I)^{-1} u_{i-1} \\
&=: \Phi(u_{i-1}),
\end{aligned}
\qquad
\begin{aligned}
(\Delta t W + S)u_i &= S u_{i-1}, \\
\Leftrightarrow u_i &= (\Delta t W + S)^{-1} S u_{i-1} \\
&=: \Phi(u_{i-1}),
\end{aligned}
$$

where S and W are *mass* and *stiffness* matrices, respectively. For details on FEM see Appendix B. Now, we demonstrate an equidistant discretization, using a FD scheme in spatial dimension and the BE method in time, simultaneously — this leads us to the following discrete approximation of Equation (3.32)

$$\frac{u_{j,i} - u_{j,i-1}}{\Delta t} - \frac{a\left(u_{j-1,i} - 2u_{j,i} + u_{j+1,i}\right)}{\Delta x^2} = g_{j,i}, \tag{3.39}$$

with $\Delta t = t_1 - t_0$ and $\Delta x = x_1 - x_0$, or equivalently

$$\left(1 + 2a\frac{\Delta t}{\Delta x^2}\right) u_{j,i} - a\frac{\Delta t}{\Delta x^2}\left(u_{j-1,i} + u_{j+1,i}\right) = u_{j,i-1} + \Delta t g_{j,i}. \tag{3.40}$$

If one takes the spatial homogeneous boundary conditions into account, one recognizes that in each time-step this is a linear system of equations

$$M u_i = u_{i-1} + \Delta t g_i, \tag{3.41}$$

of $N_x - 1$ equations for as many unknowns (as there are in the interior of $[0, 1]$, see Equation (3.33)). With Equation (3.40) and $r \coloneqq \Delta t / \Delta x^2$, the coefficient matrix is obviously

$$M = \begin{bmatrix}
1 + 2ar & -ar & 0 & \dots & 0 \\
-ar & 1 + 2ar & -ar & & \vdots \\
0 & \ddots & \ddots & \ddots & 0 \\
\vdots & & -ar & 1 + 2ar & -ar \\
0 & \dots & 0 & -ar & 1 + 2ar
\end{bmatrix}, \tag{3.42}$$

i.e.,

- $M = \text{tridiag}\left[-ar, 1 + 2ar, -ar\right]$ (when using a stencil notation);
- $M = T(f)$, where $f = 1 + 2ar - 2ar\cos\theta$ (when using a notation as a tridiagonal Toeplitz[6]

[6] Otto Toeplitz (*1 August 1881 in Breslau, German Empire (now Wroclaw, Poland); †15 February 1940 in Jerusalem, British

matrix generated by $1 + 2ar - 2ar\cos\theta$; the eigenvalues of a symmetric tridiagonal Toeplitz are known and given by the sampling of f over the equispaced τ-algebra grid [9]).

Now, denote $\Phi \coloneqq M^{-1}$ and $b_i \coloneqq \Delta t \Phi g_i$ — so, with periodic condition in time, $u_1 = u_{N_t+1}$, we conclude to the global linear system of equations, as considered in Equation (3.26). We calculate the eigenvalues of Φ, which are the reciprocals of the eigenvalues of M — the latter are well-known and given by

$$\lambda_M \in \left\{ 1 + 2ar - 2ar\cos\left(\frac{k\pi}{N_x}\right) \,\middle|\, k = 1, ..., N_x - 1 \right\}. \tag{3.43}$$

These are clearly greater than one, thus the eigenvalues of Φ are less than one, and Theorem 3.2 is applicable.

Numerical Analysis Verification

This section — and the following sections with Tables 3.6, 3.11 and 4.9 for other test equations — verifies that the algorithm's implementation executes correctly as designed, adhering to the underlying theoretical model. The error measurement,

$$\max_{j,i} |u(x_j, t_i) - u_{j,i}|, \tag{3.44}$$

focuses on the maximum absolute error across the spatial-temporal grid. Table 3.1 compares the exact solution $u(x_j, t_i)$ with the numerical approximation $u_{j,i}$ at grid points (x_j, t_i). Solutions obtained using the EW method are iterated until numerical convergence and then compared to the analytical solution. Our analysis directly observes that the BE method, serving as a first-order FD discretization method in the time dimension with its error magnitude dominating over the second-order discretization in the spatial dimension, performs as anticipated. Consequently, the deviation of the numerical solution from the analytical solution is approximately halved, aligning with the expected first-order convergence rate — this behavior agrees with theoretical expectations, demonstrating the effectiveness of both the EW method and its implementation.

Mandate of Palestine) was a German mathematician known for his work in the field of linear algebra and for the formulation of the Toeplitz matrices. His contributions have had a lasting impact on various areas of mathematics and its applications, especially in signal processing and numerical analysis, where Toeplitz matrices play a crucial role.

Table 3.1: EW error reduction for diagonal $N_t = N_x$ and different thermal diffusivity coefficients a

$N_t = N_x$	a = 0.1	a = 1	a = 10
$2^4 = 16$	4.71e-02	2.47e-02	3.11e-03
$2^5 = 32$	2.43e-02	1.30e-02	1.59e-03
$2^6 = 64$	1.22e-02	6.63e-03	7.99e-04
$2^7 = 128$	6.14e-03	3.35e-03	4.00e-04
$2^8 = 256$	3.08e-03	1.68e-03	2.00e-04
$2^9 = 512$	1.54e-03	8.44e-04	1.00e-04
$2^{10} = 1024$	7.70e-04	4.23e-04	5.01e-05

Numerical Convergence Factors

This section — alongside the following sections featuring Tables 3.7 and 3.12, 4.5, 4.7 and 4.9 for additional test equations — examines in Table 3.2 the numerical convergence factors of the EW scheme for the heat equation using FD methods in spatial dimensions and the BE methods in temporal dimension. We concentrate on the scenario of $N_t = N_x$ where we observe the scheme's behavior for uniformly discretized in time and space domains. In Table 3.2, we show the convergence factors in the $N_t = N_x$ scenario, across a range from 2^4 to 2^{10} — the study shows a consistent trend: the number of DOFs increases, the convergence factor decreases; and this suggests that the convergence rates of the EW scheme are improved when using finer discretizations, thus demonstrating the suitability of the EW scheme to high-resolution problem settings. A detailed look at the decrease in convergence factor as the thermal diffusivity coefficient a approaches zero emphasizes the significance of the sensitivity of the EW scheme convergence factor with respect to the thermal properties in the system. The results confirm the challenges of low thermal diffusivity scenario — these observations are pertinent to the recognition of the limitations of the numerical approach and may reveal the general need to investigate strategies aimed at improving the performance of numerical methods. The information presented here provides a baseline reference for the readers who might be pursuing new research on the performance of the EW scheme — the search for a more efficient computational method is necessary as the complexity to model and solve equations representing physical phenomena becomes more sophisticated —, perhaps the analysis of the EW convergence factor in the following sections could provide the reader with a reference point for future work on refining numerical algorithms to increase the efficiency of the simulation results.

Table 3.2: EW numerical convergence factors for diagonal $N_t = N_x$ and different thermal diffusivity coefficient a

$N_t = N_x$	a = 0.1	a = 1	a = 10
$2^4 = 16$	3.85e-01	4.67e-04	2.15e-14
$2^5 = 32$	3.78e-01	1.85e-04	2.84e-20
$2^6 = 64$	3.75e-01	1.03e-04	1.18e-26
$2^7 = 128$	3.75e-01	7.43e-05	1.69e-32
$2^8 = 256$	3.77e-01	6.23e-05	5.58e-37
$2^9 = 512$	3.79e-01	5.51e-05	6.37e-40
$2^{10} = 1024$	3.63e-01	5.42e-05	1.20e-41

Numerical Analysis Validation

This section presents — alongside the following sections featuring Tables 3.8-3.10, 3.13-3.15, 4.6, 4.8 and 4.9 for other test equations — Tables 3.3 through 3.5, which describe the largest eigenvalues of the inverted matrices M resulting from the discretization of the grounded $1D$+$1D$ heat equation. In the discretization process, we used FD schemes in the spatial dimensions and BE schemes in the temporal domains, over a range of N_t and N_x values ranging from 2^4 to 2^{10}, with changes in both N_t and N_x based on powers of two. The EW scheme is believed to converge with a convergence factor $\rho(\Phi^{N_t})$ according to Theorem 3.2, where ρ is the spectral radius. These tables give the spectral radii for a number of N_t and N_x pairs, which represent important evidence about the quality of the numerical scheme — in particular, they provide an indication of the stability of the numerical scheme we were using. Consequently, the checks on the eigenvalues that measure the stability of the scheme, and the checks on the convergence factor, which measures how quickly the numerical solution approaches the exact solution as the grid is refined, are closely connected. An important observation from the tables in this analysis is that the spectral radii, particularly along the diagonals of the tables, are numerically the same as the numerical convergence factors from earlier analysis, see Table 3.2: this highlight the validity of the numerical convergence factors as a robust measure of the quality and effectiveness of the numerical scheme — the validation of the numerical analysis using eigenvalues in this discussion reinforces the theoretical discourse, and this evidence underlines the practical application of the EW scheme in solving the heat equation (with a comprehensive argument about the performance dynamics of the EW scheme).

Table 3.3: $\rho(\Phi)^{N_t}$ for different N_t and N_x for $a = 0.1$

$N_t \backslash N_x$	16	32	64	128	256	512	1024
2^4	3.85e-01	3.84e-01	3.84e-01	3.84e-01	3.84e-01	3.84e-01	3.84e-01
2^5	3.79e-01	3.79e-01	3.78e-01	3.78e-01	3.78e-01	3.78e-01	3.78e-01
2^6	3.77e-01	3.76e-01	3.76e-01	3.76e-01	3.76e-01	3.76e-01	3.76e-01
2^7	3.75e-01	3.74e-01	3.74e-01	3.74e-01	3.74e-01	3.74e-01	3.74e-01
2^8	3.75e-01	3.74e-01	3.74e-01	3.74e-01	3.74e-01	3.74e-01	3.74e-01
2^9	3.74e-01	3.73e-01	3.73e-01	3.73e-01	3.73e-01	3.73e-01	3.73e-01
2^{10}	3.74e-01	3.73e-01	3.73e-01	3.73e-01	3.73e-01	3.73e-01	3.73e-01

Table 3.4: $\rho(\Phi)^{N_t}$ for different N_t and N_x for $a = 1$

$N_t \backslash N_x$	16	32	64	128	256	512	1024
2^4	4.68e-04	4.61e-04	4.59e-04	4.59e-04	4.58e-04	4.58e-04	4.58e-04
2^5	1.88e-04	1.85e-04	1.84e-04	1.84e-04	1.84e-04	1.84e-04	1.84e-04
2^6	1.06e-04	1.04e-04	1.03e-04	1.03e-04	1.03e-04	1.03e-04	1.03e-04
2^7	7.65e-05	7.48e-05	7.44e-05	7.43e-05	7.43e-05	7.43e-05	7.43e-05
2^8	6.42e-05	6.27e-05	6.24e-05	6.23e-05	6.23e-05	6.23e-05	6.23e-05
2^9	5.69e-05	5.68e-05	5.68e-05	5.68e-05	5.68e-05	5.68e-05	5.68e-05
2^{10}	5.42e-05	5.42e-05	5.42e-05	5.42e-05	5.42e-05	5.42e-05	5.42e-05

3.1.5 Fourier-Poisson-Kelvin Problem: Diffusion, Convection, and Decay

The analysis of transport phenomena in porous media, particularly the spreading and decay of solutes, is a subject of primary interest dealing with applications that span from environmental engineering to biophysics. The central mathematical model that encompasses these processes is the Fourier-Poisson[7]-Kelvin[8] problem, described by a convection-diffusion-decay equation with prescribed boundary conditions. This model offers a comprehensive context in which to understand the relationship between various components — diffusion, convection (or drift), and decay mechanisms — in the transport of a chemical solute. Consider the equation

$$\frac{\partial u(x,t)}{\partial t} = D\frac{\partial^2 u(x,t)}{\partial x^2} - \nu\frac{\partial u(x,t)}{\partial x} - \lambda u(x,t) + g(x,t), \qquad x \in [0,1], \quad t \in [0,1], \tag{3.45}$$

$$u(0,t) = u(1,t) = 0, \qquad t \in [0,1], \tag{3.46}$$

$$u(x,0) = u(x,1), \qquad x \in [0,1], \tag{3.47}$$

[7]Siméon Denis Poisson (*21 June 1781 in Pithiviers, Kingdom of France; †25 April 1840 in Sceaux, Kingdom of France) was a French mathematician and physicist known for his work on definite integrals, theory of potentials, and for the Poisson equation in electrostatics and fluid dynamics. The Poisson distribution in probability theory also bears his name, reflecting his contributions to the field of mathematical statistics.

[8]William Thomson, 1st Baron Kelvin (26 June 1824 in Belfast, United Kingdom of Great Britain and Ireland; †17 December 1907 in Largs, Scotland, United Kingdom) was a British mathematician, physicist, and engineer, best known for developing the Kelvin scale of temperature. His contributions to thermodynamics, electrical engineering, and hydrodynamics were foundational, and he played a key role in laying the first transatlantic telegraph cable.

Table 3.5: $\rho(\Phi)^{N_t}$ for different N_t and N_x for $a = 10$

$N_t \backslash N_x$	16	32	64	128	256	512	1024
2^4	2.15e-14	2.08e-14	2.06e-14	2.06e-14	2.06e-14	2.06e-14	2.06e-14
2^5	3.01e-20	2.84e-20	2.80e-20	2.79e-20	2.78e-20	2.78e-20	2.78e-20
2^6	1.32e-26	1.20e-26	1.18e-26	1.17e-26	1.17e-26	1.17e-26	1.17e-26
2^7	2.01e-32	1.76e-32	1.70e-32	1.69e-32	1.68e-32	1.68e-32	1.68e-32
2^8	7.01e-37	5.90e-37	5.65e-37	5.59e-37	5.58e-37	5.58e-37	5.57e-37
2^9	8.30e-40	6.80e-40	6.47e-40	6.39e-40	6.37e-40	6.37e-40	6.36e-40
2^{10}	1.60e-41	1.29e-41	1.22e-41	1.20e-41	1.20e-41	1.20e-41	1.20e-41

where u represents the concentration of the solute, dispersion magnitude $D > 0$ quantifies the rate at which, e.g., the solute spreads out from its initial location, accounting for both molecular diffusion and mechanical mixing, drift velocity $\nu > 0$ reflects the average velocity of the solute particles due to convection, driven by external forces like pressure gradients, and decay magnitude $\lambda > 0$ represents the rate of decrease in solute concentration over time, due to processes like chemical reactions, adsorption, or biological decay. The periodicity in time, $u(x,t) = u(x,t+\omega)$, models scenarios where the transport conditions vary in a predictable, periodic manner that may been often observed in natural and industrial processes.

This kind of consideration may be important in, e.g., environmental engineering, groundwater contamination studies, and in design of chemical reactors, where how solute is distributed as a function of time and space is crucial to predicting pollutant impact, designing efficient separation processes, or to or optimizing reaction conditions. We observe that through study of the Fourier-Poisson-Kelvin problem, one may have been seen a rich and very complex set of phenomena that are central to the study of transport processes in porous media — this real-world problem and its mathematical form with prescribed boundary conditions then provide a framework in which one can study how solutes move, spread, and degrade over time, which is highly interesting and a topic that holds promise to study and learn a lot for many scientific and engineering problems.

Exact Solution and Discretization

Given the source term

$$g(x,t) = 2\pi x(x-1)\cos(2\pi t) + (\nu(2x-1) - 2D + \lambda x(x-1))\sin(2\pi t), \tag{3.48}$$

the analytical solution to Equations (3.45)-(3.47) reads

$$u(x,t) = x(x-1)\sin(2\pi t). \tag{3.49}$$

From this point we then proceed analogously as in the case of the heat equation and calculate the tridiagonal matrix

$$M = \text{tridiag}\left[-Dr - \nu p,\ 1 + 2Dr + \lambda\Delta t,\ -Dr + \nu p\right], \tag{3.50}$$

where $r := \frac{\Delta t}{\Delta x^2}$ and $p := \frac{\Delta t}{2\Delta x}$.

Numerical Analysis Verification

The evaluation of error, represented by $\max_{j,i} |u(x_j, t_i) - u_{j,i}|$, targets the highest absolute discrepancy within the spatial-temporal domain. Demonstrated in Table 3.6, this approach benchmarks the numerical approximation $u_{j,i}$ against the exact solution $u(x_j, t_i)$ at each coordinate (x_j, t_i) — computations continue iteratively until achieving convergence, followed by a comparative analysis with the analytical solution.

Table 3.6: EW error reduction for diagonal $N_t = N_x$ and different parameters $D = \nu = \lambda$

$N_t = N_x$	$D = \nu = \lambda = 0.1$	$D = \nu = \lambda = 1$	$D = \nu = \lambda = 10$
$2^4 = 16$	4.70e-02	2.27e-02	2.78e-03
$2^5 = 32$	2.42e-02	1.20e-02	1.42e-03
$2^6 = 64$	1.22e-02	6.13e-03	7.16e-04
$2^7 = 128$	6.13e-03	3.10e-03	3.59e-04
$2^8 = 256$	3.07e-03	1.56e-03	1.80e-04
$2^9 = 512$	1.54e-03	7.81e-04	8.98e-05
$2^{10} = 1024$	7.70e-04	3.91e-04	4.49e-05

Numerical Convergence Factors

This section presents the numerical convergence factors of the EW scheme, as shown in Table 3.7, applied to the convection-diffusion-decay equation — this application employs FD methods for spatial discretization and BE methods for time-stepping, particularly in scenarios where $N_t = N_x$. The table provides the convergence factors for scenarios with $N_t = N_x$, spanning from 2^4 to 2^{10}.

Table 3.7: EW numerical convergence factors for diagonal $N_t = N_x$ and different parameters $D = \nu = \lambda$

$N_t = N_x$	$D = \nu = \lambda = 0.1$	$D = \nu = \lambda = 1$	$D = \nu = \lambda = 10$
$2^4 = 16$	3.42e-01	2.20e-04	4.11e-15
$2^5 = 32$	3.36e-01	7.21e-05	1.53e-21
$2^6 = 64$	3.32e-01	3.53e-05	1.03e-28
$2^7 = 128$	3.30e-01	2.34e-05	1.75e-35
$2^8 = 256$	3.27e-01	1.87e-05	7.87e-41
$2^9 = 512$	3.33e-01	1.67e-05	1.99e-44
$2^{10} = 1024$	3.40e-01	1.57e-05	1.43e-46

Numerical Analysis Validation

This segment details Tables 3.8-3.10, showcasing the principal eigenvalues of the inverse matrices M derived from the discretization of the $1D$+$1D$ advection-diffusion-decay equation. Utilizing FD methods for spatial discretization and BE methods for temporal propagation, the discretization spans various N_t and N_x values, each as power of two, from 2^4 to 2^{10}. In line with Theorem 3.2, it is demonstrated that our approach to the advection-diffusion-decay equation attains convergence, characterized by a convergence factor $\rho(\Phi^{N_t})$ — the tables reveal the maximal eigenvalues for every N_t and N_x pair, indicating the numerical scheme's stability and precision.

Table 3.8: $\rho(\Phi)^{N_t}$ for different N_t and N_x for $D = \nu = \lambda = 0.1$

$N_t \backslash N_x$	16	32	64	128	256	512	1024
2^4	3.85e-01	3.84e-01	3.84e-01	3.84e-01	3.84e-01	3.84e-01	3.84e-01
2^5	3.79e-01	3.79e-01	3.78e-01	3.78e-01	3.78e-01	3.78e-01	3.78e-01
2^6	3.77e-01	3.76e-01	3.76e-01	3.76e-01	3.76e-01	3.76e-01	3.76e-01
2^7	3.75e-01	3.74e-01	3.74e-01	3.74e-01	3.74e-01	3.74e-01	3.74e-01
2^8	3.75e-01	3.74e-01	3.74e-01	3.74e-01	3.74e-01	3.74e-01	3.74e-01
2^9	3.74e-01	3.73e-01	3.73e-01	3.73e-01	3.73e-01	3.73e-01	3.73e-01
2^{10}	3.74e-01	3.73e-01	3.73e-01	3.73e-01	3.73e-01	3.73e-01	3.73e-01

Table 3.9: $\rho(\Phi)^{N_t}$ for different N_t and N_x for $D = \nu = \lambda = 1$

$N_t \backslash N_x$	16	32	64	128	256	512	1024
2^4	4.68e-04	4.61e-04	4.59e-04	4.59e-04	4.58e-04	4.58e-04	4.58e-04
2^5	1.88e-04	1.85e-04	1.84e-04	1.84e-04	1.84e-04	1.84e-04	1.84e-04
2^6	1.06e-04	1.04e-04	1.03e-04	1.03e-04	1.03e-04	1.03e-04	1.03e-04
2^7	7.65e-05	7.48e-05	7.44e-05	7.43e-05	7.43e-05	7.43e-05	7.43e-05
2^8	6.42e-05	6.27e-05	6.24e-05	6.23e-05	6.23e-05	6.23e-05	6.23e-05
2^9	5.86e-05	5.73e-05	5.69e-05	5.68e-05	5.68e-05	5.68e-05	5.68e-05
2^{10}	5.60e-05	5.47e-05	5.43e-05	5.42e-05	5.42e-05	5.42e-05	5.42e-05

Table 3.10: $\rho(\Phi)^{N_t}$ for different N_t and N_x for $D = \nu = \lambda = 10$

$N_t \backslash N_x$	16	32	64	128	256	512	1024
2^4	2.15e-14	2.08e-14	2.06e-14	2.06e-14	2.06e-14	2.06e-14	2.06e-14
2^5	3.01e-20	2.84e-20	2.80e-20	2.79e-20	2.78e-20	2.78e-20	2.78e-20
2^6	1.32e-26	1.20e-26	1.18e-26	1.17e-26	1.17e-26	1.17e-26	1.17e-26
2^7	2.01e-32	1.76e-32	1.70e-32	1.69e-32	1.68e-32	1.68e-32	1.68e-32
2^8	7.01e-37	5.90e-37	5.65e-37	5.59e-37	5.58e-37	5.58e-37	5.57e-37
2^9	8.30e-40	6.80e-40	6.47e-40	6.39e-40	6.37e-40	6.37e-40	6.36e-40
2^{10}	1.60e-41	1.29e-41	1.22e-41	1.20e-41	1.20e-41	1.20e-41	1.20e-41

3.1.6 Wave Equation

The wave equation is a fundamental concept in physics and engineering, providing principles that govern waves. It is a second-order partial differential equation that is used to model the behavior of many different types of waves, which include acoustic, elastic, and electromagnetic waves that travel through materials. The inhomogeneous wave equation model adds an extra layer of complexity in that it considers external forces of the media and includes how they would affect the behavior of the wave. This equation has substantial implications in fields as diverse as geophysics, where it underpins seismic exploration, to medical science, where it informs imaging technologies. Jean-Baptiste le Rond d'Alembert[9] studied the model of a vibrating string in his seminal book from 1747 [17], for an introduction see, e.g., [48, Section 1.6]. The inhomogeneous wave equation is central to the study of wave propagation, explained by a second-order hyperbolic partial differential equation, it also captures the fact that waves propagate at finite speeds. It represents real-world wave phenomena including reflection, refraction, and diffraction. There are a couple of options for the boundary conditions and we will consider the Dirichlet[10] boundary conditions in this work. We want to investigate the behavior of the wave at the edges of an area where the wave is confined, a box in our case, i.e., the Dirichlet boundary condition includes holding the wave function fixed at the boundaries, simulating the behavior of the wave that is confined in a certain space. Multi-level iterative methods, including multi-grid algorithms, have demonstrated some effectiveness as for solving such equation [69, 112] — these methods utilize the principles of hierarchical problem solving to accelerate convergence to a solution, knowingly outperforming classical iterative approaches in both speed and efficiency, however, they are also struggling

[9] Jean-Baptiste le Rond d'Alembert (*16 November 1717 in Paris, Kingdom of France; †29 October 1783 in Paris, Kingdom of France) was a French mathematician, mechanician, physicist, philosopher, and music theorist. He is widely recognized for his contributions to the development of mathematical physics, especially in fluid dynamics, wave theory, and celestial mechanics.

[10] Johann Peter Gustav Lejeune Dirichlet (*13 February 1805 in Düren, Rhine Province, Kingdom of Prussia; †5 May 1859 in Göttingen, Kingdom of Hanover) was a German mathematician who made profound contributions to number theory, analysis, and mathematical physics. He is best known for his rigour in analysis, and for Dirichlet series that are pivotal in analytic number theory.

with selection of an appropriate coarse-grid operator for these problems [20]. Some diagonalization-based technique were proposed to overcome the poor convergence: block circulant preconditioning [88] and block $\epsilon-$circulant preconditioning [82]; introducing a weight parameter ϵ, one gets independent convergence for spatial mesh-size and time-step width, but still depends on the assumption to use the same linear time integrator for all steps.

This section is motivated by the desire to optimize multi-grid algorithms, tailoring them to reach faster rates of convergence without sacrificing the stringency of requirements due to and the demands of real-world applications. The challenges posed by the wave equation are diverse, the underlying character of the equation can cause solutions to contain discontinuities even when the initial data is smooth, which requires the careful numerical treatment given the inherent hyperbolic character of the equation. Analytic methods are limited in the face of the complexity of the wave equation, particularly in the presence of inhomogeneous conditions and non-trivial geometries. This makes computational approaches valuable, as they offer both the precision and adaptability required, especially when analytical approaches are insufficiently effective. For dealing with computational difficulties that appear in solving hyperbolic PDEs, this study looks for robust solutions, focusing on the necessary discretization techniques that convert the continuous mathematical model into a form that is computationally executable. We are most interested in the stability and accuracy of the iterative scheme over the computational domain, which is necessary due to the hyperbolic nature of the equation and the prescribed inhomogeneity. This search for efficient computational solutions to the inhomogeneous wave equation has implications that can be far-reaching and practical — having an understanding and being able to accurately model the wave propagation is necessary for interpreting data in seismic exploration, for optimizing the architectural acoustic design, and in medical imaging for diagnostic capabilities; this requires that one can solve the wave equation accurately and efficiently since understanding both the theory and the application in an accurate and efficient way will have extensive influence in the advancement of technology and in how well we understand the natural world.

Exact Solution and Discretization

Given the wave equation in a one-dimensional domain,

$$\frac{\partial^2 u}{\partial t^2} - c^2 \frac{\partial^2 u}{\partial x^2} = g(x,t), \tag{3.51}$$

where c is the wave speed, $u(x,t)$ is the wave function, and $g(x,t)$ is the source term. The specific case study within this research considers a form of inhomogeneity shaped by a sinusoidal forcing function

$$g(x,t) = (4c^2\pi - 16\pi^2)\sin(4\pi t)\sin(2\pi x), \tag{3.52}$$

which corresponds to a wave influenced by an external force oscillating in both space and time. This choice is reflective of scenarios where waves are generated or disturbed by periodic forces, common in various physical and engineering contexts. The analytical solution in this case is given by

$$u(x,t) = \sin(4\pi t)\sin(2\pi x). \tag{3.53}$$

Step 1: Discretize the Temporal Derivative

Using a central difference approximation for the second derivative in time, we get

$$\frac{\partial^2 u}{\partial t^2} \approx \frac{u^{n+1} - 2u^n + u^{n-1}}{\Delta t^2}, \tag{3.54}$$

where Δt is the time step size.

Step 2: Discretize the Spatial Derivative

Applying a central difference approximation for the spatial second derivative, we have

$$\frac{\partial^2 u}{\partial x^2} \approx \frac{u_{i+1} - 2u_i + u_{i-1}}{\Delta x^2}, \tag{3.55}$$

where Δx is the spatial step size.

Combining These Approximations

We combine the temporal and spatial discretizations into the wave equation, ensuring to keep the time step consistent across both discretizations for u^{n+1}

$$\frac{u_i^{n+1} - 2u_i^n + u_i^{n-1}}{\Delta t^2} = c^2 \frac{u_{i+1}^{n+1} - 2u_i^{n+1} + u_{i-1}^{n+1}}{\Delta x^2} + g(x_i, t_n). \tag{3.56}$$

Again, such equation forms the basis for constructing an implicit method leading to a linear system that can be solved for u_i^{n+1}, the wave function at all spatial points i at the next time step $n+1$, using EW method. To arrange this into a solvable system, we recognize that the left-hand side involves a temporal difference that relates three consecutive time steps, and the right-hand side represents a spatial operator acting on the state at the next time step. Rearranging the equation to isolate terms involving u^{n+1} gives us

$$-c^2\frac{\Delta t^2}{\Delta x^2}u_{i-1}^{n+1}+\left(1+2c^2\frac{\Delta t^2}{\Delta x^2}\right)u_i^{n+1}-c^2\frac{\Delta t^2}{\Delta x^2}u_{i+1}^{n+1}=2u_i^n-u_i^{n-1}+\Delta t^2 g(x_i,t_n). \tag{3.57}$$

This can be represented in matrix form as $M\mathbf{u}^{n+1}=2\mathbf{u}^n-\mathbf{u}^{n-1}+\mathbf{b}$, where M is the tridiagonal matrix constructed from the coefficients of u_i^{n+1} and its spatial neighbours, and **b** is the vector on the right-hand side incorporating the source term.

Step 3: Matrix Construction

Defining $w \coloneqq \left(\frac{\Delta t}{\Delta x}\right)^2$ and rearranging the equation to solve for u_{n+1}, we construct the matrix equation for the system. The matrix M embody the spatial and time discretization — the construction of M involves setting up a tridiagonal matrix where the central diagonal is modified to account for the wave equation's discretized form

$$M=\text{triadiag}\left[-c^2\cdot w,\ (1+2c^2\cdot w),\ -c^2\cdot w\right]. \tag{3.58}$$

As the matrix Φ was defined earlier, $\Phi=M^{-1}$, we now construct the 2×2-block time-stepping matrix Ψ using the following operations [33], as the time discretization in Equation (3.57) uses two previous time points, i.e., we are dealing with two-step method

- The top-left block is $-\Phi$,
- The top-right block is -2Φ,
- The bottom-left block is $2\Phi^2$,
- The bottom-right block is $4\Phi^2-\Phi$.

Thus, the matrix Ψ is constructed as

$$\Psi=\begin{bmatrix}-\Phi & -2\Phi\\ 2\Phi^2 & 4\Phi^2-\Phi\end{bmatrix}, \tag{3.59}$$

and we have

$$\begin{aligned}\mathbf{w}_n &= \begin{bmatrix} u_{2n} \\ u_{2n+1} \end{bmatrix} \\ &= \begin{bmatrix} \Phi_{2n}\left(u_{2n-1}, u_{2n-2}\right) + b_{2n} \\ \Phi_{2n+1}\left(\Phi_{2n}\left(u_{2n-1}, u_{2n-2}\right) + b_{2n}, u_{2n-1}\right) + b_{2n+1} \end{bmatrix} \\ &= \Psi_n \left(\begin{bmatrix} u_{2n-2} \\ u_{2n-1} \end{bmatrix} \right) + \begin{bmatrix} b_{2n} \\ b_{2n+1} \end{bmatrix} = \Psi\left(\mathbf{w}_n\right) + \mathbf{b}_n,\end{aligned} \tag{3.60}$$

so the EW iteration matrix Q^{wave} is given by

$$Q^{wave} = \begin{pmatrix} & \Psi & \\ & \Psi^2 & \\ & \Psi^3 & \\ & \vdots & \\ & \Psi^{N_t/2} & \end{pmatrix}. \tag{3.61}$$

Numerical Analysis Verification

The error metric $\max_{j,i} |u(x_j, t_i) - u_i^j|$ centers on identifying the peak absolute deviation throughout the spatial-temporal domain. Demonstrated in Table 3.11, it contrasts the exact solution $u(x_j, t_i)$ with the numerical solution u_i^j at the grid locations (x_j, t_i) — calculations proceed until convergence is reached, after which they are evaluated against the analytical solution.

Table 3.11: EW error reduction for diagonal $N_t = N_x$ and different parameters c

$N_t = N_x$	c = 1	c = 10	c = 100
$2^4 = 16$	2.07e-01	7.35e-01	7.16e-01
$2^5 = 32$	1.23e-01	3.98e-01	3.84e-01
$2^6 = 64$	6.44e-02	2.03e-01	1.95e-01
$2^7 = 128$	3.26e-02	1.02e-01	9.81e-02
$2^8 = 256$	1.63e-02	5.11e-02	4.91e-02
$2^9 = 512$	8.18e-03	2.56e-02	2.46e-02
$2^{10} = 1024$	4.09e-03	1.28e-02	1.23e-02

Numerical Convergence Factors

In this section, we also elucidate the numerical convergence factors associated with the EW scheme, indicated in Table 3.12 for the wave equation — this involves the use of FD method for spatial discretization and BE method for temporal advancement, with a focus on cases where $N_t = N_x$. Below, the table details the convergence factors across each matching condition of $N_t = N_x$, with values from 2^4 to 2^{10}.

Table 3.12: EW numerical convergence factors of EW for diagonal $N_t = N_x$ and different parameters c

$N_t = N_x$	c = 1	c = 10	c = 100
$2^4 = 16$	7.40e-01	5.00e-05	2.12e-21
$2^5 = 32$	8.68e-01	2.77e-04	2.07e-32
$2^6 = 64$	9.31e-01	9.79e-04	2.10e-45
$2^7 = 128$	9.65e-01	3.21e-02	3.35e-55
$2^8 = 256$	9.83e-01	1.12e-01	5.81e-52
$2^9 = 512$	9.91e-01	3.88e-01	3.05e-36
$2^{10} = 1024$	9.96e-01	6.27e-01	9.23e-21

Numerical Analysis Validation

This section introduces Tables 3.13-3.15, featuring the maximal eigenvalues of the inverse matrices M, resulting from discretizing the $1D$+$1D$ wave equation. The discretization process, incorporating FD method in spatial dimensions and BE method in temporal dimension, accommodates a range of N_t and N_x values — these values extend as powers of two from 2^4 to 2^{10}. Conforming to Theorem 3.2, the wave equation's approach is confirmed to converge, marked by a convergence factor $\rho\left(\Psi^{\frac{N_t}{2}}\right)$. Subsequent tables catalogue the peak eigenvalues for each N_t and N_x configuration, underlining the employed numerical scheme's stability and accuracy.

Table 3.13: $\rho\left(\Psi^{\frac{N_t}{2}}\right)$ for different N_t and N_x and $c = 1$

$N_t \backslash N_x$	16	32	64	128	256	512	1024
2^4	7.40e-1	7.39e-1	7.39e-1	7.39e-1	7.39e-1	7.39e-1	7.39e-1
2^5	8.58e-1	8.58e-1	8.58e-1	8.58e-1	8.58e-1	8.58e-1	8.58e-1
2^6	9.26e-1	9.26e-1	9.26e-1	9.26e-1	9.26e-1	9.26e-1	9.26e-1
2^7	9.62e-1	9.62e-1	9.62e-1	9.62e-1	9.62e-1	9.62e-1	9.62e-1
2^8	9.81e-1	9.81e-1	9.81e-1	9.81e-1	9.81e-1	9.81e-1	9.81e-1
2^9	9.90e-1	9.90e-1	9.90e-1	9.90e-1	9.90e-1	9.90e-1	9.90e-1
2^{10}	9.95e-1	9.95e-1	9.95e-1	9.95e-1	9.95e-1	9.95e-1	9.95e-1

Table 3.14: $\rho\left(\Psi^{\frac{N_t}{2}}\right)$ for different N_t and N_x and $c = 10$

$N_t \backslash N_x$	16	32	64	128	256	512	1024
2^4	3.30e-06	3.25e-06	3.24e-06	3.24e-06	3.24e-06	3.24e-06	3.24e-06
2^5	2.10e-05	2.06e-05	2.05e-05	2.04e-05	2.04e-05	2.04e-05	2.04e-05
2^6	1.02e-03	1.00e-03	1.00e-03	1.00e-03	1.00e-03	1.00e-03	1.00e-03
2^7	2.39e-02	2.37e-02	2.37e-02	2.37e-02	2.37e-02	2.37e-02	2.37e-02
2^8	1.48e-01	1.48e-01	1.48e-01	1.48e-01	1.48e-01	1.48e-01	1.48e-01
2^9	3.83e-01	3.82e-01	3.82e-01	3.82e-01	3.82e-01	3.82e-01	3.82e-01
2^{10}	6.19e-01	6.18e-01	6.18e-01	6.18e-01	6.18e-01	6.18e-01	6.18e-01

Table 3.15: $\rho\left(\Psi^{\frac{N_t}{2}}\right)$ for different N_t and N_x and $c = 100$

$N_t \backslash N_x$	16	32	64	128	256	512	1024
2^4	2.06e-21	2.02e-21	2.01e-21	2.01e-21	2.01e-21	2.01e-21	2.01e-21
2^5	1.61e-32	1.55e-32	1.53e-32	1.53e-32	1.53e-32	1.53e-32	1.53e-32
2^6	1.80e-45	1.67e-45	1.64e-45	1.63e-45	1.63e-45	1.63e-45	1.63e-45
2^7	7.86e-55	6.89e-55	6.66e-55	6.61e-55	6.59e-55	6.59e-55	6.59e-55
2^8	1.09e-51	9.07e-52	8.66e-52	8.56e-52	8.54e-52	8.53e-52	8.53e-52
2^9	3.73e-36	3.15e-36	3.02e-36	2.99e-36	2.98e-36	2.98e-36	2.98e-36
2^{10}	1.15e-20	1.03e-20	1.00e-20	9.98e-21	9.96e-21	9.95e-21	9.95e-21

3.2 Excursus on QMGRIT

Going from the EW scheme, we construct a novel multi-level algorithm QMGRIT consisting of the following seven steps corresponding to the MGRIT construction, as we observe in the Figures 3.2-3.3.

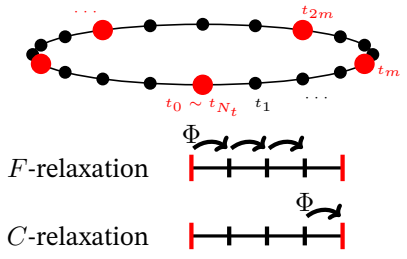

Figure 3.2: FCF-Smoothing construction with F-Points (black) and C-Points (red), F-relaxation and C-relaxation illustrated

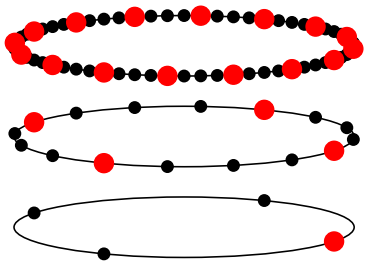

Figure 3.3: QMGRIT construction, illustrating a three-grid example with given parameter of $N_t = 64$ and coarsening factor $m = 4$

1. **Initialization:**

   - Set the number of time points to $N_t = 2^n$, the coarsening factor to $m = 2^{\alpha_m}$, and the number of levels to L = 2, firstly.
   - Partition the time points into C-Points and F-Points, such that for each set of m neighbouring points, there are $m - 1$ F-Points and one C-Point.

- Assume the first time point is a C-Point for simplicity, the number of C-Points is given by $N_c = \frac{N_t}{m}$.

2. **Fine-grid relaxation:**

   - Perform F-relaxation updating solution at F-Points using the previous time point and Φ.
   - Perform CF-relaxation for a specified number of iterations (ν):
     - Update the first C-Point using the last F-Point and Φ.
     - Update the remaining C-Points using the previous time point and Φ.
     - Perform F-relaxation within each C-relaxation iteration to update the solution at F-Points.

3. **Residual computation:**

   - Compute the residual at the first C-Point using the last F-point, Φ, and the current solution.
   - Compute the residual at the remaining C-Points using the previous C-Point, Φ, and the current solution.

4. **Coarse-grid solve:**

   - Perform γ EW iterations on the residual equation of the coarse-grid solve at the coarsest grid level, Update the time points using the time integration operator Φ_c.

5. **Coarse-grid correction:**

   - Correct the approximation at C-Points using the coarse-grid correction obtained from the coarse-grid solve.
   - Perform F-relaxation to correct the approximation at F-Points using the previous time point and Φ.

6. **Iteration:**

   - Repeat steps 2-5 until a desired level of convergence is achieved or a maximum number of iterations is reached.

7. **Return:**

   - Return the updated solution and residual.

This explicit representation of the QMGRIT algorithm focuses on the two-grid case and provides a high-level overview of the key components involved. The algorithm starts with initialization, where the time points are partitioned into C-Points and F-Points. It then proceeds with the fine-grid relaxation, residual computation, coarse-grid solve, and coarse-grid correction steps — these steps are iteratively repeated until convergence or a maximum number of iterations is reached. Finally, the updated solution and residual are returned. Furthermore, to obtain a multilevel method with L levels apply the algorithm recursively L-1 times in step 4. We write the resulting multi-grid algorithm as follows in Algorithm 2, and refer to the prototyping implementation in [5]. If problem in Equation

Algorithm 2 γ-**QMGRIT**-$\nu[A_p^{(\cdot)}, \mathbf{u}^{(\cdot)}, \mathbf{b}_p^{(\cdot)}](l+1)$:

if l is the coarsest level, L **then** smooth γ-times the coarse-system with EW iteration.
else
1. Relax on $A_p^{(l)}\mathbf{u}^{(l)} = \mathbf{b}_p^{(l)}$ using $F(CF)^\nu$-relaxations.
2. Compute and restrict residual using injection,

$$\mathbf{b}_p^{(l+1)} = R_I\left(\mathbf{b}_p^{(l)} - A_p^{(l)}\mathbf{u}^{(l)}\right)$$

3. Solve on next level: γ-**QMGRIT**-ν $[A_p^{(l+1)}, \mathbf{u}^{(l+1)}, \mathbf{b}_p^{(l+1)}]$.
3. Correct using 'ideal' interpolation, $\mathbf{u}^{(l)} \leftarrow \mathbf{u}^{(l)} + P\mathbf{u}^{(l+1)}$.
end if

(3.1) is nonlinear, QMGRIT scheme can be generalized with the Full Approximation Storage (FAS) scheme [10] in Algorithm 3. The key idea of FAS is the method it uses to solve nonlinear equations

Algorithm 3 γ-**QMGRIT**-ν **FAS**$[A_p^{(\cdot)}, \mathbf{u}^{(\cdot)}, \mathbf{b}_p^{(\cdot)}](l+1)$:

if l is the coarsest level, L **then** smooth γ-times the coarse-system with EW iteration.
else
1. Relax on $A_p^{(l)}\mathbf{u}^{(l)} = \mathbf{b}_p^{(l)}$ using $F(CF)^\nu$-relaxations.
2. Compute and restrict residual using injection,

$$\mathbf{b}_p^{(l+1)} = R\left(\mathbf{b}_p^{(l)} - A_p^{(l)}\mathbf{u}^{(l)}\right)$$

3. Solve on next level: γ-**QMGRIT**-ν **FAS**$[A_p^{(l+1)}, \mathbf{v}^{(l+1)}, A_p^{(l+1)}\left(R_I\mathbf{u}^{(l)}\right) + \mathbf{b}_p^{(l+1)}]$.
3. Correct using 'ideal' interpolation, $\mathbf{u}^{(l)} \leftarrow \mathbf{u}^{(l)} + P\left(\mathbf{v}^{(l+1)} - R_I\mathbf{u}^{(l)}\right)$.
end if

using multi-grid methods — as opposed to linear multi-grid approaches, FAS moves the solution as well as the residual to and from the coarse grid via restriction and prolongation operators; FAS can effectively resolve the nonlinear problem because FAS is dealing with the full nonlinear equation on all grid levels. By solving the coarse grid equation involving the restricted solution and the restricted

residual and interpolating the correction term back to the fine grid, a global correction to the solution is given on the finer grid.

3.2.1 Excursus to the Spectral Analysis of QMGRIT

The next step is to examine the iteration operators and analyze the two-grid structure. We consider A_p in block-form

$$A_p = \begin{pmatrix} A_{ff} & A_{fc} \\ A_{cf} & A_{cc} \end{pmatrix} \in \mathbb{R}^{N_t(N_x+1)\times N_t(N_x+1)}, \tag{3.62}$$

with

$$A_{ff} = \begin{pmatrix} \mathbb{I} & & & & & & & \\ -\Phi & \mathbb{I} & & & & & & \\ & \ddots & \ddots & & & & & \\ & & -\Phi & \mathbb{I} & & & & \\ & & & & \ddots & & & \\ & & & & & \mathbb{I} & & \\ & & & & & -\Phi & \mathbb{I} & \\ & & & & & & \ddots & \ddots \\ & & & & & & & -\Phi \quad \mathbb{I} \end{pmatrix}, \qquad A_{fc} = \begin{pmatrix} -\Phi & & \\ 0 & & \\ \vdots & & \\ 0 & & \\ & \ddots & \\ & & -\Phi \\ & & 0 \\ & & \vdots \\ & & 0 \end{pmatrix}, \tag{3.63}$$

$$A_{cf} = \begin{pmatrix} 0 & \dots & 0 & 0 & & & & & 0 & \dots & 0 & -\Phi \\ 0 & \dots & 0 & -\Phi & 0 & \dots & 0 & 0 & & & & \\ & & & & \ddots & & & & \ddots & & & \\ & & & & & 0 & \dots & 0 & -\Phi & 0 & \dots & 0 \quad 0 \end{pmatrix}. \tag{3.64}$$

It follows

$$A_p = \begin{pmatrix} \mathbb{I}_f & 0 \\ A_{cf}A_{ff}^{-1} & \mathbb{I}_c \end{pmatrix} \begin{pmatrix} A_{ff} & 0 \\ 0 & A_{cc} - A_{cf}A_{ff}^{-1}A_{fc} \end{pmatrix} \begin{pmatrix} \mathbb{I}_f & A_{ff}^{-1}A_{fc} \\ 0 & \mathbb{I}_c \end{pmatrix} \tag{3.65}$$

and

$$A_p^{-1} = \begin{pmatrix} \mathbb{I}_f & -A_{ff}^{-1}A_{fc} \\ 0 & \mathbb{I}_c \end{pmatrix} \begin{pmatrix} A_{ff}^{-1} & 0 \\ 0 & A_\Delta^{-1} \end{pmatrix} \begin{pmatrix} \mathbb{I}_f & 0 \\ -A_{cf}A_{ff}^{-1} & \mathbb{I}_c \end{pmatrix}, \tag{3.66}$$

with periodic Schur complement

$$A_\Delta \coloneqq A_{cc} - A_{cf}A_{ff}^{-1}A_{fc} = \begin{pmatrix} \mathbb{I} & & & & -\Phi^m \\ -\Phi^m & \mathbb{I} & & & \\ & -\Phi^m & \mathbb{I} & & \\ & & \ddots & \ddots & \\ & & & -\Phi^m & \mathbb{I} \end{pmatrix}. \tag{3.67}$$

We note the 'ideal' restriction operator

$$R_{ideal} \coloneqq \begin{pmatrix} -A_{cf}A_{ff}^{-1} & \mathbb{I}_c \end{pmatrix} \tag{3.68}$$

$$= \left(\begin{array}{ccccccccc|c} 0 & \dots & 0 & & & & \Phi^{m-1} & \dots & \Phi & \\ \Phi^{m-1} & \dots & \Phi & 0 & \dots & 0 & & & & \\ & & & & & & & & & \\ & & & \ddots & & & \ddots & & & \mathbb{I}_c \\ & & & & \Phi^{m-1} & \dots & \Phi & 0 & \dots & 0 \end{array}\right). \tag{3.69}$$

Then, the QMGRIT restriction operator is given by

$$R_I \coloneqq \begin{pmatrix} 0 & \mathbb{I}_c \end{pmatrix} \in \mathbb{R}^{(N_x+1)N_t/m \times (N_x+1)N_t}, \tag{3.70}$$

and the QMGRIT 'ideal' prolongation operator is given by

$$P \coloneqq \begin{pmatrix} -A_{ff}^{-1}A_{fc} \\ \mathbb{I}_c \end{pmatrix} = \left(\begin{array}{ccc} \Phi & & \\ \vdots & & \\ \Phi^{m-1} & & \\ & \ddots & \\ & & \Phi \\ & & \vdots \\ & & \Phi^{m-1} \\ \hline & & \\ & \mathbb{I}_c & \\ & & \end{array}\right) \in \mathbb{R}^{(N_x+1)N_t \times (N_x+1)^{N_t/m}}. \tag{3.71}$$

We write the iteration operator of the two-grid γ-QMGRIT-1 algorithm as

$$P(\mathbb{I}_c - A_c^{-1}A_\Delta)^\gamma(\mathbb{I}_c - A_\Delta)^1 R_I, \tag{3.72}$$

and analyze the action of the parameters $\mathbb{N} \ni \gamma,\ \nu \geq 0,\ \kappa > 0$, within the operator

$$Q(\gamma,\nu,\kappa) \coloneqq \left(P\left(\mathbb{I}_c - A_c^{-1}A_\Delta\right)^\gamma \left(\mathbb{I}_c - A_\Delta\right)^\nu R_I\right)^\kappa, \tag{3.73}$$

where A_c is the *initial value system* re-discretization of corresponding size and A_Δ is the *periodic* Schur complement.

Remark 3.6. *Before stating an analytical result, we may explicitly clarify the difference between MGRIT (see Section 2.5.1) and QMGRIT. As we have one fewer C-Point (in our construction, the last one) for QMGRIT, we efficiently demonstrate this difference by providing the explicit form of the restriction and prolongation operators, i.e., working with the generic linear equation $A\mathbf{u} = \mathbf{b}$ without reordering into the*

block-form. For MGRIT, we have

$$P = \begin{pmatrix} \mathbb{I} & & & & \\ \Phi & & & & \\ \vdots & & & & \\ \Phi^{m-1} & & & & \\ & \ddots & & & \\ & & \mathbb{I} & & \\ & & \Phi & & \\ & & \vdots & & \\ & & \Phi^{m-1} & & \\ & & & \mathbb{I} & \end{pmatrix} \text{ and } R_I = \begin{pmatrix} \mathbb{I} & & & & & & & & \\ & 0 & \cdots & 0 & \mathbb{I} & & & & \\ & & & & \ddots & & & & \\ & & & & & 0 & \cdots & 0 & \mathbb{I} \end{pmatrix}. \tag{3.74}$$

For QMGRIT we have

$$P = \begin{pmatrix} \mathbb{I} & & & & \\ \Phi & & & & \\ \vdots & & & & \\ \Phi^{m-1} & & & & \\ & \ddots & & & \\ & & \mathbb{I} & & \\ & & \Phi & & \\ & & \vdots & & \\ & & \Phi^{m-1} & & \end{pmatrix} \text{ and } R_I = \begin{pmatrix} \mathbb{I} & 0 & \dots & 0 & & & & & & & & \\ & & & & \mathbb{I} & 0 & \dots & 0 & & & & \\ & & & & & & & & \ddots & & & \\ & & & & & & & & & \mathbb{I} & 0 & \dots & 0 \end{pmatrix}. \tag{3.75}$$

Theorem 3.7. *For the grounded $dD{+}1D$ heat equation, the linear iterative error system $v^{j+1} = Q(1,\nu,\kappa)v^j$ has asymptotically stable zero solution. For $\nu = qN_c - 1$, with $\mathbb{N} \ni q \geq 1$, the order of convergence is given by*

$$\rho(Q(1,\nu,\kappa)) = \max\left\{\rho\left(\Phi^{\kappa(\nu+1)m}\right), \rho\left(\left(\Phi^m - \Phi_c\right)^\kappa \Phi^{\kappa\nu m}\right)\right\} < 1. \tag{3.76}$$

Proof. Firstly, with $\gamma = 0,\ \kappa = 1,\ \nu = 0$ we have the F-relaxation as operator $Q(0,0,1)$. The matrices

$$P\left(\mathbb{I}_c - A_\Delta\right)^\nu R_I = Q(0,\nu,1) \tag{3.77}$$

describe the two-grid 0-QMGRIT-ν, where

$$Q(0,1,1) = \begin{pmatrix} & & & & & & \Phi^m \\ & & & & & & \vdots \\ & & & & & & \Phi^{2m-1} \\ \Phi^m & & & & & & \\ \vdots & & & & & & \\ \Phi^{2m-1} & & & & & & \\ & & \ddots & & & & \\ & & & & \Phi^m & & \\ & & & & \vdots & & \\ & & & & \Phi^{2m-1} & & \end{pmatrix} \tag{3.78}$$

and

$$Q(0,\nu,1) = \begin{pmatrix} \Phi^{\nu m} & & & & & & \\ \vdots & & & & & & \\ \Phi^{\nu m+m-1} & & & & & & \\ & \ddots & & & & & \\ & & \ddots & & & & \\ & & & & \Phi^{\nu m} & & \\ & & & & \vdots & & \\ & & & & \Phi^{\nu m+m-1} & & \end{pmatrix} \tag{3.79}$$

for all $\nu \equiv qN_c$, with $\mathbb{N} \ni q \geq 1$. We define

$$B_x^y := \begin{pmatrix} \Phi^y \Phi_c^x & 0 & \dots & 0 \\ \vdots & \vdots & \vdots & \vdots \\ \Phi^{y+m-1}\Phi_c^x & 0 & \dots & 0 \end{pmatrix} \in \mathbb{R}^{(N_x+1)m \times (N_x+1)m} \tag{3.80}$$

and

$$\bar{B}_x^y := \begin{pmatrix} \left(\Phi^m - \Phi_c\right)\Phi^y\Phi_c^x & 0 & \dots & 0 \\ \vdots & \vdots & \vdots & \vdots \\ \left(\Phi^m - \Phi_c\right)\Phi^{y+m-1}\Phi_c^x & 0 & \dots & 0 \end{pmatrix} \in \mathbb{R}^{(N_x+1)m\times(N_x+1)m}. \tag{3.81}$$

Secondly, let $\gamma = \kappa = 1$. Then for $\nu = 0$ we can write the coarse-grid correction procedure with the EW scheme and F-relaxation as

$$Q(1,0,1) = \begin{pmatrix} 0 & \dots & \dots & 0 & B_0^m \\ \bar{B}_0^0 & 0 & \dots & 0 & B_1^m \\ \bar{B}_1^0 & \bar{B}_0^0 & \ddots & 0 & B_2^m \\ \vdots & \vdots & \ddots & \vdots & \vdots \\ \bar{B}_{N_c-2}^0 & \bar{B}_{N_c-3}^0 & \dots & \bar{B}_0^0 & B_{N_c-1}^m \end{pmatrix}. \tag{3.82}$$

Thirdly, for all $\nu \equiv qN_c$, with $q \geq 1$, we write

$$Q(1,\nu,1) = \begin{pmatrix} 0 & \dots & \dots & 0 & B_0^{(\nu+1)m} \\ \bar{B}_0^{\nu m} & 0 & \dots & 0 & B_1^{(\nu+1)m} \\ \bar{B}_1^{\nu m} & \bar{B}_0^{\nu m} & \ddots & 0 & B_2^{(\nu+1)m} \\ \vdots & \vdots & \ddots & \vdots & \vdots \\ \bar{B}_{N_c-2}^{\nu m} & \bar{B}_{N_c-3}^{\nu m} & \dots & \bar{B}_0^{\nu m} & B_{N_c-1}^{(\nu+1)m} \end{pmatrix}. \tag{3.83}$$

Let $\gamma = 1$ and $\nu = qN_c - 1$, with $q \geq 1$, for $\kappa \geq 1$, from Equations (3.82) and (3.83) we conclude

$$Q(1,\nu,\kappa) = \begin{pmatrix} B_0^{(\nu+1)m} & 0 & \dots & \dots & 0 \\ B_1^{(\nu+1)m} & \bar{B}_0^{\nu m} & 0 & \dots & 0 \\ B_2^{(\nu+1)m} & \bar{B}_1^{\nu m} & \bar{B}_0^{\nu m} & \ddots & 0 \\ \vdots & \vdots & \vdots & \ddots & \vdots \\ B_{N_c-1}^{(\nu+1)m} & \bar{B}_{N_c-2}^{\nu m} & \bar{B}_{N_c-3}^{\nu m} & \dots & \bar{B}_0^{\nu m} \end{pmatrix}^{\kappa}. \tag{3.84}$$

In consequence of Equation (3.84), for $\nu = qN_c - 1$, with $q \geq 1$, the eigenvalues of $Q(1,\nu,\kappa)$ are equal to zero and to the eigenvalues of $\Phi^{\kappa(\nu+1)m}$ and $\left(\Phi^m - \Phi_c\right)^{\kappa}\Phi^{\kappa\nu m}$. Therefore, we conclude to Equation

(3.76) and

$$\rho(Q(1,\nu,\kappa)) \to 0, \tag{3.85}$$

as $0 \preccurlyeq \Phi_c \preccurlyeq \Phi \preccurlyeq \mathbb{I}$, and ν, m or κ goes to infinity. □

Thus, similar to time-stepping or the EW scheme, two-grid QMGRIT eventually reduces the residual bellow a given tolerance and provides the periodic solution.

The recursive definition of QMGRIT allows us to proceed with the analysis of the three-grids algorithm, additional steps to analyze the multi-grid full algorithm continue in a similar manner. The two-grid iteration matrix for QMGRIT is

$$Q(1,1,1) = \left(\mathbb{I} - P_\Phi A_c^{-1} R_I A_p\right) P_\Phi \left(\mathbb{I} - A_\Delta\right) R_I = P_\Phi \left(\mathbb{I} - A_c^{-1} A_\Delta\right) \left(\mathbb{I} - A_\Delta\right) R_I, \tag{3.86}$$

so for the three-grid iteration matrix we have

$$Q_3(\overset{\gamma}{\overset{\shortparallel}{1}}, \overset{\nu_0}{\overset{\shortparallel}{1}}, \overset{\nu_1}{\overset{\shortparallel}{1}}, \overset{\kappa}{\overset{\shortparallel}{1}}) = \left(\mathbb{I} - P_\Phi \left(\mathbb{I}_c - Q_{2,3}^{FCF}\right) A_{p,c}^{-1} R_I A_p\right) P_\Phi \left(\mathbb{I} - A_\Delta\right) R_I, \tag{3.87}$$

where ν_0 and ν_1 describe the number of CF-smoothing steps on the fine and intermediate grids, respectively, and $Q_{2,3}^{FCF}$ is analogous to Equation (3.86). It is necessary to note that when transitioning from a fine grid to an intermediate one, an approximation of the solution through re-discretization of A_p, $A_{p,c}$ — an approximation to the periodic linear system — is used

$$A_{p,c} = \begin{pmatrix} \mathbb{I} & & & -\Phi_c \\ -\Phi_c & \mathbb{I} & & \\ & \ddots & \ddots & \\ & & -\Phi_c & \mathbb{I} \end{pmatrix} \in \mathbb{R}^{(N_x+1)\frac{N_t}{m_0} \times (N_x+1)\frac{N_t}{m_0}}, \tag{3.88}$$

where m_0 denotes the coarsening factor from the fine grid to the intermediate one. Only when transitioning from the penultimate grid to the coarsest grid, we use the $\frac{N_t}{m_0 m_1} \times \frac{N_t}{m_0 m_1}$ block matrix A_{cc}, which is the re-discretization of the initial value problem without the last time point (see Equation (3.27)), where m_1 denotes the coarsening factor from the intermediate grid to the coarsest one. Unfortunately, to the best of our knowledge, this results in the loss of the convenient structure that, in a two-grid case, allowed for the reduction of the analysis to manipulations with just the time-stepping operator.

Remark 3.8. *If we proceed with the three-grid, as*

$$\tilde{Q}_3(1,1,1,1) = \left(I - P_\Phi \left(I_c - Q_{2,3}^{FCF}\right) A_c^{-1} R_I A_p\right) P_\Phi \left(I - A_\Delta\right) R_I, \tag{3.89}$$

where again $Q_{2,3}^{FCF}$ is analog to (3.86), we are able to write the block with dominant eigenvalues of the interest for ν's as previously for the two-grid

$$\tilde{Q}_3(1,\nu_0,\nu_1,\kappa) = \begin{pmatrix}
\Phi^{(\nu_1+1)m_1}\left(I-\Phi_c^{(\nu_0+1)m_0}\right) & 0 \dots 0 & \Phi^{\nu_1 m_1}\Phi_c^{(\nu_0+1)m_0} & 0 \dots 0 & & & & & & & & & \\
\vdots & \vdots & \vdots & \vdots & & & & & & & & & \\
\Phi^{(\nu_1+2)m_1-1}\left(I-\Phi_c^{(\nu_0+1)m_0}\right) & 0 \dots 0 & \Phi^{(\nu_1+1)m_1-1}\Phi_c^{(\nu_0+1)m_0} & 0 \dots 0 & & & & & & & & & \\
\Phi^{(\nu_1+1)m_1}\Phi_c\left(I-\Phi_c^{(\nu_0+1)m_0}\right) & 0 \dots 0 & \Phi^{\nu_1 m_1}\left(\Phi^m+\Phi_c^{(\nu_0+1)m_0+1}-\Phi_c\right) & \vdots & & & & & & & & & \\
\vdots & \vdots & \vdots & \vdots & & & & & & & & & \\
\Phi^{(\nu_1+2)m_1-1}\Phi_c\left(I-\Phi_c^{(\nu_0+1)m_0}\right) & 0 \dots 0 & \Phi^{(\nu_1+1)m_1-1}\left(\Phi^m+\Phi_c^{(\nu_0+1)m_0+1}-\Phi_c\right) & 0 \dots 0 & & & & & & & & & \\
\vdots & \vdots & \dots & \vdots & & & & & & & & & \\
* & 0 \dots 0 & * & \vdots & & & & & & & & & \\
\vdots & \vdots & \vdots & \vdots & & & & & & & & & \\
* & 0 \dots 0 & * & 0 \dots 0 & \dots & * & 0 \dots 0 & * & 0 \dots 0 & * & 0 \dots 0 & * & 0 \dots 0
\end{pmatrix}^{\kappa}, \tag{3.90}$$

and the non-singular eigenvalues of this dominant block are the eigenvalues of

$$\Phi^{(\nu_1+1)m_1}$$

and the eigenvalues of $-\Phi^{(\nu_1+1)m_1}\Phi_c^{(\nu_0+1)m_0} + \Phi^{(\nu_1+1)m_1} + \Phi^{\nu_1 m_1}\Phi_c^{(\nu_0+1)m_0+1} - \Phi^{\nu_1 m_1}\Phi_c$, which is

$$\Phi^{\nu_1 m_1}\left(\left(\Phi^{m_1}-\Phi_c\right)\left(I-\Phi_c^{(\nu_0+1)m_0}\right)\right).$$

What again appears as an interesting result, it should be clearly noted that if there are negative eigenvalues in the operator Φ_c, issues with convergence due to properties of $\left(I-\Phi_c^{(\nu_0+1)m_0}\right)$ might arise. Further consideration of such an algorithm modification is out of the scope of this research.

3.2.2 Numerical Analysis Validation

We substantiate Theorem 3.7 and the associated convergence properties delineated in (3.76) through a series of numerical experiments on the grounded heat equation. The analysis, as illustrated in Figures 3.4 and 3.5, examines the QMGRIT algorithm's performance under various configurations, employing adaptive sampling strategies for the time steps, N_t, in relation to the coarsening factor, m. Figure 3.4

exemplifies the application of two-grid QMGRIT with variable number of CF-relaxations, maintaining a constant $N_c = 2^5$ and $N_x = 2^{11}$. Notably, the right subfigure accentuates the predictive accuracy of our model for convergence rates when $\nu = N_c - 1$, a key assertion of the Theorem 3.7. This predictive capability is further confirmed in the comparative analysis showcased in Figure 3.5. Here, the left subfigure signifies an optimized configuration at $N_c = 4$, and the right subfigure provides a detailed comparative analysis of $Q(1, \nu, \kappa)$ and $Q(\nu, \nu, \kappa)$. To elucidate the adaptability of our approach, we emphasize that the sampling of N_t is dynamically adjusted to satisfy the ratio $N_t/m = N_c$, thereby achieving a consistent coarse-grid resolution across varying fine-grid dimensions. In essence, the empirical data presented in our figures validate the theoretical predictions of Theorem 3.7. The convergence behavior, as anticipated by (3.76) for the cases where $\nu = N_c - 1$, aligns remarkably well with the numerical outcomes. The adaptive methodology adopted for the selection of N_t in correlation with m underpins a flexible yet rigorous framework. This framework facilitates an incisive exploration of the QMGRIT algorithm's efficiency, underlining its practical applicability and confirming its theoretical foundations. In summary, the numerical experiments presented in this section provide compelling evidence supporting the validity of Theorem 3.7 and the convergence properties described in (3.76). The adaptive sampling strategy for N_t based on the coarsening factor m has proven to be a powerful tool for analyzing the QMGRIT algorithm's performance across a wide range of grid configurations. The close agreement between the theoretical predictions and the empirical results underlines the robustness and accuracy of our mathematical framework. Moreover, the identification of convenience configurations, such as $N_c = 4$ and the effectiveness of the algorithm when $\nu = N_c - 1$, offers valuable insights for practitioners seeking to maximize the efficiency of the QMGRIT algorithm in their specific applications.

3.2.3 Ghosted QMGRIT

In this section, we present a novel paradigm for parallelizing the solution of time-depending time-periodic problems. Based on the QMGRIT algorithm and the fact that its iterations converge to an analytic solution (in time-stepping sense) starting from arbitrary initial values, we propose starting two copies of solvers with a shifted distribution at F- and C-Points (see Figure 3.6) and the subsequent predefined overlap of the two provided iteration's results (see Equation (3.97)). Thus for each iteration, we are able to compute an additional C-smoothing which may speedup the convergence. The basic idea of the application is to optimize the use of idle processors on the lower coarse levels when applying the

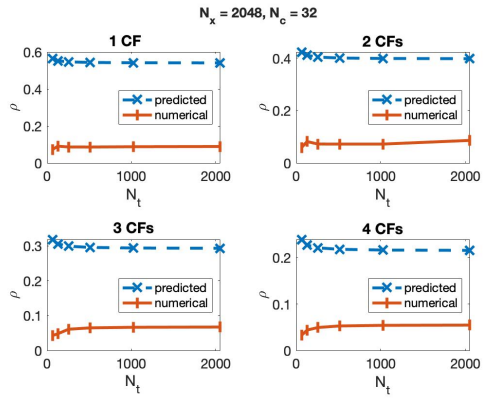

(a) Initial CF-relaxation comparison for m values, showing performance at $N_x = 2^{11}$ resolution

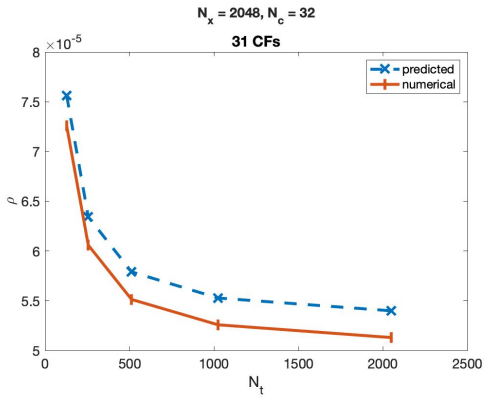

(b) Extended CF-relaxation analysis with $\nu \equiv 1 \cdot 2^5 - 1$, bringing to the forefront the convergence rates of analysis

Figure 3.4: Applying two-grid QMGRIT with 1-4 CF-relaxations (left) and $\nu \equiv 1 \cdot 2^5 - 1$ CF-relaxations (right), fixing $N_c = 2^5$, $N_x = 2^{11}$, and adaptively sampling m for N_t

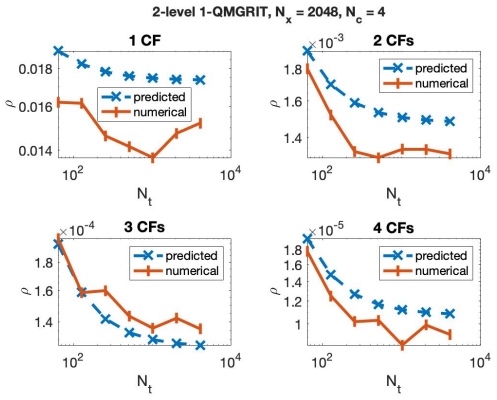

(a) By sampling N_t's (m adaptively) for the different N_x's and a set of CF-relaxations we screen a greedy, light and fast constellation, where $N_c = 4$

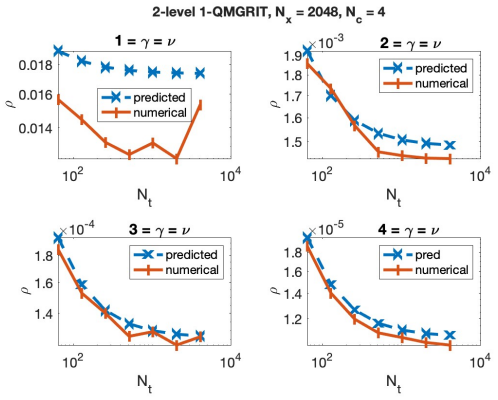

(b) Equivalently to $Q(1, \nu, \kappa)$ on the two last subplots blocks for $\nu = 1, 2, 3, 4$ we observe the numerical behaviour of $Q(\nu, \nu, \kappa)$ with $\gamma = \nu = 1, 2, 3, 4$, again, comparing with (3.76) on $Q(1, \nu, \kappa)$

Figure 3.5: Comparative analysis of QMGRIT efficiency across different configurations, focusing on adaptive sampling strategies for m (based on N_t), and evaluating the numerical behavior of $Q(\gamma, \nu, \kappa)$ for varying γ and ν values. The left subfigure identifies a light, fast, and efficient configuration with $N_c = 4$, while the right subfigure explores detailed comparisons of $Q(1, \nu, \kappa)$ and $Q(\nu, \nu, \kappa)$, illustrating the algorithm's performance.

multilevel algorithm — however, a straightforward algorithmic two-grid application is also possible, as in the case of sub-optimal processor load-sharing, e.g., as in the case of the two-grid algorithm application and having more processors than necessary for optimal loading of all processors by given fixed discretization size.

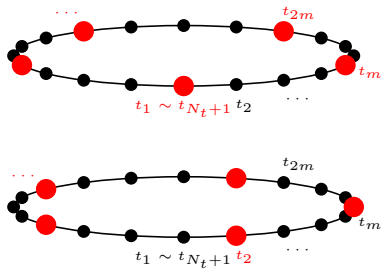

Figure 3.6: gQMGRIT Construction: Illustration of two copies of the temporal grid, showing the shifted distribution at F-Points (black) and C-Points (red)

We consider the matrix system Equation (3.26) and note two restriction operators. The first one is the standard QMGRIT restriction operator

$$R_1 := \begin{pmatrix} \mathbb{I} & 0 & \dots & 0 & & & & & & & \\ & & & & \mathbb{I} & 0 & \dots & 0 & & & \\ & & & & & & & & \ddots & & \\ & & & & & & & & & \mathbb{I} & 0 & \dots & 0 \end{pmatrix}. \tag{3.91}$$

The second one is the restriction operator with the shifted distribution at F and C points

$$R_2 := \begin{pmatrix} 0 & \mathbb{I} & 0 & \dots & 0 & & & & & & \\ & & & & & \mathbb{I} & 0 & \dots & 0 & & \\ & & & & & & & & & \ddots & \\ & & & & & & & & & \mathbb{I} & 0 & \dots \end{pmatrix}. \tag{3.92}$$

Furthermore, we consider two prolongation operators with the shifted distribution at F and C points. That is, the classical P_1 and the shifted copy ones, P_2

$$P_1 := \begin{pmatrix} \mathbb{I} & & \\ \Phi & & \\ \vdots & & \\ \Phi^{m-1} & & \\ & \ddots & \\ & & \mathbb{I} \\ & & \Phi \\ & & \vdots \\ & & \Phi^{m-1} \end{pmatrix}, \qquad P_2 := \begin{pmatrix} & & \Phi^{m-1} \\ \mathbb{I} & & \\ \Phi & & \\ \vdots & & \\ \Phi^{m-1} & & \\ & \ddots & \\ & & \mathbb{I} \\ & & \Phi \\ & & \vdots \\ & & \Phi^{m-2} \end{pmatrix}. \tag{3.93}$$

In addition, we note two interchangeable operators, which give us the possibility of creating the desired calculation by plaiting the braid of two solutions after two simultaneous iterations. Through this plaiting, all points in the resulting solution have undergone an F-relaxation.

$$G_1 := \begin{pmatrix} 0 & & & & & & \\ & \mathbb{I} & & & & & \\ & & \ddots & & & & \\ & & & \mathbb{I} & & & \\ & & & & 0 & & \\ & & & & & \mathbb{I} & \\ & & & & & & \ddots \\ & & & & & & & \mathbb{I} \\ & & & & & & & & 0 \end{pmatrix}, \qquad G_2 := \begin{pmatrix} \mathbb{I} & & & & & & \\ & 0 & & & & & \\ & & \ddots & & & & \\ & & & 0 & & & \\ & & & & \mathbb{I} & & \\ & & & & & 0 & \\ & & & & & & \ddots \\ & & & & & & & 0 \\ & & & & & & & & \mathbb{I} \end{pmatrix}. \tag{3.94}$$

Once more, with A_c as the initial value system re-discretization and A_Δ as the periodic Schur complement, we construct two copies of two-grid QMGRIT application as follows

$$Q_1 \coloneqq P_1(\mathbb{I}_c - A_c^{-1}A_\Delta)(\mathbb{I}_c - A_\Delta)R_1 \tag{3.95}$$

and

$$Q_2 \coloneqq P_2(\mathbb{I}_c - A_c^{-1}A_\Delta)(\mathbb{I}_c - A_\Delta)R_2, \tag{3.96}$$

so that the iteration operator of the two-grid gQMGRIT is defined as

$$Q_g \coloneqq G_1 Q_1 + G_2 Q_2. \tag{3.97}$$

Exploiting the operators structure, the following result holds.

Theorem 3.9.

$$\|Q_g\|_{max} < \|Q_1\|_{max} \tag{3.98}$$

and

$$\|Q_g\|_1 < \|Q_1\|_1. \tag{3.99}$$

Proof. For the sake of readability and a better graphic visualization of large matrices — due to space limitations on a small sheet of paper and for a better visual introduction to the gQMGRIT operators, we present a proof for $N_t = 8$ and $N_c = 4$ (where $m = {}^{N_t}/_{N_c} = 2$). The generalization to any feasible combination of m, N_c, and N_t follows the same approach. We will use the calculus from Theorem 3.7 and write down the first operator

$$Q_1 = \begin{pmatrix}
0 & 0 & 0 & 0 & \Phi^{2m} & 0 & 0 & 0 \\
0 & 0 & 0 & 0 & \Phi^{3m-1} & 0 & 0 & 0 \\
0 & 0 & 0 & 0 & \Phi^{2m}\Phi_c & 0 & \Phi^m(\Phi^m - \Phi_c) & 0 \\
0 & 0 & 0 & 0 & \Phi^{3m-1}\Phi_c & 0 & \Phi^{2m-1}(\Phi^m - \Phi_c) & 0 \\
\Phi^m(\Phi^m - \Phi_c) & 0 & 0 & 0 & \Phi^{2m}\Phi_c^{N_c-2} & 0 & \Phi^m\Phi_c(\Phi^m - \Phi_c) & 0 \\
\Phi^{2m-1}(\Phi^m - \Phi_c) & 0 & 0 & 0 & \Phi^{3m-1}\Phi_c^{N_c-2} & 0 & \Phi^{m+1}\Phi_c(\Phi^m - \Phi_c) & 0 \\
\Phi^m\Phi_c(\Phi^m - \Phi_c) & 0 & \Phi^m(\Phi^m - \Phi_c) & 0 & \Phi^{2m}\Phi_c^{N_c-1} & 0 & \Phi^m\Phi_c^2(\Phi^m - \Phi_c) & 0 \\
\Phi^{2m-1}\Phi_c(\Phi^m - \Phi_c) & 0 & \Phi^{2m-1}(\Phi^m - \Phi_c) & 0 & \Phi^{3m-1}\Phi_c^{N_c-1} & 0 & \Phi^{2m-1}\Phi_c^2(\Phi^m - \Phi_c) & 0
\end{pmatrix}. \tag{3.100}$$

For the given discretization parameters, the second operator is

$$Q_2 = \begin{pmatrix} 0 & \Phi^3\Phi_c\left(\Phi^2-\Phi_c\right) & 0 & \Phi^3\left(\Phi^2-\Phi_c\right) & 0 & \Phi^5\Phi_c^3 & 0 & \Phi^3\Phi_c^2\left(\Phi^2-\Phi_c\right) \\ 0 & 0 & 0 & 0 & 0 & \Phi^4 & 0 & 0 \\ 0 & 0 & 0 & 0 & 0 & \Phi^5 & 0 & 0 \\ 0 & 0 & 0 & 0 & 0 & \Phi^4\Phi_c & 0 & \Phi^2\left(\Phi^2-\Phi_c\right) \\ 0 & 0 & 0 & 0 & 0 & \Phi^5\Phi_c & 0 & \Phi^3\left(\Phi^2-\Phi_c\right) \\ 0 & \Phi^2\left(\Phi^2-\Phi_c\right) & 0 & 0 & 0 & \Phi^4\Phi_c^2 & 0 & \Phi^2\Phi_c\left(\Phi^2-\Phi_c\right) \\ 0 & \Phi^3\left(\Phi^2-\Phi_c\right) & 0 & 0 & 0 & \Phi^5\Phi_c^2 & 0 & \Phi^3\Phi_c\left(\Phi^2-\Phi_c\right) \\ 0 & \Phi^2\Phi_c\left(\Phi^2-\Phi_c\right) & 0 & \Phi^2\left(\Phi^2-\Phi_c\right) & 0 & \Phi^4\Phi_c^3 & 0 & \Phi^2\Phi_c^2\left(\Phi^2-\Phi_c\right) \end{pmatrix}. \tag{3.101}$$

Therefore, we can directly conclude the gQMGRIT operator

$$Q_g = \begin{pmatrix} 0 & \Phi^3\Phi_c\left(\Phi^2-\Phi_c\right) & 0 & \Phi^3\left(\Phi^2-\Phi_c\right) & 0 & \Phi^5\Phi_c^3 & 0 & \Phi^3\Phi_c^2\left(\Phi^2-\Phi_c\right) \\ 0 & 0 & 0 & 0 & \Phi^5 & 0 & 0 & 0 \\ 0 & 0 & 0 & 0 & 0 & \Phi^5 & 0 & 0 \\ 0 & 0 & 0 & 0 & \Phi^5\Phi_c & 0 & \Phi^3\left(\Phi^2-\Phi_c\right) & 0 \\ 0 & 0 & 0 & 0 & 0 & \Phi^5\Phi_c & 0 & \Phi^3\left(\Phi^2-\Phi_c\right) \\ \Phi^3\left(\Phi^2-\Phi_c\right) & 0 & 0 & 0 & \Phi^5\Phi_c^2 & 0 & \Phi^3\Phi_c\left(\Phi^2-\Phi_c\right) & 0 \\ 0 & \Phi^3\left(\Phi^2-\Phi_c\right) & 0 & 0 & 0 & \Phi^5\Phi_c^2 & 0 & \Phi^3\Phi_c\left(\Phi^2-\Phi_c\right) \\ \Phi^3\Phi_c\left(\Phi^2-\Phi_c\right) & 0 & \Phi^3\left(\Phi^2-\Phi_c\right) & 0 & \Phi^5\Phi_c^3 & 0 & \Phi^3\Phi_c^2\left(\Phi^2-\Phi_c\right) & 0 \end{pmatrix}. \tag{3.102}$$

Now, we calculate the maximum norm

$$\begin{aligned} \|Q_g\|_{\max} &= \max_{1\le i,j\le 8(N_x+1)} |\left(Q_g\right)_{ij}| \\ &= \max\{\|\Phi^3\left(\Phi^2-\Phi_c\right)\|_{\max}, \|\Phi^5\|_{\max}\} \\ &= \|\Phi^5\|_{\max} \\ &< \|\Phi^4\|_{\max} = \|Q_2\|_{\max} \\ &= \|Q_1\|_{\max}. \end{aligned}$$

This leads to (3.98). Considering the columns, we further observe the action of gQMGRIT paradigm, which involves the division of all columns, and particularly the fifth dominant block-column of Q_1 (corresponding to the sixth block-column of Q_2) into two distinct parts. Thus, (3.99) is evident. □

Remark 3.10. *Since Q_2 is obtained by circularly shifting the elements of Q_1, we can express their rela-*

tionship using the permutation matrix S as follows

$$Q_2 = S^t Q_1 S, \tag{3.103}$$

where S is the permutation matrix given by

$$S = \begin{pmatrix} 0 & 1 & \cdots & 0 \\ \vdots & \vdots & \ddots & \vdots \\ 0 & 0 & \cdots & 1 \\ 1 & 0 & \cdots & 0 \end{pmatrix}. \tag{3.104}$$

Thus, we can conclude that Q_1 and Q_2 are similar matrices, $Q_1 \sim Q_2$, which implies that they share the same eigenvalues, while their eigenvectors are related by the permutation matrix S. In other words, if λ is an eigenvalue of Q_1 with corresponding eigenvector $\mathbf{v}$, then λ is also an eigenvalue of Q_2 with corresponding eigenvector $S^t\mathbf{v}$.

3.2.4 Alternative Analysis Methodology with SAMA

Semi-Algebraic Mode Analysis expands the analysis possibilities available in the toolkit for analysis of multi-grid methods generalizing LFA — this method creatively merges LFA in space with an exact algebraic approach in time to provide a new perspective, which is a contemporary and precise way to analyze multi-grid methods. SAMA's inception, credited to Friedhoff and MacLachlan[11], noted a prominent advance in the predictive analysis of such methods, particularly valuable for systems characterized by non-circulant matrices which multi-grid iteration matrices often exhibit [20, 40, 42, 59, 72].

When dealing with periodic problems, where the system matrix traditionally assumes a circulant structure conducive to LFA, the QMGRIT method's iteration matrix presents a challenge because of its non-circulant nature — this complexity arises from approximating the coarse problem with an initial value problem within QMGRIT, rendering LFA less effective (see Appendix A) and thus elevating the importance of SAMA for our analysis. By using SAMA, we produce a richer understanding of the QMGRIT method by obtaining an algebraic decomposition that shows the method's eigenvalue structure, which is essential for predicting performance accurately. By representing matrices for time

[11] Scott P. MacLachlan is a mathematician recognized for his contributions to numerical analysis, particularly in the development of multi-grid and AMG methods. His work has advanced the efficiency and theoretical understanding of computational methods for solving partial differential equations in scientific and engineering applications.

stepping and spatial discretization with the Kronecker[12] product, we also illustrate the algebraic sophistication of SAMA's approach. We write

$$A_p \mathbf{u}_p = \left(J \otimes \mathbb{I}_{N_x} + \mathbb{I}_{N_t} \otimes \mathcal{O}\right) \mathbf{u}_p = \mathbf{b}_p, \tag{3.105}$$

where

$$J = \frac{1}{\Delta t} \begin{pmatrix} 1 & & & & -1 \\ -1 & 1 & & & \\ & -1 & 1 & & \\ & & -1 & 1 & \\ & & & \ddots & \ddots \end{pmatrix}, \qquad \mathcal{O} = \frac{1}{\Delta x^2} \begin{pmatrix} 2 & -1 & & & \\ -1 & 2 & -1 & & \\ & \ddots & \ddots & \ddots & \\ & -1 & 2 & -1 & \\ & & -1 & 2 & \end{pmatrix}. \tag{3.106}$$

Then, we have

$$A_p = \begin{pmatrix} J_0 + \mathcal{O} & & & & J_{-1} \\ J_{-1} & J_0 + \mathcal{O} & & & \\ & \ddots & \ddots & & \\ & & & J_{-1} & J_0 + \mathcal{O} \end{pmatrix} \tag{3.107}$$

with $J_0 = (1/\Delta t)\,\mathbb{I}_{N_x}$ and $J_{-1} = -(1/\Delta t)\,\mathbb{I}_{N_x}$. Applying the SAMA, which involves block-wise Fourier transformation, $\mathcal{F}$, and permutation of the system matrix, $\mathcal{P}$, such that the time direction is the innermost, we obtain

$$\mathcal{P}^{-1}\mathcal{F}^{-1} A_p \mathcal{F}\mathcal{P} = \begin{pmatrix} B_1^{(A_p)} & & & \\ & B_2^{(A_p)} & & \\ & & \ddots & \\ & & & B_{N_x}^{(A_p)} \end{pmatrix}, \tag{3.108}$$

[12] Leopold Kronecker (*7 December 1823 in Liegnitz, Prussia (now Legnica, Poland); †29 December 1891 in Berlin, Germany) was a German mathematician known for his work in algebra, number theory, and the foundations of mathematics. Kronecker's contributions include the Kronecker delta and the Kronecker product, as well as his views on the philosophy of mathematics, particularly his dictum: 'God made the integers; all else is the work of man'.

where

$$B_k^{(A_p)} = \begin{pmatrix} j_0 + \lambda_k & & & j_{-1} \\ j_{-1} & j_0 + \lambda_k & & \\ & \ddots & \ddots & \\ & & j_{-1} & j_0 + \lambda_k \end{pmatrix}, \tag{3.109}$$

and also

$$\mathcal{P}^{-1}\mathcal{F}^{-1}P_\Phi\mathcal{F}\mathcal{P} = \begin{pmatrix} B_1^{(P_\Phi)} & & & \\ & B_2^{(P_\Phi)} & & \\ & & \ddots & \\ & & & B_{N_x-1}^{(P_\Phi)} \end{pmatrix}, \tag{3.110}$$

where $B_k^{(P_\Phi)} = \mathbb{I}_{N_t/m} \otimes v$ with $v = \left(1, \lambda_k, \lambda_k^2, \ldots, \lambda_k^{m-1}\right)^T$. Furthermore,

$$B_k^{(\hat{A}_p)} = \begin{pmatrix} 1 & & & -\hat{\lambda}_k \\ -\hat{\lambda}_k & 1 & & \\ & \ddots & \ddots & \\ & & -\hat{\lambda}_k & 1 \end{pmatrix}, \qquad B_k^{(\hat{A}_c)} = \begin{pmatrix} 1 & & & \\ -\hat{\lambda}_{c;k} & 1 & & \\ & \ddots & \ddots & \\ & & -\hat{\lambda}_{c;k} & 1 \end{pmatrix} \tag{3.111}$$

with the eigenvalues $\hat{\lambda}_k = \left(1 + \frac{4\Delta t}{\Delta x^2}\sin^2\left(\frac{k\pi}{2N_x}\right)\right)^{-1}$ for the fine equations system, and $\hat{\lambda}_{c;k} = \left(1 + \frac{4m\Delta t}{\Delta x^2}\sin^2\left(\frac{k\pi}{2N_x}\right)\right)^{-1}$ for the coarse one. Complementing the analysis we also note the following

$$B_k^{\left(S^F\right)} = \begin{pmatrix} Z^{\left(S^F\right)} & & & \\ & Z^{\left(S^F\right)} & & \\ & & \ddots & \\ & & & Z^{\left(S^F\right)} \end{pmatrix}, \qquad B_k^{\left(S^C\right)} = \begin{pmatrix} Z^{\left(S^C\right)} & & & \hat{\lambda}_k\hat{e}_1\hat{e}_m^T \\ \hat{\lambda}_k\hat{e}_1\hat{e}_m^T & Z^{\left(S^C\right)} & & \\ \ddots & \ddots & & \\ & \hat{\lambda}_k\hat{e}_1\hat{e}_m^T & & Z^{\left(S^C\right)} \end{pmatrix} \tag{3.112}$$

with

$$Z^{\left(S^F\right)} = \begin{pmatrix} 1 & & & \\ & \hat{\lambda}_k & & \\ & & \hat{\lambda}_k^2 & \\ & & & \vdots \\ & & & \hat{\lambda}_k^{m-1} \end{pmatrix}, \qquad Z^{\left(S^C\right)} = \begin{pmatrix} 0 & & & & \\ & 1 & & & \\ & & 1 & & \\ & & & \ddots & \\ & & & & 1 \end{pmatrix}, \tag{3.113}$$

$\hat{e}_1 = [1, 0, 0, \ldots, 0]^T$, and $\hat{e}_m = [0, \ldots, 0, 0, 1]^T$. Putting the corresponding matrices together into the iteration operator for each eigenvalue in spatial dimension, we get

$$B_k^{Q(1,1,1)} = \left(\mathbb{I} - B_k^{(P_\Phi)} \left(B_k^{\left(\hat{A}_c\right)} \right)^{-1} B_k^{(R_I)} B_k^{(\hat{A}_p)} \right) B_k^{\left(S^F\right)} B_k^{\left(S^C\right)} B_k^{\left(S^F\right)}, \tag{3.114}$$

and so define the SAMA prediction on the convergence factor for an iteration

$$\rho_{\text{sama}}\left(Q(1,1,1)\right) \coloneqq \sup_k \left\{ \left\| B_k^{Q(1,1,1)} \right\|_2 \right\}. \tag{3.115}$$

In our investigation, we include the SAMA as more of a sidekick for our previously done spectral study of the QMGRIT. This method helps us understand the dynamics of the multi-grid method more fully than we would get if we only had the spectral study — especially since this iteration matrix of QMGRIT is non-circulant. On top, we hope this work exemplifies how SAMA is a very robust framework and how it complements the depth and insight gained from doing a spectral study by hand — this framework is also the embodiment of how utilizing SAMA could provide a useful predictive indicator of convergence and an extension of the analysis that we propose in this research. Incorporating SAMA with spectral analysis of QMGRIT in Section 3.2.1 manifests a deepened understanding of its behavior, that may help us to understand the theoretical and practical consequences of the work in the field of computational mathematics.

Numerical Validation with SAMA

Following definition of gQMGRIT in Equation (3.97), definition of SAMA prediction in (3.115) and Remark 3.10, in this section, we utilize the SAMA methodology, applying it to both the QMGRIT and the gQMGRIT algorithms — this approach allows us to compare these two methods in terms of analytical predictions on convergence behaviour. Applying the QMGRIT algorithm and comparing it with

the gQMGRIT, we analyze both using SAMA on the grounded $1D$+$1D$ heat equation — this analysis is vital for understanding the convergence behaviour of these algorithms and for evaluating their performance in practical applications.

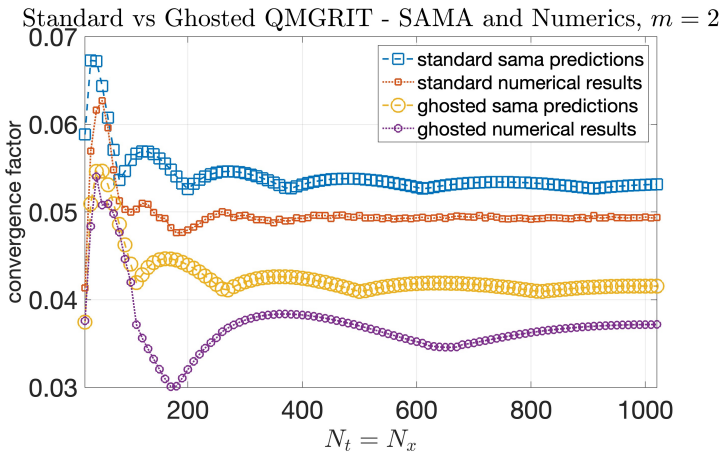

Figure 3.7: A discrete composition of convergence behavior as functions of $N_t = N_x$ in four samplings with one hundred realizations: two numerical calculations and two analytic SAMA predictions (for QMGRIT and gQMGRIT, respectively). The SAMA analysis accurately predicts the numerical behavior of the algorithms, showcasing the distinct advantage of the gQMGRIT paradigm over the standard QMGRIT application.

Our numerical findings suggest the superiority of the gQMGRIT approach over the counterpart, the plain QMGRIT, and we verify that we can obtain **30%** more efficient convergence factors for the given heat equation model problem, as proved in the SAMA methodology — the improvement for the heat equation model problem, as proven by the SAMA methodology, is remarkable and indicates profound improvement in algorithm performance and convergence rate. From Figures 3.7 and 3.8, we collect a comprehensive data set of numerical $1D$+$1D$-dimensional grounded heat equation simulations and respective analysis calculations for the convergence factor. These figures illustrate the superior performance of the gQMGRIT algorithm, demonstrating its potential for significantly improving the convergence rate in solving the heat equation. The additive representation of the convergence rate improvement, as depicted in Figure 3.8, provides a clear and quantifiable measure of the gQMGRIT's advantage over QMGRIT, further validating the SAMA methodology as a powerful tool for predicting and comparing the performance of numerical algorithms. For a comparison of SAMA with LFA see Appendix A.

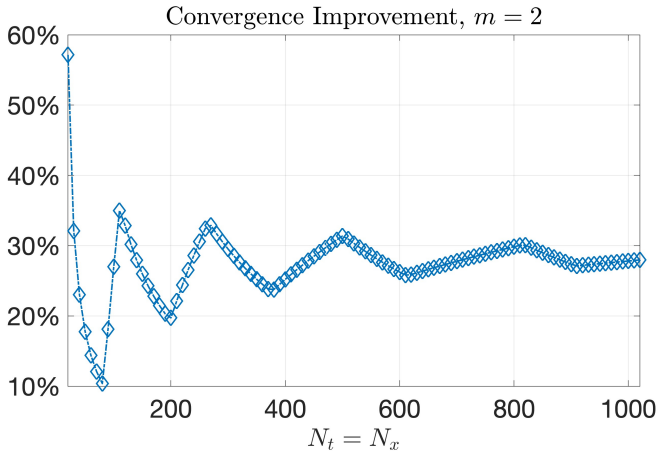

Figure 3.8: Using the formula $100\left(\frac{\rho_{\mathsf{sama}}\left(T^{(1,1,2)}_{\mathrm{QMGRIT}}\right)}{\rho_{\mathsf{sama}}\left(T_{\mathrm{gQMGRIT}}\right)}-1\right)\%$, this figure plots an additive representation of the algorithmic convergence rate improvement of the gQMGRIT algorithm compared to the QMGRIT.

3.2.5 Comparison with periodic Parareal

Parareal-End

To derive the Parareal for time-periodic problems, one uses the relationship of the Parareal algorithm to the multiple-shooting method [46]. To this end, one notes the fitting conditions fulfilled by the solution $\mathbf{u}$,

$$\mathbf{U}_1 - \mathbf{u}_N\left(T_1, \mathbf{U}_N\right) = 0, \mathbf{U}_2 - \mathbf{u}_1\left(T_2, \mathbf{U}_1\right) = 0, \ldots, \mathbf{U}_N - \mathbf{u}_{N-1}\left(T_N, \mathbf{U}_{N-1}\right) = 0, \tag{3.116}$$

where $\mathbf{u}_n\left(T_{n+1}, \mathbf{U}_n\right), n = 1, \ldots, N$, denotes the solution at T_{n+1} of the corresponding problem with initial value $\mathbf{U}_n$. These fitting conditions form a nonlinear system of equations

$$\mathbf{F}(\mathbf{U}) = 0, \quad \mathbf{U} = \left(\mathbf{U}_1^{\mathbf{T}}, \mathbf{U}_2^{\mathbf{T}}, \ldots, \mathbf{U}_N^{\mathbf{T}}\right)^{\mathbf{T}}, \tag{3.117}$$

and applying Newton's[13] method to solve it leads to

$$\mathbf{U}^{k+1} = \mathbf{U}^k - J_F^{-1}\left(\mathbf{U}^k\right)\mathbf{F}\left(\mathbf{U}^k\right), \tag{3.118}$$

[13]Sir Isaac Newton (*25 December 1642 in Woolsthorpe, Lincolnshire, England; †20 March 1727 in Kensington, Middlesex, England) was an English mathematician, physicist, astronomer, and author, widely recognized as one of the most influential scientists of all time and a key figure in the scientific revolution. His work *Philosophiæ Naturalis Principia Mathematica* (Mathematical Principles of Natural Philosophy), first published in 1687.

where the Jacobian[14] J_F of $\mathbf{F}$ is given by

$$J_F = \begin{pmatrix} I & & & & -\frac{\partial \mathbf{u}_N}{\partial \mathbf{U}_N}\left(T_1, \mathbf{U}_N^k\right) \\ -\frac{\partial \mathbf{u}_1}{\partial \mathbf{U}_1}\left(T_2, \mathbf{U}_1^k\right) & I & & & \\ & -\frac{\partial \mathbf{u}_2}{\partial \mathbf{U}_2}\left(T_3, \mathbf{U}_2^k\right) & I & & \\ & \ddots & \ddots & & \\ & & -\frac{\partial \mathbf{u}_{N-1}}{\partial \mathbf{U}_{N-1}}\left(T_N, \mathbf{U}_{N-1}^k\right) & I \end{pmatrix}. \tag{3.119}$$

Multiplying (3.118) with $J_F\left(U^k\right)$, we get the recurrence of the multiple shooting method applied to the time-periodic problem [46]

$$\begin{aligned} \mathbf{U}_1^{k+1} &= \mathbf{u}_N\left(T_1, \mathbf{U}_N^k\right) + \frac{\partial \mathbf{u}_N}{\partial \mathbf{U}_N}\left(T_1, \mathbf{U}_N^k\right)\left(\mathbf{U}_N^{k+1} - \mathbf{U}_N^k\right), \\ \mathbf{U}_{n+1}^{k+1} &= \mathbf{u}_n\left(T_{n+1}, \mathbf{U}_n^k\right) + \frac{\partial \mathbf{u}_n}{\partial \mathbf{U}_n}\left(T_{n+1}, \mathbf{U}_n^k\right)\left(\mathbf{U}_n^{k+1} - \mathbf{U}_n^k\right), \quad n = 1, \ldots, N-1. \end{aligned} \tag{3.120}$$

Approximating the exact solution in the multiple shooting method (3.120) by an accurate numerical approximation, denoted by F (the fine propagator), $\mathbf{u}_n\left(T_{n+1}, \mathbf{U}_n^k\right) \approx F\left(T_{n+1}, T_n, \mathbf{U}_n^k\right)$, and if one approximates the term from the Jacobian by a FD of a *cheap* numerical approximation, denoted by G (the coarse propagator),

$$\frac{\partial \mathbf{u}_n}{\partial \mathbf{U}_n}\left(T_{n+1}, \mathbf{U}_n^k\right)\left(\mathbf{U}_n^{k+1} - \mathbf{U}_n^k\right) \approx G\left(T_{n+1}, T_n, \mathbf{U}_n^{k+1}\right) - G\left(T_{n+1}, T_n, \mathbf{U}_n^k\right), \tag{3.121}$$

then one gets the following Parareal algorithm, PP-PC[15] [46], for the time-periodic problems

$$\begin{aligned} \mathbf{U}_1^{k+1} &= F\left(T_{N+1}, T_N, \mathbf{U}_N^k\right) + G\left(T_{N+1}, T_N, \mathbf{U}_N^{k+1}\right) - G\left(T_{N+1}, T_N, \mathbf{U}_N^k\right), \\ \mathbf{U}_{n+1}^{k+1} &= F\left(T_{n+1}, T_n, \mathbf{U}_n^k\right) + G\left(T_{n+1}, T_n, \mathbf{U}_n^{k+1}\right) - G\left(T_{n+1}, T_n, \mathbf{U}_n^k\right), \quad n = 1, \ldots, N-1. \end{aligned} \tag{3.122}$$

Similarly, one gets another, 'relaxed' one, method, PP-IC[16] [46],

$$\begin{aligned} \mathbf{U}_1^{k+1} &= \mathbf{U}_{N+1}^k, \\ \mathbf{U}_{n+1}^{k+1} &= F\left(T_{n+1}, T_n, \mathbf{U}_n^k\right) + G\left(T_{n+1}, T_n, \mathbf{U}_n^{k+1}\right) - G\left(T_{n+1}, T_n, \mathbf{U}_n^k\right), \quad n = 1, \ldots, N. \end{aligned} \tag{3.123}$$

[14] Carl Gustav Jacob Jacobi (*10 December 1804 in Potsdam, Kingdom of Prussia; †18 February 1851 in Berlin, Kingdom of Prussia) was a German mathematician, making pivotal contributions to elliptic functions, differential equations, and mechanics. Jacobi's work in developing the theory of Jacobi elliptic functions and the application of his methods to the theory of dynamics has had a profound impact on the development of mathematics in the 19th century.

[15] Periodic Parareal - Periodic Coarse

[16] Periodic Parareal - Initial Coarse

Note the distinction in the index n's range between the two approaches: for the first, n ranges from 1 to $N-1$, while for the second, n extends from 1 to N, inclusively.

QMGRIT-End

Our objective is to delineate the periodic Parareal algorithm within the framework of QMGRIT. We will adopt the methodology outlined in [49] for this representation. To this end, we apply the periodic Parareal technique to our periodic linear equation system, as detailed in Equation (3.124), discretized on C-Points, according to Equation (3.126) — so, let

$$A\mathbf{u} \equiv \begin{pmatrix} \mathbb{I} & & & & -\Phi \\ -\Phi & \mathbb{I} & & & \\ & -\Phi & \mathbb{I} & & \\ & & \ddots & \ddots & \\ & & & -\Phi & \mathbb{I} \end{pmatrix} \cdot \begin{pmatrix} u_1 \\ u_2 \\ u_3 \\ \vdots \\ u_N \end{pmatrix} = \begin{pmatrix} b_1 \\ b_2 \\ b_3 \\ \vdots \\ b_N \end{pmatrix} \equiv \mathbf{b}. \tag{3.124}$$

We define

$$A_c \coloneqq \begin{pmatrix} \mathbb{I} & & & & -\Phi_c \\ -\Phi_c & \mathbb{I} & & & \\ & -\Phi_c & \mathbb{I} & & \\ & & \ddots & \ddots & \\ & & & -\Phi_c & \mathbb{I} \end{pmatrix} \tag{3.125}$$

and write

$$A_c\mathbf{u}_c = \mathbf{b}_c, \tag{3.126}$$

where $\mathbf{b}_c$ is the discretized on the C-Points modified right hand side of some given ODE. Furthermore, we calculate

$$A_\Delta \mathbf{u}_c = R_{ideal}\mathbf{b} = \mathbf{b}_c. \tag{3.127}$$

Applying the Parareal algorithm (3.122) to solve the linear system (3.126) induced from the given ODE, we write

$$\begin{aligned} u_{1,c}^{k+1} &\coloneqq \Phi^m u_{N,c}^k + b_{1,c} + \Phi_c u_{N,c}^{k+1} - \Phi_c u_{N,c}^k, \\ u_{i+1,c}^{k+1} &\coloneqq \Phi^m u_{i,c}^k + b_{i+1,c} + \Phi_c u_{i,c}^{k+1} - \Phi_c u_{i,c}^k, \quad i = 1, 2, \ldots, N-1. \end{aligned} \tag{3.128}$$

It follows,

$$\mathbf{u}_c^{(k+1)} = \mathbf{u}_c^{(k)} + A_c^{-1}\left(\mathbf{b}_c - A_\Delta \mathbf{u}_c^{(k)}\right), \tag{3.129}$$

so when solving the Equation (3.127), one is therefore able to denote the error propagation operator of the periodic Parareal PP-PC by

$$P(\mathbb{I}_c - A_c^{-1}A_\Delta)R_I, \tag{3.130}$$

and then, relaxing the scheme by approximating on the coarse grid the matrix A_c with the matrix $\tilde{A}_c$, whereas

$$\tilde{A}_c \coloneqq \begin{pmatrix} \mathbb{I}_R & & & & \\ -\Phi_c & \mathbb{I}_R & & & \\ & -\Phi_c & \mathbb{I}_R & & \\ & & \ddots & \ddots & \\ & & & -\Phi_c & \mathbb{I}_R \end{pmatrix}, \tag{3.131}$$

one denotes error propagation operator for the periodic Parareal PP-IC, considered up to a projection map that glues endpoints in time, by the following expression

$$P(\mathbb{I}_c - \tilde{A}_c^{-1}A_\Delta)R_I. \tag{3.132}$$

This representation inherently includes the modulo projection map adjustment, making PP-IC equivalent to the two-grid 1-QMGRIT-0 method, i.e., the PP-IC provides the solution at all time points, with the first time point being a copy of the last time point, and in contrast, the two-grid 1-QMGRIT-0 method provides the solution at all time points except the last one, which can be appended as a copy of the first time point, yielding the same result as the PP-IC solution.

3.3 Intermediate Conclusion

To wrap up, this chapter was devoted to the introduction and the underlying theory of the QMGRIT algorithm, which provides a new alternative to classical multi-grid methods for the solution of periodic time-dependent PDEs — it has shown the extension of the application of the QMGRIT algorithm to situations where standard two-grid methods could be applied, as well as the possibility of further scal-

ing up for the efficient and scalable solving of PDEs in a parallel programming context. This chapter, accessing the primary four objectives of this thesis, sets the stage for subsequent numerical experiments by the following.

- Providing the mathematical model and the constituent algorithms that form the QMGRIT method, which illustrates its unique multi-level structure and its special operators to address periodicity in the time domain.
- Discussing the advantages of QMGRIT over classical MGRIT and comparing theoretically with known two-grid PinT algorithms.
- Focusing on the respective convergence rates estimation methodologies, such as spectral analysis and SAMA
- Providing the strategy for integrating QMGRIT into existing HPC platforms, such as the gQMGRIT parallelization paradigm, to exploit its performance and its capabilities in parallel and scalable computations.

Our numerical investigations will further verify the theory presented and solidify the effectiveness and efficiency of the QMGRIT method across a number of periodic problems, and provide empirical evidence that the QMGRIT algorithm has the potential to change the way periodic problems are solved in computational science and engineering in terms of speed and robustness — as we progress, the results in conjunction with those of both the analytical and numerical studies will help us to comprehend the potential of QMGRIT alongside its limitations and possible advancements, which will be the basis for drawing then our summary and conclusions in the final chapter.

Chapter 4

Numerical Experiments

This chapter will examine the convergence and performance of QMGRIT by applying it to different test problems. The scalability of the linear and non-linear model problem will be investigated, and numerical results will be compared with the analytical solution, in the first test case of the coaxial cable problem in Section 4.1. After this, we show results on the acceleration of computations by applying QMGRIT to a linear and non-linear test model of an electrical machine in Section 4.2. We also compare the numerical results with the analytical solution and examine whether QMGRIT converges for the convection-diffusion-decay test equation in Section 4.3. After that, we examine the convergence of QMGRIT for the test wave equation case, also comparing the provided solutions to the analytical solution, while reviewing the wave equation as a two-variable problem in Section 4.4. Lastly, in order to clarify the possible relationship between the following two solving approaches, we will conduct an empirical study on QMGRIT's usage as a preconditioner for the Generalized Minimal Residual (GMRES) method in Section 4.5.

4.1 Coaxial Cable Problem

In a specified, finite domain Ω within $\mathbb{R}^3$ and during a time interval $\mathcal{I} = [t_0, t_{\text{end}}]$ that belongs to $\mathbb{R} \geq 0$, the behavior of electromagnetic fields within $\Omega \times \mathcal{I}$ is determined by Maxwell's equations [75]

$$\nabla \times E = -\partial_t B, \qquad \nabla \times H = \partial_t D + J, \tag{4.1}$$

$$\nabla \cdot B = 0, \qquad \nabla \cdot D = \rho, \tag{4.2}$$

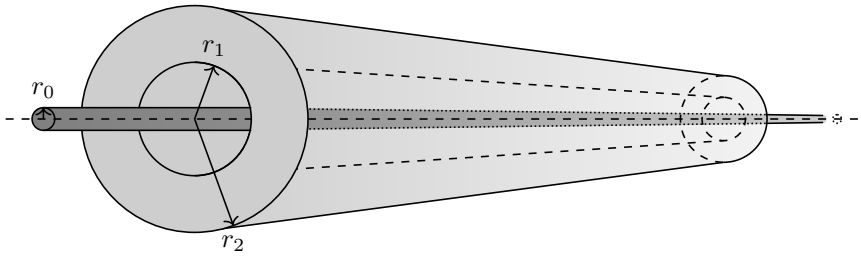

Figure 4.1: Illustration of a cable with a central conductor (see also [38]), including a $2D$ cross-sectional view in x-y-plane. The wire is represented by the central dark grey region, $0 \leq r \leq r_0$, while the conducting sheath is shown in lighter grey, $r_1 \leq r \leq r_2$, and the space between r_0 and r_1 is filled with the air.

accompanied by appropriate initial and boundary conditions at time t_0 and along $\partial\Omega$, respectively. In our scenario, involving constitutive relation between mentioned physical quantities, these foundational equations are augmented by relationships

$$D = \varepsilon E, \quad J = \sigma E + J_s, \quad B = \mu H. \tag{4.3}$$

Here, H denotes the magnetic field intensity, B the magnetic flux density, E the electric field intensity, D the electric displacement field. J, $J_\sigma = \sigma E$, $J_d = \partial_t D$ and J_s signify, respectively, the total, Ohmic, displacement, and source current densities, with ρ denoting the charge density. The constants $\sigma \geq 0$, $\varepsilon > 0$, and $\mu > 0$, respectively, represent the electrical conductivity, permittivity, and magnetic permeability of the material, assumed here to be scalar quantities [41].

This work explores the scenario where the displacement current, indicative of capacitive effects, is minor compared to the source currents, expressed as

$$\|J_d\| = \|\partial_t D\| \ll \|J_s\|. \tag{4.4}$$

A discussion on the model's accuracy in the described approximation is available in [106]. Ignoring the displacement current, i.e., setting $\partial_t D = 0$ in Maxwell's equations, introduces the concept of the magnetoquasistatic approximation, also known as the *eddy current problem* — this approach explains the *skin effect*, where increasing frequency causes currents to concentrate near the surface of a conductor (see [41] and [75, Chapter 5.18]).

4.1.1 The Partial Differential Equation

Within the magnetoquasistatic approximation, we employ the magnetic vector potential A to both characterize magnetic fields and, implicitly, electric fields through temporal derivatives — this streamlines the electromagnetic phenomena under the assumption of negligible displacement currents. The electric field E is derived from the time rate of change of A, effectively simplifying the analysis

$$E = -\partial_t A, \tag{4.5}$$

leading to a PDE written with the curl-curl operator

$$\nabla \times (\nu \nabla \times A) + \sigma \frac{\partial A}{\partial t} = J_s, \tag{4.6}$$

where $\nu = \mu^{-1}$ denotes again the reluctivity (inverse of permeability), σ represents the conductivity; J_s is the source current density from external source, expressed as $J_s(x, y, z, t) = J_0(x, y, z) \sin(\omega t)$ with $\omega = 2\pi f$, linking to the source's frequency f. For cases with minimal spatial variation along one dimension, it is practical to limit the analysis to a $2D$ cross-section, the x-y-cross-section in our test case, as illustrated in Figure 4.1 — this reduction permits assumptions

$$J_s = (0, 0, J_{s,z}), \tag{4.7}$$

$$B = (B_x, B_y, 0), \tag{4.8}$$

$$A = (0, 0, A_z), \tag{4.9}$$

that to further simplify the governing equations. Focusing on the z-component of A, we reduce the Equation (4.6) to

$$\nabla \cdot (\nu \nabla A_z(x, y, t)) + \sigma \frac{\partial A_z(x, y, t)}{\partial t} = J_{s,z}, \tag{4.10}$$

which mirrors the structure of the heat equation (see Section 3.1.4), distinguished by the non-negative conductivity σ [41] (when comparing with thermal diffusivity coefficient a).

4.1.2 Derivation of the Analytical Solution

To obtain an analytical solution for the Equation (4.6), we will consider further symmetries. The series of transformation and simplification from the original PDE that describes electromagnetic phenomena

are specified by a number of mathematical steps. The final outcome of this process is documented in [41], but the intermediate steps are omitted — thus, we will undertake the task of exploring these steps independently.

1. By transitioning to **polar coordinates** and exploiting the radial symmetry of the coaxial structure (assuming no angular variation), we build on (4.10) and simplify equation (4.6) further — this adjustment aligns the physical symmetries of the coaxial cable with the mathematical model

$$\overset{\substack{polar\ coordinates \\ \partial A_z(\varphi,r,t)/\partial\varphi=0}}{\Longleftrightarrow} -\frac{1}{r}\frac{\partial}{\partial r}\left(r\nu\frac{\partial A_z(r,t)}{\partial r}\right)+\sigma\frac{\partial A_z(r,t)}{\partial t}=J_0(r,t). \tag{4.11}$$

2. The application of **phasor calculus**[1] transforms the time-domain equation into the frequency domain, facilitating the analysis of the system's steady-state response to sinusoidal inputs — from Equation (4.11) we proceed to

$$\overset{\substack{phasor \\ calculus}}{\Longleftrightarrow} -\frac{1}{r}\frac{\partial}{\partial r}\left(r\nu\frac{\partial A_z(r)\cos(\omega t+\varphi_0)}{\partial r}\right)+\sigma\frac{\partial A_z(r)\cos(\omega t+\varphi_0)}{\partial t}=J_0(r)\cos(\omega t+\varphi_0). \tag{4.12}$$

3. Adjusting for **phase shift**, specifically setting the initial phase to zero, focuses the analysis on the real components — simplifying the mathematical treatment by neglecting phase shifts in sinusoidal functions — so, the Equation (4.12) leads to

$$\overset{\varphi_0=0}{\Longleftrightarrow} -\frac{1}{r}\frac{\partial}{\partial r}\left(r\nu\frac{\partial\Re\left\{A_z(r)e^{i\omega t}\right\}}{\partial r}\right)+\sigma\frac{\partial\Re\left\{A_z(r)e^{i\omega t}\right\}}{\partial t}=\Re\{J_0(r)e^{i\omega t}\}. \tag{4.13}$$

4. Through the use of **differential calculus** — the equation is decomposed into real and imaginary parts —, and concentrating on the real part from (4.13) we get

$$\overset{\substack{differential \\ calculus}}{\Longleftrightarrow} \Re\left\{-\frac{1}{r}\frac{\partial}{\partial r}\left(r\nu\frac{\partial A_z(r)}{\partial r}\right)e^{i\omega t}\right\}+\Re\left\{i\omega\sigma A_z(r)e^{i\omega t}\right\}=\Re\{J_0(r)e^{i\omega t}\}. \tag{4.14}$$

5. A bijective **time shift** is applied to (4.14) to provide the imaginary component of the system's response, allowing for a forthcoming employment of both magnitude and phase aspects of the

[1] Phasor calculus represents sinusoidal functions as complex numbers, transforming time-domain Maxwell's equations into frequency-domain algebraic equations for simplified analysis of linear, time-invariant electromagnetic systems with sinusoidal steady-state signals [55].

magnetic vector potential linked to the source current density

$$\overset{t\hookrightarrow t-\frac{\pi}{2\omega}}{\Longleftrightarrow} \Im\left\{-\frac{1}{r}\frac{\partial}{\partial r}\left(r\nu\frac{\partial A_z(r)}{\partial r}\right)e^{i\omega t}\right\}+\Im\left\{i\omega\sigma A_z(r)e^{i\omega t}\right\}=\Im\{J_0(r)e^{i\omega t}\}. \tag{4.15}$$

6. The **combination of real and imaginary formulations** leads to a comprehensive equation that considers both the magnitude and phase of the system's response — this equation, in its simplified form, directly relates the magnetic vector potential A_z with the source current density J_0

$$\overset{(4.14)+i\cdot(4.15)}{\Longrightarrow} -\frac{1}{r}\frac{\partial}{\partial r}\left(r\nu\frac{\partial A_z(r)}{\partial r}\right)e^{i\omega t}+i\omega\sigma A_z(r)e^{i\omega t}=J_0(r)e^{i\omega t}. \tag{4.16}$$

Each step in the previous sequence of six reformulation steps systematically refines and transforms the problem into a form amenable to analytical solution. From Equation (4.16) we get

$$\overset{\cdot e^{-i\omega t}}{\Longleftrightarrow} -\frac{1}{r}\frac{\partial}{\partial r}\left(r\nu\frac{\partial A_z(r)}{\partial r}\right)+i\omega\sigma A_z(r)=J_0(r), \tag{4.17}$$

showcasing the mathematical strategies employed in solving the PDE and/or simulating electromagnetic fields within coaxial cables — this modelling leads further to a series of following equations, each representing different regions within the cable, see Figure 4.1, and their respective boundary conditions. The following set of equations delineates the formulations across these different regions

$$\Longrightarrow \begin{cases} -\frac{1}{r}\frac{\partial}{\partial r}\left(r\frac{\partial A_z(r)}{\partial r}\right)=\mu_0 J_0, & \text{for } r<r_0 \\ -\frac{1}{r}\frac{\partial}{\partial r}\left(r\frac{\partial A_z(r)}{\partial r}\right)=0, & \text{for } r_0<r<r_1 \\ -\frac{1}{r}\frac{\partial}{\partial r}\left(r\nu_2\frac{\partial A_z(r)}{\partial r}\right)+i\omega\sigma_2 A_z(r)=0, & \text{for } r_1<r<r_2 \\ H_\varphi(r)=-\nu\frac{\partial A_z(r)}{\partial r}. & \end{cases} \tag{4.18}$$

Whereas the formulations across different radial distances from the coaxial cable's centre are derived under following specific assumptions.

- **Inside the inner conductor** $(r<r_0)$: The magnetic vector potential $A_z^{(0)}(r)$ and the corresponding magnetic field strength $H_\varphi^{(0)}$ are derived considering the presence of the source current density J_0; the solution reflects the physical behavior of the magnetic fields within the inner conductor.

- **In the insulating region** $(r_0 < r < r_1)$: This region is characterized by the absence of free currents, leading to a simpler form of the magnetic vector potential $A_z^{(1)}(r)$ and magnetic field strength $H_\varphi^{(1)}$; the logarithmic nature of the potential in this region stems from the cylindrical geometry of the problem.

- **Within the outer conductor** $(r_1 < r < r_2)$: Here, the impact of the material's properties, including its conductivity σ_2 and permeability μ_2, on the magnetic vector potential $A_z^{(2)}(r)$ and field strength $H_\varphi^{(2)}$ is considered; the solution involves modified Bessel[2] functions, reflecting the complex behavior in this conductive region under alternating currents.

So, a set of equations in (4.18) can be resolved into

$$\Longrightarrow \begin{cases} A_z^{(0)}(r) = -\frac{J_0 r^2 \mu_0}{4} - C_0 \ln(r) - C_5, & \text{for } r < r_0 \\ H_\varphi^{(0)} = \frac{J_0 r}{2}, & \text{for } r < r_0 \\ A_z^{(1)}(r) = C_3 \ln(r) + C_4, & \text{for } r_0 < r < r_1 \\ H_\varphi^{(1)} = -C_3 \frac{1}{r\mu_0}, & \text{for } r_0 < r < r_1 \\ A_z^{(2)}(r) = C_1 \frac{I_0(\xi r)}{I_0(\xi r_2)} + C_2 \frac{K_0(\xi r)}{K_0(\xi r_2)}, & \text{for } r_1 < r < r_2 \\ H_\varphi^{(2)}(r) = -C_1 \nu_2 \xi \frac{I_1(\xi r)}{I_0(\xi r_2)} + C_2 \nu_2 \xi \frac{K_1(\xi r)}{K_0(\xi r_2)}, & \text{for } r_1 < r < r_2 \\ |A_z(0)| < \infty \\ A_z^{(0)}(r_0) = A_z^{(1)}(r_0) \\ H_\varphi^{(0)}(r_0) = H_\varphi^{(1)}(r_0) \\ A_z^{(1)}(r_1) = A_z^{(2)}(r_1) \\ H_\varphi^{(1)}(r_1) = H_\varphi^{(2)}(r_1) \\ A_z^{(2)}(r_2) = 0, \end{cases} \tag{4.19}$$

with the Helmholtz[3] constant $\xi \coloneqq (1+i)/\delta$, where $\delta \coloneqq \sqrt{2/\omega\mu_2\sigma_2}$ is the *skin depth* of the tube region.

[2] Friedrich Wilhelm Bessel (*22 July 1784 in Minden, Minden-Ravensberg, Holy Roman Empire; †17 March 1846 in Königsberg, Kingdom of Prussia) was a German mathematician, astronomer, and geodesist, best known for his work in astronomy on the parallax of 61 Cygni, which allowed for the determination of the distance from the Earth to a star. His contributions to mathematics include the development of Bessel functions, critical for the solutions of certain differential equations with applications in physics and engineering.

[3] Hermann von Helmholtz (*31 August 1821 in Potsdam, Kingdom of Prussia; †8 September 1894 in Charlottenburg, German Empire) was a German physicist and physician, renowned for his contributions to the understanding of the conservation of energy, electrodynamics, thermodynamics, and acoustics. His work laid foundational principles for the fields of biomechanics and visual and auditory perception, influencing both science and philosophy.

I_α and K_α are zeroth-order modified Bessel functions of the first and second kind, respectively. Furthermore, the continuity conditions at the boundaries between different regions ensure the physical feasibility of the solution, as follows.

- The continuity of the magnetic vector potential and magnetic field strength across the interfaces at $r = r_0$ and $r = r_1$ leads to a set of equations for determining the constants C_0, C_1, C_2, C_3, C_4, and C_5.

- The Helmholtz constant ξ, related to the skin depth δ, plays a key role in describing the eddy current, the electromagnetic field's penetration into the outer sheath.

Solving (4.19) leads to

$$
\Longrightarrow \begin{cases}
A_z^{(0)}(r) = -\frac{J_0 r^2 \mu_0}{4} - C_5, & \text{for } r < r_0 \\
H_\varphi^{(0)}(r) = \frac{J_0 r}{2}, & \text{for } r < r_0 \\
A_z^{(1)}(r) = C_3 \ln(r) + C_4, & \text{for } r_0 < r < r_1 \\
H_\varphi^{(1)}(r) = -C_3 \frac{1}{r\mu_0}, & \text{for } r_0 < r < r_1 \\
A_z^{(2)}(r) = C_1 \frac{I_0(\xi r)}{I_0(\xi r_2)} + C_2 \frac{K_0(\xi r)}{K_0(\xi r_2)}, & \text{for } r_1 < r < r_2 \\
H_\varphi^{(2)}(r) = -C_1 \nu_2 \xi \frac{I_1(\xi r)}{I_0(\xi r_2)} + C_2 \nu_2 \xi \frac{K_1(\xi r)}{K_0(\xi r_2)}, & \text{for } r_1 < r < r_2 \\
C_1 = -C_2, & \\
C_2 = \left(\left(\frac{I_1(\xi r_1)}{I_0(\xi r_2)} + \frac{K_1(\xi r_1)}{K_0(\xi r_2)} \right) \nu_2 \xi \right)^{-1} \frac{J_0 r_0^2}{2 r_1}, & \\
C_3 = -\frac{J_0 r_0^2 \mu_0}{2}, & \\
C_4 = C_2 \left(\frac{I_0(\xi r_1)}{I_0(\xi r_2)} - \frac{K_0(\xi r_1)}{K_0(\xi r_2)} \right) + \frac{J_0 r_0^2 \mu_0}{2} \ln(r_1), & \\
C_5 = -\frac{J_0 r_0^2 \mu_0}{4} + \frac{J_0 r_0^2 \mu_0}{2} \ln(r_0) - C_4. &
\end{cases} \tag{4.20}
$$

Upon computing the Bessel functions I_α and K_α, we determine the constants C_i for $i = 1, 2, 3, 4, 5$, enabling the calculation of A_z and H_φ across the three specified radial domains. The final step to obtain the analytical solution for the desired cable modelling involves transitioning back to the time domain — this is achieved by multiplying the frequency domain solutions by $\exp(i\omega t)$ and taking the real part, thus capturing the electromagnetic fields' temporal behavior across these domains.

4.1.3 Model Parameters

This section outlines explicitly the particular parameters and configuration of a cylindrical tube model, illustrated in Figure 4.1. The model features a conducting wire within a pipe, characterized by distinct material properties and geometric dimensions [41] , and consists of a straight cylindrical tube, with a

Table 4.1: Overview of Model Parameters and Material Properties

Parameter	Value/Description
R	Radius of the tube = 0.0254 m
r_0	Radius of the wire = $0.1R$
r_1	Inner radius of the pipe = $0.5R$
r_2	Outer radius of the pipe = R
I_ω	Current amplitude = 100 A
f	Frequency = 50 Hz
ω	Angular frequency = $2\pi f$ rad/s
ν_0, ν_1, ν_2	Reluctivity of regions = $\mu_0^{-1}, \mu_1^{-1}, \mu_2^{-1}$ respectively
μ_0, μ_1	Permeability of the wire and air = 795774.71545948^{-1} H/m
μ_2	Permeability of the tube = $1000\mu_0$ H/m
σ_2	Conductivity of the tube = 10000000 S/m
$J_0^{(1)}(r)$	Current density in the wire = $^{100}/_{\pi r_0^2}$ A/m^2
$J_0^{(2)}(r), J_0^{(3)}(r)$	Current density in air and tube = 0 A/m^2

conducting wire at its centre carrying a current $I_\omega = 100$, resulting in a current density $J_0^{(1)} = I_\omega/(\pi r_0^2)$ that varies sinusoidally at an angular frequency ω. The wire, with radius $r_0 = 0.00254$, is encased within a pipe characterized by inner and outer radii $r_1 = 0.0157$ and $r_2 = 0.0254$, respectively. Eddy currents in the wire are neglected, implying $\sigma_0 = \sigma_1 = 0$. The intervening space between the wire and the pipe is filled with air. The material properties specified for each region detailed in Table 4.1.

4.1.4 Non-linear Model Formulation

In models of significant practical relevance, the governing relationships of material properties frequently display nonlinear characteristics. A critical aspect to consider, especially within the context of eddy current analysis, is the saturation phenomenon prevalent in magnetic materials — this can be mathematically represented as

$$H = \nu(\|B\|_2)B, \tag{4.21}$$

where $\nu(\cdot)$ denotes a suitable monotonic function characterized by well-established properties, as detailed in [4]. Incorporating this non-linear material behaviour leads to the formulation of a non-linear

version of the eddy current problem

$$\nabla \cdot (\nu(\|\nabla A\|_2)\nabla A_z(x,y,t)) + \sigma \frac{\partial A_z(x,y,t)}{\partial t} = J_{s,z}. \tag{4.22}$$

The operator exhibits a specific form of non-linearity, which is influenced by the derivative of the variable under consideration, reminiscent of the well-known p-Laplace equation [41].

4.1.5 Numerics of QMGRIT

For a brief discussion on FEM see Appendix B. In our exploration, we look into the testing of varying γ in the γ-QMGRIT algorithm. Specifically, we employ a three-grid γ-QMGRIT and γ-QMGRIT FAS algorithms complemented by a standard FCF-relaxation strategy. The algorithms are applied to a $2D + 1D$ model problem, utilizing FEM on a triangulated spatial domain. This problem incorporates partially equal to zeros jumping coefficients and employs BE methods for spatial and temporal dimensions, respectively. Thus navigating the challenges of a differential-algebraic equation system.

Linear Problem

Table 4.2 quantifies the impact of changing the electrical conductivity, σ_2, and the number of coarse EW iterations, γ, on computational efficiency. We clarify that the conductivity in other regions, i.e., σ_0 and σ_1, is unchanged with the details presented in Table 4.1. We present the number of iterations required to achieve a tolerance of 10^{-5}, underlining the interaction between σ_2 and γ. On the leftmost column of the table, we list σ_2 values. The remaining columns enumerate the needed iterations required to reach this tolerance for an array of γ values ranging between 1 and 32. We observe a constant trend: as σ_2 increases, the number of iterations to achieve the tolerance also increases. On the other hand, for each value of σ_2, as γ increases, we observe that the number of iterations required decreases. This observation accentuates that changing the number of coarse EW iterations has a impactful change on the computational performance, especially as σ_2 increases.

Parallelization Result

Figure 4.2 depicts the strong scaling performance of the 65-QMGRIT algorithm with a tolerance of 10^{-5} for a spatial-temporal problem. The x-axis consists of cores with numbers from 2^1 to 2^8, and the y-axis consists of the time to solve in seconds (on a log scale). The graph shows two lines, the

Table 4.2: Iterations required to achieve tolerance across varying σ_2 and γ values

σ_2 \ γ	1	2	4	8	16	32
1.0e+05	6	5	5	5	5	5
3.2e+05	13	6	5	5	5	5
1.0e+06	37	18	10	5	4	4
3.2e+06	102	50	26	13	7	4
1.0e+07	291	139	71	36	18	9

65-QMGRIT line, and what we term the *ideal* scaling line — the ideal scaling line is what the solver would achieve if it had a doubling of the number of cores and that halved the solve time. The 65-QMGRIT line decreases rapidly and tracks with the ideal scaling line perfectly when the numbers of cores increase from 2^1 to 2^4. This indicates that the strong scaling performance is very good, i.e., as the users adds more cores, the solver is making efficient use of the extra cores, and they will observe a direct speedup in the amount of time. As the number of cores continues to increase from 2^4 to 2^8, there is still a decrease in time to solve; however, it decreases less rapidly than when increasing from 2^1 to 2^4. This is a common behavior in parallel algorithms because running a larger number of cores does increase the communication overhead, and it will become increasingly more difficult to evenly balance the amount of work. Even though when the we add more cores past approximately 24, and the 65-QMGRIT line deviates from the ideal scaling line, the 65-QMGRIT algorithm still enables a pretty good amount of scaling and speedup. The time needed to solve the problem is reduced from approximately 2^{15} seconds on 2^1 cores to about 2^9 seconds on 2^8 cores — a significant decrease in the time needed to solve the problem. In all, the figure demonstrates the strong scaling behavior of the 65-QMGRIT algorithm showing good performance and speedup up to 2^4 cores, and continued scaling, though at a more gradual pace, as the number of cores increases. The simulations were conducted on an Intel Xeon Phi Cluster consisting of four 1.4 GHz Intel Xeon Phi processors.

Non-linear Problem

In Table 4.3, analogously to the linear problem, the computational efficiency for non-linear scenarios is catalogued meticulously in terms of changes of electrical conductivity, σ_2, and the number of coarse EW iterations, γ. The conductivity values for the other regions, outlined in Table 4.1, are kept constant to ensure a consistent basis for comparison. The table details the iterations to satisfy a tolerance level of 10^{-5} for each region, illustrating how σ_2 and γ are related. The first column represents various σ_2 values that were investigated, and the following columns account for the number of iterations necessary

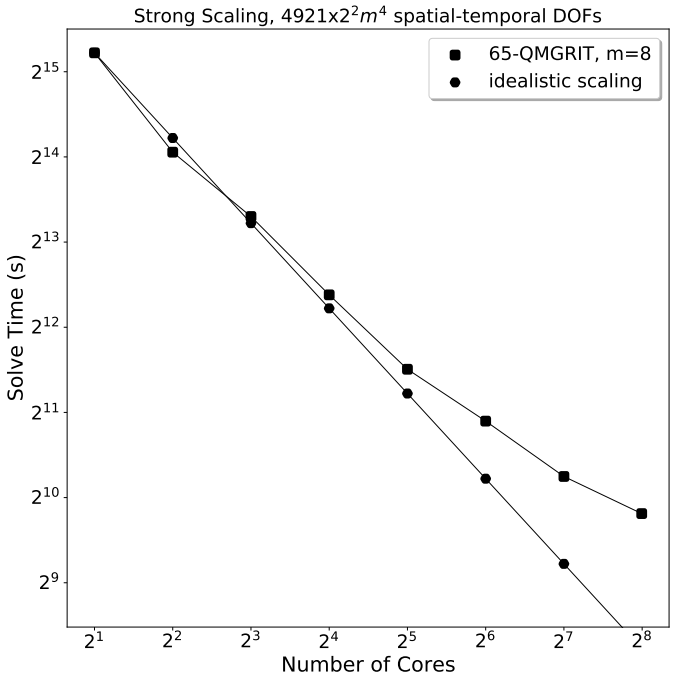

Figure 4.2: Scaling results with the five-grid 65-QMGRIT and tolerance 10^{-5}

to satisfy the defined tolerance for a range of γ, from 1 to 32. From the data represented, there is again a noticeable trend. A higher σ_2 value required more iterations to satisfy the tolerance, which was also the case for linear constellation. For increasing values of γ, a lower number of iterations were necessary for each corresponding σ_2 value investigated — the significance of γ in being able to lower the iteration count with a higher σ_2 value in a non-linear calculation is therefore noteworthy.

Table 4.3: Iterations required to achieve tolerance across varying σ_2 and γ values in non-linear computations

σ_2 \ γ	1	2	4	8	16	32
1.0e+05	6	4	4	4	4	4
3.2e+05	14	7	4	4	4	4
1.0e+06	38	14	10	7	4	4
3.2e+06	57	58	27	10	9	7
1.0e+07	110	163	66	18	23	13

Summing up, firstly used for the cable problem here, the new — in comparison with MGRIT — intrinsic algorithmic leverage parameter, γ, which is based on the periodic iterative EW routine for solving the coarse grid problem, provides a powerful tool for leveraging the convergence performance

of QMGRIT.

4.2 Electrical Machine

We approach a challenging problem from the industrial engineering discourse, extensively studied in recent years using PinT methods. Therefore, we note only briefly the consideration to a generalization of the Coaxial Cable Problem application, a coupled equations system, which we will now introduce in the forthcoming section. For more details, refer to [64, 65, 115, 116], and especially [66].

4.2.1 Numerical Experiments with QMGRIT and Machine — Speedup

In this section, we consider the governing parabolic PDE coupled with two kinematic equations for a squirrel-cage induction motor steady-state modelling. We demonstrate the advantage of the algorithmic non-invasiveness, parallel scalability, and high accuracy of the novel QMGRIT scheme in a modern industrial task. We use an external 3kW four-pole electric machine model 'im_3_kw', as illustrated in Figure 4.3, whose definition assumes a two-dimensional vector potential formulation of a magnetic field problem [24] — it means we consider a simplification of Maxwell's equations so that only the components of the current respectively induction densities orthogonal to a machine's spatial two-dimensional cross-section respectively the machine's shaft are taken into account [57, 107]. The two kinematic equations with the periodic boundary condition in time are

$$\theta_t = \nu \quad \text{and} \quad I\nu_t + C\nu + \kappa\theta = T(\mathbf{u}), \tag{4.23}$$

where θ and ν is the rotor angular displacement and the rotor angular velocity, respectively, I the moment of inertia, C and κ the friction and the torsion coefficient, respectively, $\mathbf{u} \in \mathbb{R}^n$ is the vector of (line-integrated) magnetic vector potentials, and T is the mechanical excitation given by the magnetic field. The no-load condition is considered levying the periodic operation of the motor [6, 47]. Our QMGRIT and QMGRIT FAS implementations extend an existing, efficient construction of the MGRIT algorithm applied to the non-invasive machine simulation in the Python package PyMGRIT [63]; whereas the non-invasive time step calculations are carried out utilizing an external, widely tunable library GetDP [25, 54], which is a FEM solver adapted for an integration in time with the BE

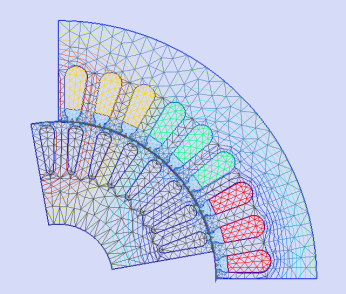

Figure 4.3: Mesh view of the four-pole induction motor from the GetDP library [54]

method. As a stopping criterion we consider the Euclidean[4] norm of a space-time residual of the main electrical machine characteristics, Joule[5] losses and rotor torque, less than 10^{-3}. The following tests were performed on an Intel Xeon Phi cluster consisting of four 1.4 GHz Intel Xeon Phi processors. In an invasive manner, similar work was done in [3]. We inspect the model problem settings with linear reluctivity and represent results in Figure 4.4 and in Figure 4.5. The calculation shows that the

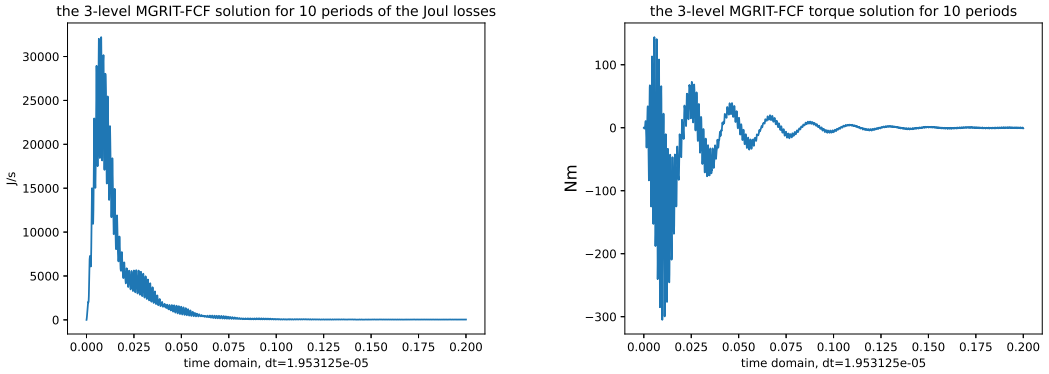

(a) The Joule losses solution discretized in time

(b) The rotor torque solution discretized in time

Figure 4.4: The electrical machine behaviour discretized in time with a (biased) representation on the steady-state simulation by the 10th period

time-stepping solution reaches the periodic solution at the 19th period. Table 4.4 lists experiments on speedup with three-grid QMGRIT solvers for the model problem discretized on a space-time grid of size 4449×1024 coarsing by $m_0 = m_1 = 8$ in time; whereas the periodic Parareal, PP-IC [46], respectively

[4] Euclid (*circa 300 BCE in Alexandria, Ptolemaic Egypt) was an ancient Greek mathematician often referred to as the "father of geometry." His most famous work, "Elements," is a comprehensive compilation of geometry knowledge of his time and has been one of the most influential works in the history of mathematics; his systematic approach and axiomatic method have laid the foundations for modern mathematical rigour and logical reasoning.

[5] James Prescott Joule (*24 December 1818 in Salford, Lancashire, England; †11 October 1889 in Sale, Cheshire, England) was an English physicist and brewer, best known for his research in thermodynamics and for establishing the mechanical equivalent of heat. His discoveries led to the development of the first law of thermodynamics and laid the foundation for the modern field of energy conservation.

the time-stepping, the MGRIT, and the Parareal [83] solves are performed on a space-time grid of size 4449×1024 respectively 4449×19456. Table 4.4 provides an in-depth comparison of the performance improvements achieved through various configurations of the MGRIT and QMGRIT algorithms. The analysis concentrates on the speedup in time to the periodic solution for the machine model, utilizing a discretized space-time grid and harnessing the computational power of an Intel Xeon Phi cluster.

Table 4.4: When modelling the steady-state of the machine, we show a speedup in time-to-solution compared to the periodic solution. We compare the algorithms MGRIT and QMGRIT, respectively, with time-stepping applied to the model discretized on a space-time grid of size 4449×19456 and 4449×1024. Tests were performed on an Intel Xeon Phi Cluster consisting of four 1.4 GHz Intel Xeon Phi processors.

Algorithm	1-level **Time step** 1 processor	two-grid **Parareal** 128 processors	two-grid **Per. Parareal** 128 processors	two-grid **Per. Parareal** 32 processors	three-grid **MGRIT** 128 processors	three-grid **MGRIT** 128 processors
Coarsing	-	$m_0 = 152$	$m_0 = 8$	$m_0 = 32$	$m_0 = 8, m_1 = 8$	$m_0 = 152, m_1 = 8$
Speedup *in time to the periodic solution*	1	2.98	4.39	9.16	1.68	2.26

Algorithm	1-level **Time step** 1 processor	three-grid **1-QMGRIT** 128 processors	three-grid **2-QMGRIT** 128 processors	three-grid **3-QMGRIT** 128 processors	three-grid **4-QMGRIT** 128 processors
Coarsing	-	$m_0 = m_1 = 8$	$m_0 = m_1 = 8$	$m_0 = m_1 = 8$	$m_0 = m_1 = 8$
Speedup *in time to the periodic solution*	1	8.48	12.05	13.74	14.63

Key insights. The Table 4.4 showcases the effectiveness of the MGRIT and QMGRIT algorithms in accelerating the time to reach a periodic solution in computational models.

- The transition from traditional time-stepping (1 processor) to a two-grid Parareal [83] approach on 128 processors yields a speedup factor of **2.98**, demonstrating the basic efficiency of parallel solving.
- Implementing PP-IC [46] with optimal coarsening strategies, where the number of coarse time intervals equals the number of processors ($m_0 = 32$ for 32 processors and $m_0 = 8$ for 128 processors), significantly improves performance. However, the speedup factor of **9.16** on 32 processors is notably higher than the speedup factor of **4.39** on 128 processors. This difference is due to the increased communication overhead and reduced workload per processor when using more processors, potentially limiting the algorithm's scalability — these findings suggest the necessity of multi-grid development, which allows for simultaneous calculations on multiple levels or grids, enabling feasible scalability on a larger number of processors.
- The introduction of a third level in the algorithm further improves the speedup, with the three-

grid 1-QMGRIT configuration achieving an **8.48** speedup factor. This improvement is even more pronounced in configurations with enhanced γ-QMGRIT strategies, $\gamma = 2, 3, 4$, culminating in a **14.63** speedup factor for the three-grid 4-QMGRIT setup. The results are again underlining the importance of QMGRIT's algorithmic parameter γ.

Increased speeds were observed when quantized multi-grid strategies and processor mapping were used in HPC environments. The process reconstitution and processor configuration uncovered by the QMGRIT algorithm show promise in improving the overall time for solving large problems.

Remark 4.1. *In general, our experiments with results on speedup provide neither a minimum nor a maximum of the speedup. First, because there is ample reason to debate the fairness of comparison based on the starting constellations for the different approaches, such as the number of additional CF-relaxations, the coarsening factors, the randomness by the initial values or the number of EW relaxations for QMGRIT, the nested iteration application, etc. Second, the load of processors that maximizes the potential for parallelism for both approaches differs not only a priori due to the number of points required to simulate with both approaches at a fixed discretization size, but also depends on a particular parallel architecture and implementation. Therefore, performance modelling may be a part of future research, e.g., see [44, 66].*

Figure 4.5 is used to illustrate a comparison between the QMGRIT solution and the biased seeking of the machine steady-state simulation at the 10th period. Subfigures 4.5a and 4.5b show the Joule loss and the rotor torque solutions, discretized in time, at one period. Subfigure 4.5c shows the periodical rotor torque and Joule loss solutions, discretized in time for one period. For the steady-state simulation of the electrical machine at the 10th periods, the bias is considerable, as can be observed visually. To achieve a QMGRIT solution, the MGRIT algorithm requires more or fewer periods depending on the predefined tolerance and material parameter settings. When considering linear material parameters, the MGRIT algorithm requires 19 periods to reach a tolerance of 10^{-3}, as stated in Figure 4.5, and 26 periods to reach a tolerance of 10^{-5}. Considering non-linear material parameters, the MGRIT algorithm requires 16 periods to reach a tolerance of 10^{-3} and 22 periods to reach a tolerance of 10^{-5}. These findings underline the critical importance of choosing the *right number* of periods a priori, when modelling with the MGRIT algorithm to obtain accurate periodic solutions. The QMGRIT algorithm does well in the simulation of the true steady-state behavior of the electrical machine, dealing a priori with the only one period, thus overcoming the limitation of simulations over some fixed amount of periods with MGRIT.

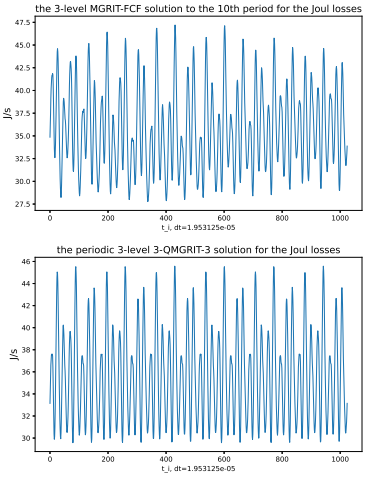

(a) Joule losses solutions of MGRIT (top, 10th period) and QMGRIT (bottom) discretized in time to one period

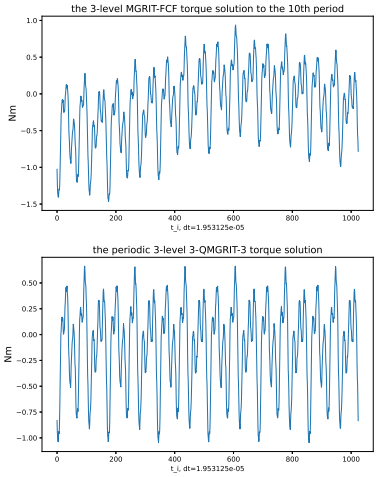

(b) Rotor torque solutions of MGRIT (top, 10th period) and QMGRIT (bottom) discretized in time to one period

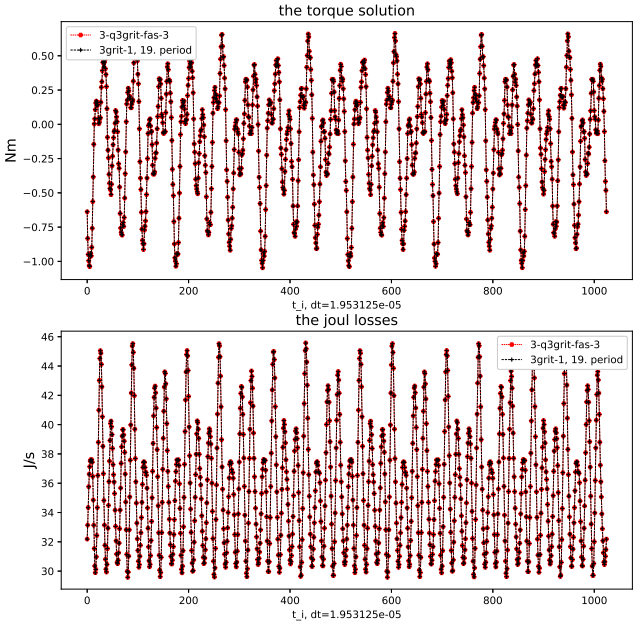

(c) Periodic rotor torque and Joule losses solutions obtained by QMGRIT

Figure 4.5: Comparison of MGRIT and QMGRIT solutions: the machine's steady-state simulation at the 10th vs. 19th period vs. periodic QMGRIT solution

4.3 Convection-Diffusion-Decay Equation

Building on the discussion of Section 3.1.5, we address the following topic: the convergence behavior analysis of the multi-grid method.

4.3.1 Multi-grid Convergence

This section presents a convergence comparison between numerical convergence and analytical convergence for each of the two-grid and three-grid approaches. We examine the convergence factors that arise from QMGRIT, as well as the convergence factors obtained from an analytical convergence analysis for two-grid and three-grid (explicitly calculating the eigenvalues of the three-grid iteration operator) approaches; these four tables are presented in Tables 4.5 and 4.6 for the two-grid and in Tables 4.7 and 4.8 for the three-grid specifically. This comparison allows us to determine the correspondence

Table 4.5: Two-grid QMGRIT numerical convergence factors for diagonal $N_t = N_x$ and different parameters $D = \nu = \lambda$

$N_t = N_x$	$D = \nu = \lambda = 0.1$	$D = \nu = \lambda = 1$	$D = \nu = \lambda = 10$
$2^4 = 16$	3.05e-01	4.92e-02	8.59e-04
$2^5 = 32$	2.92e-01	8.08e-02	4.01e-03
$2^6 = 64$	2.92e-01	8.86e-02	1.49e-02

Table 4.6: Two-grid QMGRIT analytical convergence factors for diagonal $N_t = N_x$ and different parameters $D = \nu = \lambda$

$N_t = N_x$	$D = \nu = \lambda = 0.1$	$D = \nu = \lambda = 1$	$D = \nu = \lambda = 10$
$2^4 = 16$	3.05e-01	4.94e-02	8.69e-04
$2^5 = 32$	2.95e-01	8.14e-02	4.11e-03
$2^6 = 64$	2.92e-01	8.96e-02	1.49e-02

Table 4.7: Three-grid QMGRIT numerical convergence factors for diagonal $N_t = N_x$ and different parameters $D = \nu = \lambda$

$N_t = N_x$	$D = \nu = \lambda = 0.1$	$D = \nu = \lambda = 1$	$D = \nu = \lambda = 10$
$2^4 = 16$	3.30e-01	4.93e-02	8.94e-04
$2^5 = 32$	2.86e-01	7.04e-02	4.59e-03
$2^6 = 64$	2.70e-01	1.06e-01	1.70e-02

between the numerical results and the expected behavior of the analytical results, and evaluates how well QMGRIT can solve the convection-diffusion-decay equation.

Table 4.8: Three-grid QMGRIT analytical convergence factors for diagonal $N_t = N_x$ and different parameters $D = \nu = \lambda$

$N_t = N_x$	$D = \nu = \lambda = 0.1$	$D = \nu = \lambda = 1$	$D = \nu = \lambda = 10$
$2^4 = 16$	3.30e-01	5.13e-02	9.32e-04
$2^5 = 32$	2.87e-01	7.08e-02	4.69e-03
$2^6 = 64$	2.70e-01	9.90e-02	1.74e-02

Open Problem 1. ***Objective: The convection-diffusion-decay equation with periodic boundary conditions of the first type — pure boundary value problem on a semi-infinite domain [84].*** *In this open problem, our attention is drawn to the exploration of Equation (4.24), particularly with in Equation (4.25) — on contrary to Equations (3.45)-(3.47) — posited periodic boundary value conditions (that alternatively may be seen as time-periodic initial value conditions in spatial dimension). Our interests continue with parallel efforts for the wave equation, with a particular interest in applications to medical imaging. The aim of the concern is the Fourier-Poisson-Kelvin problem for diffusion with convection and decay given by the equations*

$$u_t = Du_{xx} - \nu u_x - \lambda u, \qquad x > 0, t \in \mathbb{R}, \tag{4.24}$$

$$u(0,t) = g(t), \qquad g(t+\omega) = g(t), \qquad t \in \mathbb{R}, \tag{4.25}$$

where u represents the concentration of a substance, e.g., such as a drug or a biological marker, moving through a biological medium. This is influenced by dispersion $D > 0$, drift velocity $\nu > 0$, decay $\lambda > 0$, and the function $g(t)$ that is a bounded, continuous function, showing ω-periodicity, which can reflect, e.g., the cyclical nature of biological processes or treatment schedules — in the field of medical science, the equation may play a big role, resolving the dispersion and transport of pharmaceuticals in the human body and the subsequent diffusion processes in tissues. Moreover, modelling the dispersion and magnification of micro-, nano- or macro-particles in biological environments may also play an important role in understanding how these foreign substances could move in cellular environments — these models are essential for drug delivery systems, target therapy, and designing medical treatments that need to control the distribution and concentration of active substances very precisely. An analytical solution exists under specific conditions, presenting a foundation for further exploration within applications, in particular the solution for a bounded, continuous function g on $\mathbb{R}$ is [84]

$$u(x,t) = \frac{2}{\sqrt{\pi}} e^{\nu x/2D} \int_0^\infty e^{-\eta^2 - \frac{(\lambda+\nu^2/4D)x^2}{4D\eta^2}} f\left(t - \frac{x^2}{4D\eta^2}\right) d\eta. \tag{4.26}$$

This suggests that if g is ω-periodic, then so is $c(x,t)$, offering intriguing possibilities for, e.g., cyclic treatment strategies in medical protocols.

Still, when dealing with possibility to solve the equation analytically to be able to apply the solution to a real-world problems, there are considerable computational obstacles when trying to put this theory into practice. As we moved to apply the multi-grid algorithm developed during the research to this specific problem, we discovered that a complex interaction of challenges faced us — despite the fervent effort, best intentions, careful use of available time and resources, we were unable to apply the algorithm successfully. This experience demonstrates the complexity of the problem. It also demonstrates the fact that the current methodology may have limitations under some circumstances. We therefore pose this as an openly, unsolved problem for the community. We are looking for any and all new thoughts, new strategies, and a possible rethinking of the current algorithms, including those suggested in this work. The potential for contributions to medicine from the numerical methodology to solve the convection-diffusion-decay equation with periodic boundary conditions are significant — there is potential for future researchers to see this problem as a pathway for contributing to a field which intersects mathematical models and understanding of complex biological systems.

4.4 Wave Equation

Open Problem 2. *Even with looking at this in great detail the multi-grid method is not completely successful in tackling the discrete, one-dimensional system as presented in Section 3.1.6. Indeed, this is the second open problem in this thesis — we must deal with this instability which does not lend itself to the traditional understanding of numerical solutions to the wave equation as well as a more profound examination of the relationship between discretization approaches and multi-grid methods. In an effort improve upon this, we will moving forward to analyze a two-variable system.*

4.4.1 Two-variable System — Discretization and Numerical Solution

The inhomogeneous wave equation presents a complex model that describes wave dynamics under the influence of external forces. Now, its numerical resolution requires the equation to be expressed as a system of first-order equations, capturing the wave's displacement u and velocity v — these equations

are

$$\frac{\partial u}{\partial t} = v, \tag{4.27}$$

$$\frac{\partial v}{\partial t} = c^2 \nabla^2 u + g(x,t), \tag{4.28}$$

where c denotes the wave speed and $g(x,t)$ the external force. The numerical approach to solving these equations is again rooted in their discretization in both space and time.

Temporal Discretization

Temporal discretization is treated using the BE method. This method necessitates the solution of a system of algebraic equations at each time step, updating the wave function by incorporating the boundary and initial conditions inherent to the wave equation — the updates of the equations for u and v at each time step n using the BE method are given by

$$u_i^{n+1} = u_i^n + \Delta t \cdot v_i^{n+1}, \tag{4.29}$$

$$v_i^{n+1} = v_i^n + \Delta t \cdot \left(c^2 \frac{u_{i+1}^{n+1} - 2u_i^{n+1} + u_{i-1}^{n+1}}{\Delta x^2} + g(x_i, t_{n+1}) \right). \tag{4.30}$$

Discrete Laplacian Operator and Spatial Discretization

The spatial domain is discretized into a finite grid, leading to the approximation of spatial derivatives using FD. The discrete Laplacian operator $\mathcal{O}$, which arises from the central difference approximation of the second spatial derivative, is constructed as

$$\mathcal{O} = \frac{1}{\Delta x^2} \begin{bmatrix} -2 & 1 & 0 & \cdots & 0 & 0 \\ 1 & -2 & 1 & \cdots & 0 & 0 \\ 0 & \ddots & \ddots & \ddots & \vdots & \vdots \\ \vdots & \cdots & 1 & -2 & 1 & 0 \\ 0 & \cdots & 0 & 1 & -2 & 1 \\ 0 & \cdots & 0 & 0 & 1 & -2 \end{bmatrix}. \tag{4.31}$$

Moreover, the second-order spatial derivative incorporating the time-stepping for the two-variable wave equation can be discretized using FD schemes, yielding a tridiagonal matrix

$$M = \begin{bmatrix} 1 & 0 & 0 & \cdots & 0 & 0 & 0 \\ 0 & -\frac{c^2\Delta t^2}{2\Delta x^2} & 1+\frac{c^2\Delta t^2}{\Delta x^2} & -\frac{c^2\Delta t^2}{2\Delta x^2} & \cdots & \ddots & 0 \\ 0 & 0 & \ddots & \ddots & \ddots & \ddots & \vdots \\ 0 & \vdots & \cdots & -\frac{c^2\Delta t^2}{2\Delta x^2} & 1+\frac{c^2\Delta t^2}{\Delta x^2} & -\frac{c^2\Delta t^2}{2\Delta x^2} & 0 \\ 0 & 0 & \cdots & 0 & 0 & 0 & 1 \end{bmatrix}, \tag{4.32}$$

where Δx is the spatial step size, and c is the wave speed. Note that the boundary conditions are applied to the first and last rows, ensuring that the operator does not apply beyond the computational domain.

Construction of the Time-Stepping Block Matrix

For the two-variable time-stepping routine, a 2×2 block matrix F is constructed, enabling the simultaneous update of the displacement u and the velocity v. The matrix F is explicitly defined in terms of its sub-matrices as follows

$$F = \begin{bmatrix} F_u & \Delta t \cdot F_u \\ F_v & I + \Delta t \cdot F_v \end{bmatrix}, \tag{4.33}$$

where

$$F_u = M^{-1}, \tag{4.34}$$

with M being the matrix arising from the discretization of the second-order spatial derivatives of u, incorporating the wave speed c and time step Δt. The matrix F_v is defined as

$$F_v = c^2 \cdot \Delta t \cdot \mathcal{O} \cdot F_u, \tag{4.35}$$

which incorporates the acceleration term due to the spatial variation of the displacement field and the external force represented by the discrete Laplacian operator $\mathcal{O}$. To apply the Dirichlet boundary conditions, a diagonal matrix D_{BC} is constructed with ones on the diagonal, except for the entries corresponding to the boundary nodes, which are set to zero. The modified time-stepping block matrix $\tilde{F}$ incorporating the boundary conditions is then obtained by

$$\tilde{F} = D_{BC} \cdot F. \tag{4.36}$$

The assembly of matrix $\tilde{F}$ facilitates the update of both displacement and velocity fields within each time step, ensuring that the iterative solver captures dynamics of the inhomogeneous wave equation while satisfying the prescribed Dirichlet boundary conditions. The one-grid solution results, as presented in Table 4.9, provide a baseline for evaluating the possible performance of the multi-grid algorithm — the table compares the numerical and predicted convergence factors for different problem sizes, ranging from $N_t = N_x = 2^4$ to 2^{10}. The close agreement between the numerical and predicted values indicates the accuracy of the theoretical analysis and serves as a foundation to assess the possible efficiency gains achieved through the multi-grid approach.

Table 4.9: EW results for $N_t = N_x$ and $c = 1$

$N_t = N_x$	Error	Numerical Convergence Factor	Predicted Convergence Factor
$2^4 = 16$	1.18e-01	8.71e-01	8.59e-01
$2^5 = 32$	6.37e-02	9.22e-01	9.26e-01
$2^6 = 64$	3.25e-02	9.64e-01	9.62e-01
$2^7 = 128$	1.63e-02	9.91e-01	9.81e-01
$2^8 = 256$	8.18e-03	9.91e-01	9.90e-01
$2^9 = 512$	4.35e-03	9.95e-01	9.95e-01
$2^{10} = 1024$	2.05e-03	9.98e-01	9.98e-01

4.4.2 Two-grid Solution

Convergence Overview for $m = 2$

This subsection presents the analysis of convergence behaviour as influenced by the number of coarse-fine smoothing steps within the multi-grid algorithm framework. The CF smoothing steps are helpful in improving the convergence rate, and their optimization is important for the efficiency of the multi-grid solver. Figures 4.6 and 4.7 illustrate the convergence behaviour of the two-grid solution with a coarsening factor of $m = 2$ at discretization levels $N_t = N_x = 2^6$ and 2^7, respectively. The plots compare the numerically obtained convergence factors with the predicted values for different numbers of CF-smoothing steps. The close agreement between the numerical and predicted results validates the accuracy of the convergence prediction model in Theorem 3.76 and accentuates the limited effectiveness of the observed CF-smoothing steps number in reducing the error at both resolution levels.

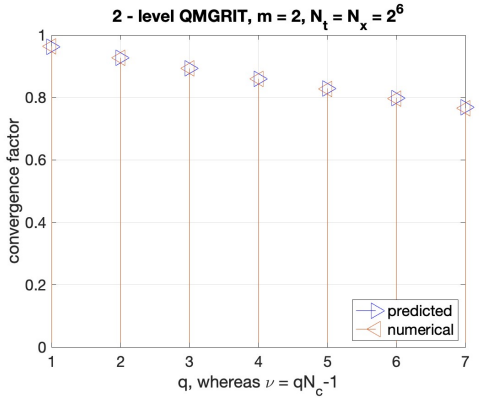

Figure 4.6: Convergence factor review for a coarsening factor $m = 2$ at discretization level $N_t = N_x = 2^6$. The plot displays the convergence factors obtained with different numbers of CF-smoothing steps. The numerical results are juxtaposed with the predicted outcomes, indicating the efficacy of each smoothing step count. The alignment between numerical and predicted data points suggests that the model used to predict convergence factors is accurate for this number of smoothing steps at the given discretization level.

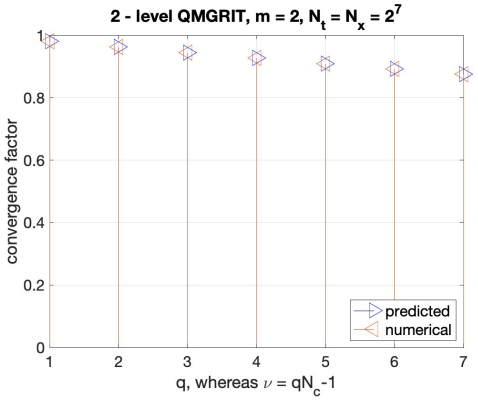

Figure 4.7: Convergence factor review for a coarsening factor $m = 2$ at a higher discretization level $N_t = N_x = 2^7$. The plot similarly compares the numerical and predicted convergence factors as the number of CF-smoothing steps varies. Consistency between numerical and predicted values is observed, indicating that the solver's performance is limitedly maintained when increasing the discretization points, but this suggests also that the increasing the CF-smoothing steps may improve relaxation of the error at both levels of discretization.

Convergence Overview for $m = 4$

This subsection examines how varying the number of CF-smoothing steps affects the convergence factors at a coarsening factor of $m = 4$. Figures 4.8 and 4.9 present the convergence analysis for a coarsening factor of $m = 4$ at discretization levels $N_t = N_x = 2^6$ and $N_t = N_x = 2^7$, respectively. The plots compare the numerically obtained convergence factors with the predicted values across a range of CF-smoothing steps, when applying the results from Theorem 3.7. The close agreement between the numerical results and predictions, even at the bigger coarsing factor, demonstrates the robustness of the solver and its ability to maintain efficiency with an increased coarsening — these findings may provide guidance for selecting the number of CF-smoothing steps to achieve decent convergence at different discretization scales.

Tabulated Data

Table 4.10 presents the convergence factors obtained from the two-grid solution for various problem sizes $N_t = N_x$, numbers of CF smoothing steps ν, and EW iterations γ. The results demonstrate the impact of these parameters on the convergence behaviour of the multi-grid solver. As the problem size increases, the convergence factors tend to approach unity, indicating slower convergence rates.

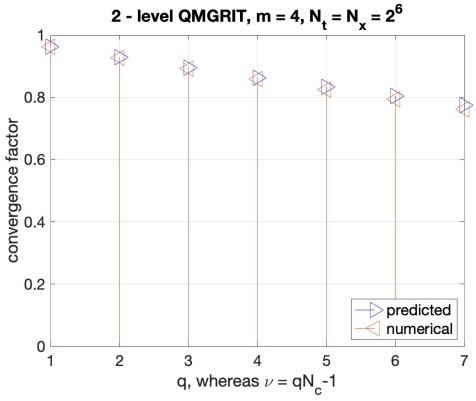

Figure 4.8: Convergence factor review with $m = 4$ and discretization level $N_t = N_x = 2^6$. The plot compares the convergence factors obtained numerically with respect those predicted across a range of CF-smoothing steps. The close correspondence between the numerical results and predictions at this level of discretization indicates that the prediction model is reliable. The variance in convergence factors with different CF-smoothing step counts may provide valuable information for selecting the most efficient number of steps to optimize convergence.

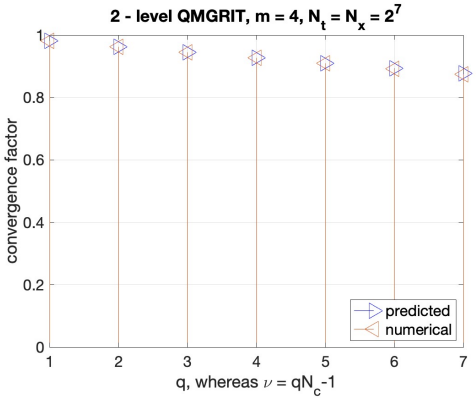

Figure 4.9: Convergence factor review with $m = 4$ at a higher discretization level $N_t = N_x = 2^7$. Here, the numerical and predicted convergence factors are also compared as the CF-smoothing steps vary. Despite the finer discretization, the results do not deviate from the predictions, suggesting that the solver maintains its efficacy with an increased number of smoothing steps according to the theoretical results. This underlines the robustness of the solver and may help to determine the necessary number of CF-smoothings for feasible convergence at different discretization scales.

Increasing the number of CF smoothing steps and EW iterations generally leads to improved convergence factors, especially for larger problem sizes. These findings stress the importance to carefully seek further and select the algorithmic parameters optimizing the performance of the solver for the wave equation.

Table 4.10: Results of a two-grid solutions for $N_t = N_x$ of the wave equation with different number of CF-smoothings and EW iterations, $m = 2$

$N_t = N_x$	$\gamma = 1$			$\gamma = 2$			$\gamma = 5$		
	$\nu = 1$	$\nu = 2$	$\nu = 5$	$\nu = 1$	$\nu = 2$	$\nu = 5$	$\nu = 1$	$\nu = 2$	$\nu = 5$
$2^6 = 64$	8.79e-01	8.85e-01	9.04e-01	8.34e-01	8.32e-01	8.30e-01	6.03e-01	6.08e-01	6.01e-01
$2^7 = 128$	9.31e-01	9.34e-01	9.39e-01	9.09e-01	9.08e-01	9.06e-01	7.65e-01	7.68e-01	7.68e-01
$2^8 = 256$	9.63e-01	9.64e-01	9.66e-01	9.51e-01	9.51e-01	9.50e-01	8.70e-01	8.71e-01	8.71e-01

4.4.3 Three-grid and Four-grid Solutions

Table 4.11 presents the convergence factors obtained from the three-grid solution for various problem sizes, numbers of CF-smoothing steps, and EW iterations. Compared to the two-grid solution, the three-grid approach generally exhibits improved convergence factors, especially for larger problem sizes and higher numbers of CF-smoothing steps and EW iterations — this improvement in

convergence behaviour can be attributed to the additional level of coarse-grid correction introduced by the three-grid scheme, which further reduces the low-frequency error components and accelerates the total convergence rate. Table 4.12 presents the convergence factors obtained from the four-grid

Table 4.11: Three-grid, Convergence Factors for Various Parameters, $N_t = N_x$, $m = 2$

$N_t = N_x$	$\gamma = 1$			$\gamma = 2$			$\gamma = 5$		
	$\nu = 1$	$\nu = 2$	$\nu = 5$	$\nu = 1$	$\nu = 2$	$\nu = 5$	$\nu = 1$	$\nu = 2$	$\nu = 5$
$2^6 = 64$	8.06e-01	8.47e-01	9.46e-01	6.98e-01	6.89e-01	6.81e-01	5.61e-01	5.25e-01	4.94e-01
$2^7 = 128$	8.93e-01	8.88e-01	9.37e-01	8.23e-01	8.20e-01	8.16e-01	6.37e-01	6.17e-01	6.23e-01
$2^8 = 256$	9.40e-01	9.38e-01	9.36e-01	9.02e-01	9.02e-01	9.00e-01	7.62e-01	7.59e-01	7.51e-01

solution for various problem sizes, numbers of CF-smoothing steps, and EW iterations. The four-grid approach introduces an additional level of coarse-grid correction compared to the three-grid scheme, which could further improve the convergence behaviour, especially for larger problem sizes — but the improvement in convergence factors is not pronounced, as by the transition from two-grid to three-grid solutions, suggesting a diminishing return in performance as the number of grid levels increases. The results from the three-grid and four-grid solutions demonstrate limited effectiveness of multi-grid

Table 4.12: Four-grid, Convergence Factors for Various Parameters, $N_t = N_x$, $m = 2$

$N_t = N_x$	$\gamma = 1$			$\gamma = 2$			$\gamma = 5$		
	$\nu = 1$	$\nu = 2$	$\nu = 5$	$\nu = 1$	$\nu = 2$	$\nu = 5$	$\nu = 1$	$\nu = 2$	$\nu = 5$
$2^6 = 64$	8.30e-01	9.28e-01	6.75e-01	7.64e-01	7.02e-01	6.15e-01	7.54e-01	6.28e-01	5.69e-01
$2^7 = 128$	9.02e-01	8.89e-01	9.68e-01	8.13e-01	8.14e-01	7.84e-01	7.84e-01	7.21e-01	6.91e-01
$2^8 = 256$	9.41e-01	9.37e-01	9.48e-01	8.92e-01	8.84e-01	8.69e-01	8.12e-01	7.71e-01	7.69e-01

methods in accelerating the convergence of the wave equation solver. The incorporation of multiple coarse-grid correction levels may allow for efficient reduction of low-frequency error components, leading to faster convergence rates — but the optimal choice of the number of grid levels may depend on the specific problem size and the desired balance between convergence speed and computational complexity.

4.4.4 Four-grid and Five-grid Solutions — Achieving a 'Convenient' Convergence Factor at the Cost of High Computational Overhead

The search for higher rates of convergence in multi-grid can often lead investigators to contemplate the prospect of looking at even higher levels of grid hierarchy. This subsection covers this area of exploration in which we consider convergence performance and computational expense for four-grid and five-grid solutions for the two-variable wave equation. We conduct four-grid and five-grid experiments to understand the scalability and optimality of the method under investigation. Notably, in this study,

we are willing to accept significantly higher computational costs in order to achieve the well desired convergence properties. Furthermore, the calculation of the numerical convergence factor differs from all previous solutions, as it captures all iterations, including the first one (which is usually much better than the converged convergence factor), via the geometric mean of convergence factors between iterations — this approach sets the following analysis apart from our earlier discussions.

Four-grid Solution

Table 4.13 presents the convergence factors obtained from the four-grid solution for various combinations of smoothing steps ν and coarse-grid iterations γ. The results demonstrate a general trend of improving convergence factors with increasing γ and ν. However, it is important to recognize that the computational cost associated with higher values of these parameters can be substantial.

Table 4.13: Convergence factors for the four-grid solution with various smoothing steps ν and coarse-grid iterations γ, $N_t = N_x = 2^8$, $m = 2$; the lowest convergence factor attained is marked in green

γ	Convergence Factors				
	$\nu = 16$	$\nu = 32$	$\nu = 64$	$\nu = 128$	$\nu = 256$
16	5.81e-01	6.19e-01	4.39e-01	3.01e-01	2.00e-01
32	6.37e-01	5.88e-01	4.62e-01	3.19e-01	2.00e-01
64	5.86e-01	5.65e-01	4.72e-01	2.99e-01	1.57e-01
128	6.32e-01	5.32e-01	4.25e-01	3.35e-01	1.79e-01
256	6.26e-01	5.88e-01	4.49e-01	3.70e-01	2.20e-01

Five-grid Solution

Table 4.14 presents the convergence factors obtained from the five-grid solution for various combinations of smoothing steps ν and coarse-grid iterations γ. The results exhibit a similar trend to the four-grid solution, with improving convergence factors as γ and ν increase, but the computational cost associated with the five-grid solution is even higher than that of the four-grid solution. While the four-grid and five-grid solutions demonstrate the potential for achieving 'convenient' convergence factors, it is essential to consider the trade-off between convergence improvement and computational cost. The excessive computational cost associated with these higher-level grid hierarchies, γ, and ν may render them impractical for many applications, particularly those with time-sensitive requirements or limited computational resources. In summary, the multi-grid techniques showcase the ability to achieve improved convergence factors for the wave equation, when leverage with γ and ν — but the pursuit of these improvements comes at the expense of significantly increased computational cost. Further care-

ful consideration must be given to the balance between convergence performance and computational efficiency when selecting the appropriate level of grid hierarchy for a given problem and numbers of EW iterations or CF-relaxations.

Table 4.14: Convergence factors for the five-grid solution with various smoothing steps ν and coarse-grid iterations γ, $N_t = N_x = 2^8$, $m = 2$; the lowest convergence factor attained is marked in green

γ	Convergence Factors				
	$\nu = 16$	$\nu = 32$	$\nu = 64$	$\nu = 128$	$\nu = 256$
16	6.28e-01	6.34e-01	4.51e-01	2.15e-01	1.72e-01
32	7.13e-01	6.29e-01	4.73e-01	2.88e-01	1.05e-01
64	7.26e-01	6.39e-01	4.93e-01	3.40e-01	1.28e-01
128	7.20e-01	6.49e-01	4.61e-01	2.72e-01	1.69e-01
256	7.20e-01	6.33e-01	4.27e-01	2.53e-01	1.29e-01

4.5 Interplay with QMGRIT on GMRES — Empirical Analysis

Yousef Saad[6] and Martin H. Schultz[7] developed the GMRES method in 1986 [104]. The GMRES method is used to solve large, sparse linear systems of equations that are non-symmetric. It is a method that has been successfully used in a wide range of computational applications in applied mathematics and HPC, most notably for its ability to tackle non-symmetric matrices — the algorithm computes an approximation of the solution in a Krylov[8] subspace by minimizing the residual of the equation, providing a sequence of approximate solutions that decrease the residual and refine the solution, while acknowledging the effect of the matrix on the space of possible solutions. The GMRES method can be used with preconditioner, which has become common in modeling time-dependent partial differential equations — the next section discusses preconditioning with QMGRIT and the first studies of the GMRES method using the QMGRIT as preconditioner while looking at the effect of the number of QMGRIT iterations. The investigations of this section will evaluate efficiency, convergence, and accuracy and reason on its potential utility in an HPC environment.

[6] Yousef Saad is a contemporary mathematician and computer scientist, widely recognized for his contributions to numerical linear algebra and iterative methods for solving large-scale linear systems. His work on the development of efficient algorithms, such as the conjugate gradient method and GMRES, has had a significant impact on computational science and engineering.

[7] Martin H. Schultz is an American mathematician known for his pioneering work in the development of sparse matrix technology and iterative methods in numerical linear algebra. His contributions have been fundamental to the advancement of computational methods used in scientific computing and engineering, particularly through his work on the generalized minimal residual method.

[8] Alexey Nikolayevich Krylov (*15 August 1863 in Visyaga, Simbirsk Governorate, Russian Empire; †26 October 1945 in Leningrad, Soviet Union) was a Soviet mathematician, naval engineer, and physicist known for his work in applied mathematics and for the development of methods to solve linear operator equations, leading to what is now known as Krylov subspace methods.

Preconditioning

In this section, we employ a single three-grid QMGRIT iteration as a preconditioner for the GMRES method, utilizing the MATLAB function `gmres`. By applying this preconditioning strategy to a range of problem sizes, with $N_x = N_t$ varying from 2^4 to 2^{10}, we aim to assess its impact on the convergence behavior and computational efficiency of the iterative solver. The results of this investigation are presented in the following Table 4.15, which focuses on the relationship between problem size, preconditioning, and the performance of the GMRES algorithm. The table presents a comparison of

Table 4.15: Time-to-solution performance comparison, pointing out the significant impact of QMGRIT as a preconditioner for GMRES; -1 indicates failing convergence

$N_t = N_x$	2^4	2^5	2^6	2^7	2^8	2^9	2^{10}
GMRES	8.19e-1	1.02e-1	3.83e+0	4.58e+1	-1	-1	-1
QMGRIT	1.50e-1	1.54e-1	7.20e-1	2.72e+0	1.38e+1	1.15e+2	4.40e+3
QMGRIT+GMRES	5.05e-2	2.61e-2	8.22e-2	2.96e-1	1.55e+0	1.37e+1	-1

time-to-solution performance for GMRES, QMGRIT, and QMGRIT+GMRES across different problem sizes. The maximum number of iterations for the GMRES and QMGRIT application alone is set to $\frac{N_x N_t}{2}$, for QMGRIT+GMRES to five iterations. The solution tolerance (the norm of the global space-time residual for QMGRIT and relative residual error for GMRES) to be 10^{-5}. Here are following some key observations and insights.

- GMRES alone struggles to solve larger problems efficiently, as indicated by the -1 values for $N_t = N_x \geq 2^8$. This means that GMRES reaches its limit[9] in terms of computational resources for these problem sizes.

- QMGRIT alone performs better than GMRES for larger problem sizes, successfully solving problems up to $N_t = N_x = 2^{10}$, but the time-to-solution for QMGRIT increases significantly as the problem size grows, reaching $4.40e+3$ seconds for $N_t = N_x = 2^{10}$.

- The combination of QMGRIT and GMRES (QMGRIT+GMRES) demonstrates the impressive performance improvement. Regardless of the problem's discretization size, the GMRES, when preconditioned with QMGRIT, consistently achieved convergence within just four iterations. For problem sizes up to $N_t = N_x = 2^9$, QMGRIT+GMRES achieves a much lower time-to-solution

[9]Specifically, on the provided personal computer, the requested arrays exceed MATLAB's maximum array size preference of 32 GB, leading to resource limitations.

compared to QMGRIT alone — this accentuates the effectiveness of using QMGRIT as a preconditioner for GMRES. The efficiency gain of QMGRIT+GMRES over QMGRIT alone becomes more pronounced as the problem size increases. At $N_t = N_x = 2^9$, QMGRIT+GMRES takes only $1.37e+1$ seconds, while QMGRIT alone takes $1.15e+2$ seconds — this represents a reduction in time-to-solution of approximately **88%**, illustrating the significant impact of preconditioning.

- The scalability of the QMGRIT+GMRES approach is evident from the consistent performance improvement across increasing problem sizes. For the largest problem size tested, with $N_t = N_x = 2^{10}$, QMGRIT+GMRES fails to provide a solution, as indicated by the -1 value. This suggests that there may be limitations to the scalability of the preconditioning strategy for extremely large problems — the issue is not due to QMGRIT not working effectively in the given combination of QMGRIT+GMRES, but rather because there may be insufficient memory when constructing a global spatiotemporal matrix and allocating a certain number of vectors of the appropriate size needed for GMRES.

A summary of QMGRIT being used as a preconditioner for GMRES is provided herein, emphasizing the improvement in performance observed, particularly as the problem size increases. The results successfully incorporate the QMGRIT with GMRES. They demonstrate a significant speedup in time-to-solution, thereby easing the development of advanced preconditioning techniques for HPC environments to solve challenging problems. While the approach may suffer from scalability restraints for very large problems, efficiency gains underscore the worthwhile pursuit of such techniques. The results confirm the effectiveness of QMGRIT as a preconditioner, which leads to more efficiently using computation and a better performing solver for a range of problems. Therefore indicate that it is the role of modern preconditioner in computational mathematics and scientific computing, which should be a point of interest for future work in PinT methods for hyperbolic problems like the wave equation.

To wrap up, this research provides new contributions from exploring the impact of algorithmic parameter optimization on convergence and scalability; the role of preconditioning in boosting solver efficiency is highlighted, particularly in the case of a hyperbolic PDE — these discoveries advance PinT methods and present considerations for future research that may enrich and generalize PinT techniques[10].

[10] Here, we acknowledge the diversity of possible approaches to parallelizing GMRES itself, as evidenced by multiple implementations [13, 21, 28, 93, 110]. Furthermore, the exploration of *flexible* GMRES variants in the context of non-linear preconditioning may provide the way for further solver capabilities [12, 56, 102], namely by combining QMGRIT FAS and flexible GMRES.

Chapter 5

Summary, Conclusions and Future Work

The chapter will summarize the key results of the dissertation study in relation to the research aims and questions, value and contribution, and review the limitations of the study and suggested areas for future research. The Quotient Multi-grid Reduction in Time algorithm, developed and implemented in this study, has shown potential to solve complex problems in science and engineering, and in particular for periodic time-dependent partial differential equations.

5.0.1 Summery, Achievement of Research Aims and Objectives

This study outlines the QMGRIT algorithm for efficaciously scaling and solving periodic time-dependent PDEs in HPC environments — the research covers a series of topics, which have a common theme: the derivation, development, analysis, and application of QMGRIT. It is anticipated that this research will advance computational mathematics, and solve challenging problems that arise in the scientific and engineering domains. Addressing the primary four objectives of this dissertation, the major contributions and findings of the thesis include the following.

- We have laid out the principle of Eternal Wanderlust, and although the idea is obviously not unique in its novelty, it has become evident in Theorem 3.2 how transitions from period to period in time carry information with the eigenvalues of the spatial integration function. Then, we were able to utilize the EW principle for the context of multi-grid algorithm — the development of

the QMGRIT algorithm extends the capabilities of traditional two-grid and multi-grid methods — it introduces a multi-level framework and specialized operators to deal with periodicity in the temporal domain. Furthermore, the introducing of γ as algorithmic parameter for QMGRIT provides an exquisite leveraging tool for the solver's performance (see Section 3.2 and Algorithm 2 within).

- By performing theoretical analysis and empirical comparison of QMGRIT with existing PinT methods, bringing to the forefront its potential for faster convergence and improved parallel efficiency, we accurately examined the immanent structure of the QMGRIT operator in Theorem 3.7. Furthermore, we defined the iterative structure of multi-grid generalization. We approach distinguishing QMGRIT and ideas of near-laying periodic two-grid method based on Parareal analytically in Section 3.2.5 and then comparing the approaches on the Electrical Machine problem numerically in Section 4.2.

- The gratifying finding of the study, validated by SAMA application, is the introduction of the gQMGRIT parallelization paradigm in Section 3.2.3 to optimize resource usage and reduce computation times across various possible applications — it promises generic power-saving in numerical simulations.

- Numerical experiments demonstrating QMGRIT's effectiveness and scalability across a range of periodic problems, including the heat equation, convection-diffusion-decay equation, coaxial cable problem, steady-state of an electric motor, and wave equation. Particularly, Table 4.4 and Table 4.15 are underlining the results for (industrially challenging) parabolic PDE problem and (computationally challenging) hyperbolic PDE problem, respectively.

The investigation presented in this thesis has significance for the progression of computational methodologies in science and engineering and provides tools to overcome challenging time-periodic phenomena effectively; the findings from this work are expected to inspire other advances to HPC and allow the solution of more challenging problems.

5.0.2 Limitations of the Study

The raison d'être of this thesis, and this chapter in particular, is not only to describe the main achievements of the work, as in the previous paragraph, or to outline possible next steps in research, as in

the following paragraph, but also to recognize limitations and weaknesses, drawing a clear line of self-assessment.

- As observed in research on initial value problems in the PinT context, we encountered challenges with periodic domains — our limited success with hyperbolic problems revealed algorithmic performance issues, which some might describe as multi-grid scaling degradation. Nevertheless, we propose successful strategies to overcome these issues, including expanding on smoothing intensity for QMGRIT in Section 4.4.4, and combinations with GMRES for preconditioning in Section 4.5. Still, this experience prompts a more precise discussion about the somewhat 'heuristic topology' underlying the 'quotient' term in the QMGRIT algorithm's name. It may be beneficial to revisit foundational ideas (e.g., [78]) with careful attention to detail. Furthermore, the thesis lacks a pure V-cycle analysis, an omission stemming from the generic complexities of research process — for instance, in three-level algorithms or higher, approximating periodic problems with multiple *shortened* initial value problems (Remark 3.8) proves ineffective. However, the operator in 3.90 emerges with elegant simplicity, highlighting the general limitation in research time afterwards. It is noteworthy that with $r = \Delta t/\Delta x^2$ and $\Delta t = \Delta x$, increasing DOF through spatial refinement, similarly as in the case, where the thermal diffusivity $a \to 0$, leads consequently to that the time-step matrix tends towards identity — this aspect constrains the breadth of the date of some numerical tests for considered test equations, particularly due to the constraint $N_t = N_x$.

5.0.3 Directions for Future Research

Expanding upon the limitations, findings and insights gained in this dissertation, we suggest several directions beneficial for future research.

- Collaborate with industry partners to apply QMGRIT to real-world engineering and scientific challenges to validate its applicability in practical environments and to understand areas for the further possible optimization.

- Expand the possibilities of the applications of QMGRIT idea to a broader set of problems, including quasi-periodic, almost-periodic, and stochastic PDEs, to potentially extend the demonstration of its universality and robustness.

- Investigate the integration of QMGRIT with emerging computational paradigms like machine

learning or even quantum computing to investigate potential synergies for new solution methodologies.

- Consider the theoretical foundations of QMGRIT in more detail, particularly in relation to electronic band structures calculations, photonic orbits calculation, and to the class of complex valued functions, e.g. to the class of Schrödinger [1] equations, to extend its application to quantum mechanical problems or the study of time crystals.
- Refine the gQMGRIT parallelization strategy and investigate alternative methods that improve the scalability and efficiency of QMGRIT in an HPC setting. Specifically, combine GMRES with gQMGRIT as preconditioner.

5.0.4 Concluding Thought

This dissertation has demonstrated that QMGRIT can drive progress in scientific computing and facilitate resolving difficult problems in many scientific and engineering fields — the results of this study can serve as a sound platform for further research, which may lead to new progress in HPC and the design of cutting-edge computational tools. To the very end it is obvious that the QMGRIT algorithm is presented as a new and promising multi-level approach to efficiently solving time-dependent PDEs with periodic boundary conditions in time.

[1] Erwin Schrödinger (*12 August 1887 in Vienna, Austria-Hungary; †4 January 1961 in Vienna, Austria) was an Austrian physicist and Nobel laureate known for his foundational contributions to quantum mechanics. Schrödinger's wave equation, formulated in 1926, revolutionized the understanding of the behavior of subatomic particles and is a cornerstone of modern quantum theory.

Appendix A

LFA vs. SAMA

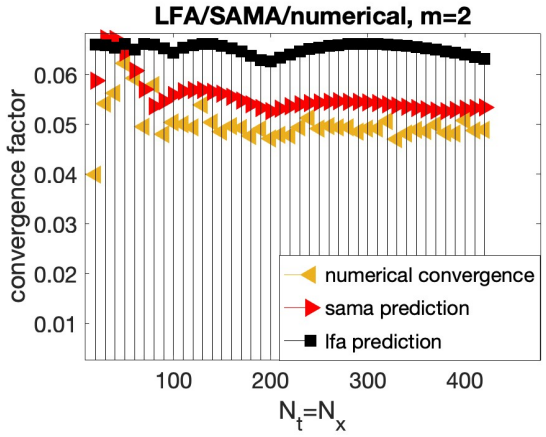

Figure A.1: LFA vs. SAMA Comparison, $m = 2$

We build upon the comprehensive analysis presented by [20]. We apply the LFA and SAMA analysis methodologies to the two-grid QMGRIT method for the grounded heat equation (see Section 3.1.4). Varying the spatial and temporal grid sizes such that $N_t = N_x$, as a byproduct of the research, we gain valuable insights from the Figures A.1-A.3. The LFA consistently overestimates the amplitude of convergence factors, while SAMA exhibits a remarkable correspondence with the numerical results — the excellent results of SAMA, which deals with time-similar dimension algebraically, are not surprising in this context, as it represents a generalization and modern evolution of the analysis methodology developed within the LFA, which was founded almost fifty years ago by [10] — SAMA, as presented by [42], builds upon the foundation laid by LFA and extends its capabilities to provide a more accurate and comprehensive analysis of multi-grid algorithms. The mentioned figures clearly

demonstrate the convergence behavior of the QMGRIT method for different values of m, the coarsening factor — while $N_t = N_x$ increase, and as m increases from two to five and finally to ten, we observe a consistent behaviour in convergence rates, with SAMA closely matching the numerical results. The convergence factors are bounded by ≈ 0.11 and this observation underlines the high effectiveness of QMGRIT algorithm for the parabolic PDE. Therefore, an analyzing the QMGRIT for the grounded heat equation within SAMA methodology yields valuable insights into solver convergence behavior and performance — furthermore, in contrast to the overestimation by LFA, the close agreements between SAMA and numerical results underline the significance to employ state-of-the-art analysis techniques to guide the development and refinement of PinT multi-grid algorithms for PDEs.

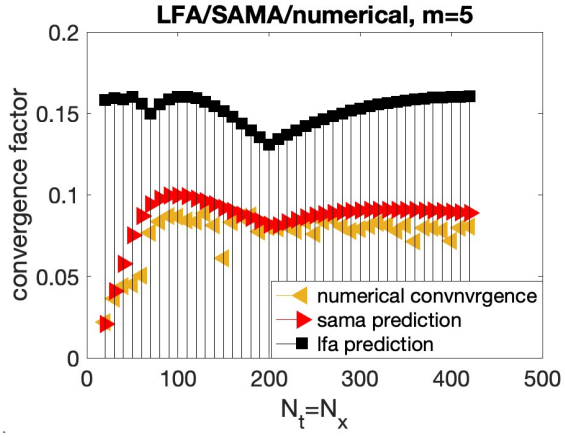

Figure A.2: LFA vs. SAMA Comparison, $m = 5$

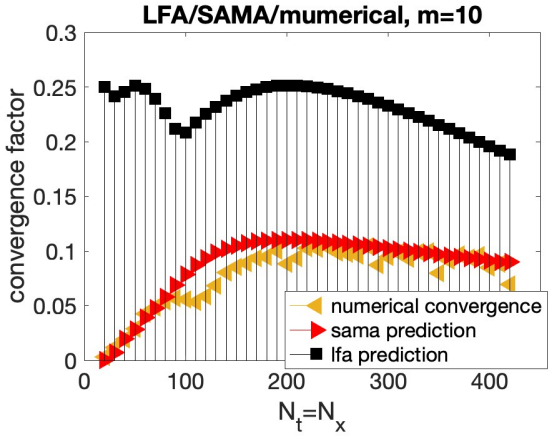

Figure A.3: LFA vs. SAMA Comparison, $m = 10$

Appendix B

FEM

The Finite Element Method (FEM) is a powerful numerical technique for solving challenging PDEs by discretizing the problem domain into smaller, simpler elements. FEM is widely used due to its ability to deal with complex geometries and provide accurate approximate solutions for a wide range of physical problems. We will adopt the methodologies outlined in [99, 105] and references within for the construction of FEM on triangular grids. The core idea of FEM is to partition the domain Ω into smaller elements, such as triangles in $2D$, and approximate the PDE locally on these elements using basis functions within a variational or *weak* formulation, as illustrated in Figure B.1a — the local approximations are then assembled to form a global system of equations, representing a discrete version of the original problem, exemplified by the hexagonal tiling and its triangular subdivisions shown in Figure B.1b. FEM relies on various function spaces, such as the Lebesgue[1] space

$$L^2(\Omega) \coloneqq \left\{ f : \Omega \to \mathbb{R} \;\middle|\; \int_\Omega |f|^2 < \infty \right\}, \tag{B.1}$$

and Sobolev[2] spaces $W^{s,p}(\Omega)$, defined as

$$W^{s,p}(\Omega) \coloneqq \left\{ \phi \in L^p(\Omega) \;\middle|\; \partial^\alpha \phi \in L^p(\Omega), |\alpha| \leq s \right\}, \tag{B.2}$$

[1] Henri Léon Lebesgue (*28 June 1875 in Beauvais, France; †26 July 1941 in Paris, France) was a French mathematician best known for his theory of integration, which was fundamental in the development of modern analysis. His introduction of the Lebesgue integral revolutionized the way mathematicians measure functions, significantly impacting the fields of real analysis and probability theory.

[2] Sergei L'vovich Sobolev (*6 October 1908 in St. Petersburg, Russian Empire; †3 January 1989 in Moscow, Soviet Union) was a Soviet mathematician who made foundational contributions to the field of functional analysis, partial differential equations, and mathematical physics. Best known for introducing the concept of Sobolev spaces, which are critical in the study of partial differential equations and their numerical solutions.

where $s \in \mathbb{Z}_+$ and $1 \leq p < \infty$. The Hilbert spaces $H^s(\Omega)$,

$$H^s(\Omega) \coloneqq \left\{ u \in C_0^\infty(\Omega)' \;\middle|\; u = U|_\Omega \text{ for some } U \in W^{s,2}\left(\mathbb{R}^d\right) \right\}, \tag{B.3}$$

where $s \in \mathbb{Z}_+$, particularly $H^1(\Omega)$ and its subspace

$$H_0^1(\Omega) \coloneqq \left\{ v \in H^1(\Omega) \;\middle|\; v = 0 \text{ on } \partial\Omega \right\}, \tag{B.4}$$

play a fundamental role in FEM formulations. The discretization process involves creating a triangulation $\mathcal{T}_h$ of the domain, numbering the nodes $\{x_{n,m}\}$ (vertices of the triangles), and constructing a set of nodal basis functions $\{\varphi_{n,m}\}$, demonstrated in Figure B.1. The discrete solution space V_h, a subspace of $H^1(\Omega)$, consists of continuous piece-wise linear functions on each element $K \in \mathcal{T}_h$

$$V_h \coloneqq \left\{ v_h \in C(\overline{\Omega}) \;\middle|\; v_h|_K \in \mathbb{P}_1, \forall K \in \mathcal{T}_h \right\}, \tag{B.5}$$

where $\mathbb{P}_1$ is the space of linear polynomials

$$\mathbb{P}_1 \coloneqq \left\{ p(x_1, x_2) = a_0 + a_1 x_1 + a_2 x_2 \;\middle|\; a_0, a_1, a_2 \in \mathbb{R} \right\}, \tag{B.6}$$

shown in Figure B.1a. The subspace V_h^0 contains functions that vanish on the boundary $\partial\Omega$. In the time-dependent case, FEM employs time-stepping schemes to approximate the solution at each time-step by solving a weak formulation of the PDE

$$\begin{cases} \text{Find } u^{n+1} \in H^1(\Omega) \text{ such that} \\ \delta_n \displaystyle\int_\Omega \nabla u^{n+1} \cdot \nabla \varphi + \int_\Omega u^{n+1} \varphi = \int_\Omega u^n \varphi + \delta_n \int_\Omega f^{n+1} \varphi, \quad \forall \varphi \in H_0^1(\Omega), \end{cases} \tag{B.7}$$

where δ_n is the time step size and f^{n+1} is the source term at time t^{n+1}. The discrete variational formulation leads to a linear system involving the stiffness matrix W, the mass matrix M, and the *load* vector $\mathbf{f}^{n+1}$

$$(\delta_n W + M)\mathbf{u}^{n+1} = M\mathbf{u}^n + \mathbf{f}^{n+1}. \tag{B.8}$$

The solution vector $\mathbf{u}^{n+1}$ represents the approximate solution at the nodes of the triangulation. The subsequent paragraphs will provide more details on the construction of the stiffness and mass matrices,

which are central components of the FEM formulation.

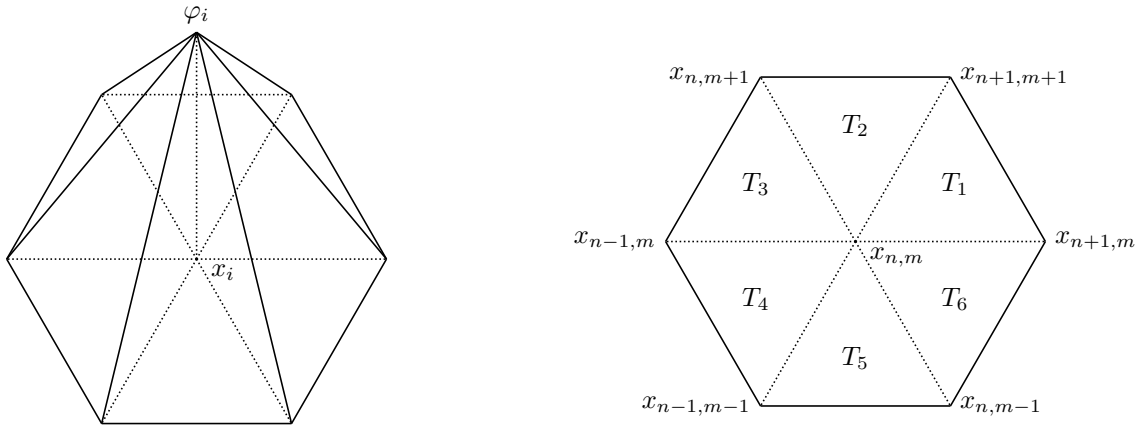

(a) Nodal basis function φ_i associated with node x_i within a finite element mesh

(b) A hexagon divided into sub-triangles T1 to T6 around node $x_{n,m}$

Figure B.1: Illustration of (a) the nodal basis function and element subdivision used in FEM mesh generation and (b) a hexagon with its local numbering and division into triangles

Stiffness matrix The stiffness matrix W captures the relationship between forces and displacements in the system — it is constructed as

$$W \coloneqq \begin{bmatrix} 0 & \int_{T_2\cup T_3} \nabla\varphi_{n,m+1}\cdot\nabla\varphi_{n,m}\mathbf{dx} & \int_{T_1\cup T_2} \nabla\varphi_{n+1,m+1}\cdot\nabla\varphi_{n,m}\mathbf{dx} \\ \int_{T_3\cup T_4} \nabla\varphi_{n-1,m}\cdot\nabla\varphi_{n,m}\mathbf{dx} & \int_{\cup_{i=1}^6 T_i} \nabla\varphi_{n,m}\cdot\nabla\varphi_{n,m}\mathbf{dx} & \int_{T_1\cup T_6} \nabla\varphi_{n+1,m}\cdot\nabla\varphi_{n,m}\mathbf{dx} \\ \int_{T_4\cup T_5} \nabla\varphi_{n-1,m-1}\cdot\nabla\varphi_{n,m}\mathbf{dx} & \int_{T_5\cup T_6} \nabla\varphi_{n,m-1}\cdot\nabla\varphi_{n,m}\mathbf{dx} & 0 \end{bmatrix}. \tag{B.9}$$

Mass matrix The mass matrix M reflects the system's inertial properties — it is defined by

$$M \coloneqq \begin{bmatrix} 0 & \int_{T_2\cup T_3} \varphi_{n,m+1}\varphi_{n,m}\mathbf{dx} & \int_{T_1\cup T_2} \varphi_{n+1,m+1}\varphi_{n,m}\mathbf{dx} \\ \int_{T_3\cup T_4} \varphi_{n-1,m}\varphi_{n,m}\mathbf{dx} & \int_{\cup_{i=1}^6 T_i} \varphi_{n,m}\varphi_{n,m}\mathbf{dx} & \int_{T_1\cup T_6} \varphi_{n+1,m}\varphi_{n,m}\mathbf{dx} \\ \int_{T_4\cup T_5} \varphi_{n-1,m-1}\varphi_{n,m}\mathbf{dx} & \int_{T_5\cup T_6} \varphi_{n,m-1}\varphi_{n,m}\mathbf{dx} & 0 \end{bmatrix}. \tag{B.10}$$

The FEM approach devises stiffness and mass matrices to capture the physical system. Let us examine into the calculation specifics. Consider the transformation defined by

$$\begin{pmatrix} x_1 \\ x_2 \end{pmatrix} = F_H(\widehat{\mathbf{x}}) \coloneqq B_H \begin{pmatrix} \widehat{x}_1 \\ \widehat{x}_2 \end{pmatrix} + b_H, \tag{B.11}$$

where the transformation matrix B_H and bias vector b_H are given by

$$B_H \coloneqq \begin{pmatrix} x_{n+1,m} - x_{n,m} & x_{n+1,m+1} - x_{n+1,m} \\ y_{n+1,m} - y_{n,m} & y_{n+1,m+1} - y_{n+1,m} \end{pmatrix}, \quad b_H \coloneqq \begin{pmatrix} x_{n,m} \\ y_{n,m} \end{pmatrix}. \tag{B.12}$$

This transformation aids to map a reference triangle onto the finite elements and their gradients as follows

$$\widehat{\varphi}_{k,l} = \varphi_{n+k,m+l} \circ F_H, \quad \nabla \widehat{\varphi}_{k,l} = B_H^t \left(\nabla \varphi_{n+k,m+l} \circ F_H \right). \tag{B.13}$$

The mapping of basis functions $\widehat{\varphi}_{k,l}$ under transformation F_H yields

$$\begin{aligned}
\widehat{\varphi}_{1,0}(\widehat{x},\widehat{y}) &= \begin{cases} \widehat{x} - \widehat{y}, & (\widehat{x},\widehat{y}) \in \widehat{T}_1 \\ \widehat{x}, & (\widehat{x},\widehat{y}) \in \widehat{T}_6, \end{cases} \qquad \widehat{\varphi}_{1,1}(\widehat{x},\widehat{y}) = \begin{cases} \widehat{y}, & (\widehat{x},\widehat{y}) \in \widehat{T}_1, \\ \widehat{x}, & (\widehat{x},\widehat{y}) \in \widehat{T}_2, \end{cases} \\
\widehat{\varphi}_{0,1}(\widehat{x},\widehat{y}) &= \begin{cases} \widehat{y} - \widehat{x}, & (\widehat{x},\widehat{y}) \in \widehat{T}_2, \\ \widehat{y}, & (\widehat{x},\widehat{y}) \in \widehat{T}_3, \end{cases} \qquad \widehat{\varphi}_{-1,0}(\widehat{x},\widehat{y}) = \begin{cases} -\widehat{x}, & (\widehat{x},\widehat{y}) \in \widehat{T}_3, \\ \widehat{y} - \widehat{x}, & (\widehat{x},\widehat{y}) \in \widehat{T}_4, \end{cases} \\
\widehat{\varphi}_{-1,-1}(\widehat{x},\widehat{y}) &= \begin{cases} -\widehat{y}, & (\widehat{x},\widehat{y}) \in \widehat{T}_4, \\ -\widehat{x}, & (\widehat{x},\widehat{y}) \in \widehat{T}_5, \end{cases} \qquad \widehat{\varphi}_{0,-1}(\widehat{x},\widehat{y}) = \begin{cases} \widehat{x} - \widehat{y}, & (\widehat{x},\widehat{y}) \in \widehat{T}_5, \\ -\widehat{y}, & (\widehat{x},\widehat{y}) \in \widehat{T}_6, \end{cases} \\
\widehat{\varphi}_{0,0}(\widehat{x},\widehat{y}) &= \begin{cases} 1 - \widehat{x}, & (\widehat{x},\widehat{y}) \in \widehat{T}_1, \\ 1 - \widehat{y}, & (\widehat{x},\widehat{y}) \in \widehat{T}_2, \\ 1 + \widehat{x} - \widehat{y}, & (\widehat{x},\widehat{y}) \in \widehat{T}_3, \\ 1 + \widehat{x}, & (\widehat{x},\widehat{y}) \in \widehat{T}_4, \\ 1 + \widehat{y}, & (\widehat{x},\widehat{y}) \in \widehat{T}_5, \\ 1 - \widehat{x} + \widehat{y}, & (\widehat{x},\widehat{y}) \in \widehat{T}_6, \end{cases}
\end{aligned} \tag{B.14}$$

with the integral transformations being calculated accordingly to the integration by substitution[3] for multiple variables to capture the interaction within the elements,

$$\int_T \varphi_{n+k,m+l}\varphi_{n,m} = |\det(B_H)| \int_{\widehat{T}} \widehat{\varphi}_{k,l}\widehat{\varphi}_{0,0}, \tag{B.15}$$

enabling the forthcoming evaluation of stiffness and mass matrices — the integration over triangular elements is performed as follows

$$\begin{aligned}
\int_T \nabla\varphi_{n+k,m+l} \cdot \nabla\varphi_{n,m} &= |\det(B_H)| \int_{\widehat{T}} (\nabla\varphi_{n+k,m+l} \circ F_H) \cdot (\nabla\varphi_{n,m} \circ F_H) && \text{(B.16)}\\
&= |\det(B_H)| \int_{\widehat{T}} \left(B_H^{-t}\nabla\widehat{\varphi}_{k,l}\right) \cdot \left(B_H^{-t}\nabla\widehat{\varphi}_{0,0}\right) && \text{(B.17)}\\
&= |\det(B_H)| \int_{\widehat{T}} C_H \nabla\widehat{\varphi}_{k,l} \cdot \nabla\widehat{\varphi}_{0,0} && \text{(B.18)}\\
&= |\det(B_H)| \left(c_{11}^H \widehat{S}_{xx} + c_{12}^H \widehat{S}_{xy} + c_{21}^H \widehat{S}_{yx} + c_{22}^H \widehat{S}_{yy}\right) && \text{(B.19)}\\
&= |\det(B_H)| \left(c_{11}^H \widehat{S}_{xx} + 2c_{12}^H \widehat{S}_{xy} + c_{22}^H \widehat{S}_{yy}\right), && \text{(B.20)}
\end{aligned}$$

where $C_H = B_H^{-1}B_H^{-t}$, and $\widehat{S}_{xx}$, $\widehat{S}_{xy}$, $\widehat{S}_{yy}$, respectively, are structured matrices representing the discretized domain's spatial derivatives

$$C_H = \begin{pmatrix} c_{11}^H & c_{12}^H \\ c_{21}^H & c_{22}^H \end{pmatrix} \coloneqq B_H^{-1}B_H^{-t}, \tag{B.21}$$

[3] If sloppily formulated, because otherwise one would shall calculate the derivation of F_H and trace the following theorem's statement, in some extend, a corollary nowadays [122]: that was first proposed by Euler when he developed the notion of double integrals in 1769, although expanded to triple integrals by Lagrange[4] in 1773, and first generalized to n variables by Ostrogradsky[5] in 1836 — specifically, let U be an open subset of $\mathbf{R}^n$ and $\varphi : U \to \mathbf{R}^n$ be a bi-Lipschitz mapping, let $f : \varphi(U) \to \mathbb{R}$ be measurable, then $\int_{\varphi(U)} f(x)dx = \int_U (f \circ \varphi)(x)|\det D\varphi(x)|dx$ (in the sense that if either integral exists, or is properly infinite, then so does the other one, and they have the same value).

[4] Joseph-Louis Lagrange (*25 January 1736 in Turin, Kingdom of Sardinia; †10 April 1813 in Paris, France) was an Italian-French mathematician and astronomer. Renowned for his contributions to the fields of analysis, number theory, and both classical and celestial mechanics, Lagrange's work, including the Lagrangian mechanics framework, has profoundly influenced the development of mathematical physics and engineering.

[5] Mikhail Ostrogradsky (*24 September 1801 in Pashennaya, Poltava Governorate, Ukraine; †1 January 1862 in Poltava, Ukraine) was a Ukrainian mathematician and physicist. Known for his contributions to the theory of partial differential equations, calculus of variations, and the divergence theorem in vector calculus, Ostrogradsky's work has had a lasting impact on mathematical physics and engineering.

and

$$\widehat{S}_{xx} = \begin{pmatrix} 0 & \int_{\widehat{T}_2\cup\widehat{T}_3} \partial_x\widehat{\varphi}_{0,1}\cdot\partial_x\widehat{\varphi}_{0,0}\mathbf{dx} & \int_{\widehat{T}_1\cup\widehat{T}_2} \partial_x\widehat{\varphi}_{1,1}\cdot\partial_x\widehat{\varphi}_{0,0}\mathbf{dx} \\ \int_{\widehat{T}_3\cup\widehat{T}_4} \partial_x\widehat{\varphi}_{-1,0}\cdot\partial_x\widehat{\varphi}_{0,0}\mathbf{dx} & \int_{\bigcup_{i=1}^6\widehat{T}_i} \partial_x\widehat{\varphi}_{0,0}\cdot\partial_x\widehat{\varphi}_{0,0}\mathbf{dx} & \int_{\widehat{T}_1\cup\widehat{T}_6} \partial_x\widehat{\varphi}_{1,0}\cdot\partial_x\widehat{\varphi}_{0,0}\mathbf{dx} \\ \int_{\widehat{T}_4\cup\widehat{T}_5} \partial_x\widehat{\varphi}_{-1,-1}\cdot\partial_x\widehat{\varphi}_{0,0}\mathbf{dx} & \int_{\widehat{T}_5\cup\widehat{T}_6} \partial_x\widehat{\varphi}_{0,-1}\cdot\partial_x\widehat{\varphi}_{0,0}\mathbf{dx} & 0 \end{pmatrix} \tag{B.22}$$

$$= \begin{pmatrix} 0 & 0 & 0 \\ -1 & 2 & -1 \\ 0 & 0 & 0 \end{pmatrix}, \tag{B.23}$$

$$\widehat{S}_{xy} = \begin{pmatrix} 0 & \int_{\widehat{T}_2\cup\widehat{T}_3} \partial_x\widehat{\varphi}_{0,1}\cdot\partial_y\widehat{\varphi}_{0,0}\mathbf{dx} & \int_{\widehat{T}_1\cup\widehat{T}_2} \partial_x\widehat{\varphi}_{1,1}\cdot\partial_y\widehat{\varphi}_{0,0}\mathbf{dx} \\ \int_{\widehat{T}_3\cup\widehat{T}_4} \partial_x\widehat{\varphi}_{-1,0}\cdot\partial_y\widehat{\varphi}_{0,0}\mathbf{dx} & \int_{\bigcup_{i=1}^6\widehat{T}_i} \partial_x\widehat{\varphi}_{0,0}\cdot\partial_y\widehat{\varphi}_{0,0}\mathbf{dx} & \int_{\widehat{T}_1\cup\widehat{T}_6} \partial_x\widehat{\varphi}_{1,0}\cdot\partial_y\widehat{\varphi}_{0,0}\mathbf{dx} \\ \int_{\widehat{T}_4\cup\widehat{T}_5} \partial_x\widehat{\varphi}_{-1,-1}\cdot\partial_y\widehat{\varphi}_{0,0}\mathbf{dx} & \int_{\widehat{T}_5\cup\widehat{T}_6} \partial_x\widehat{\varphi}_{0,-1}\cdot\partial_y\widehat{\varphi}_{0,0}\mathbf{dx} & 0 \end{pmatrix} \tag{B.24}$$

$$= \begin{pmatrix} 0 & 1 & -1 \\ 1 & -2 & 1 \\ -1 & 1 & 0 \end{pmatrix}, \tag{B.25}$$

$$\widehat{S}_{yy} = \begin{pmatrix} 0 & \int_{\widehat{T}_2\cup\widehat{T}_3} \partial_y\widehat{\varphi}_{0,1}\cdot\partial_y\widehat{\varphi}_{0,0}\mathbf{dx} & \int_{\widehat{T}_1\cup\widehat{T}_2} \partial_y\widehat{\varphi}_{1,1}\cdot\partial_y\widehat{\varphi}_{0,0}\mathbf{dx} \\ \int_{\widehat{T}_3\cup\widehat{T}_4} \partial_y\widehat{\varphi}_{-1,0}\cdot\partial_y\widehat{\varphi}_{0,0}\mathbf{dx} & \int_{\bigcup_{i=1}^6\widehat{T}_i} \partial_y\widehat{\varphi}_{0,0}\cdot\partial_y\widehat{\varphi}_{0,0}\mathbf{dx} & \int_{\widehat{T}_1\cup\widehat{T}_6} \partial_y\widehat{\varphi}_{1,0}\cdot\partial_y\widehat{\varphi}_{0,0}\mathbf{dx} \\ \int_{\widehat{T}_4\cup\widehat{T}_5} \partial_y\widehat{\varphi}_{-1,-1}\cdot\partial_y\widehat{\varphi}_{0,0}\mathbf{dx} & \int_{\widehat{T}_5\cup\widehat{T}_6} \partial_y\widehat{\varphi}_{0,-1}\cdot\partial_y\widehat{\varphi}_{0,0}\mathbf{dx} & 0 \end{pmatrix} \tag{B.26}$$

$$= \begin{pmatrix} 0 & -1 & 0 \\ 0 & 2 & 0 \\ 0 & -1 & 0 \end{pmatrix}. \tag{B.27}$$

Following the FEM framework, we evaluate from (B.9)–(B.10) the mass matrix M and stiffness matrix W further, which are pivotal in numerically building up the system's dynamic behavior — the determinant of the transformation matrix B_H, reflecting the geometric transformations applied to the

finite elements, plays a key role here, as observed in B.15 and illustrated via the appendix-footnote B afterwards. Thus, the mass matrix is given by

$$M = |\det(B_H)| \begin{pmatrix} 0 & 1/12 & 1/12 \\ 1/12 & 1/2 & 1/12 \\ 1/12 & 1/12 & 0 \end{pmatrix}, \tag{B.28}$$

indicating the distribution of mass across the elements and the stiffness matrix, encapsulating the system's response to e.g. elastic deformations, is expressed as

$$W = |\det(B_H)| \left(c_{11}^H \begin{pmatrix} 0 & 0 & 0 \\ -1 & 2 & -1 \\ 0 & 0 & 0 \end{pmatrix} + 2c_{12}^H \begin{pmatrix} 0 & 1 & -1 \\ 1 & -2 & 1 \\ -1 & 1 & 0 \end{pmatrix} + c_{22}^H \begin{pmatrix} 0 & -1 & 0 \\ 0 & 2 & 0 \\ 0 & -1 & 0 \end{pmatrix} \right). \tag{B.29}$$

Both factored by the determinant of B_H to account for the element's orientation and scale.

Calculation for a *hexagon-stencil*: The previous considerations lead us to the following conclusion. For any specific triangular element inducing a spatial $2D$ hexagonal tiling characterized by side length h, and angles α and β, we can calculate a revealing result

$$B_H = \begin{pmatrix} h & -\frac{h\sin(\alpha)\cos(\beta)}{\sin(\alpha+\beta)} \\ 0 & \frac{h\sin(\alpha)\sin(\beta)}{\sin(\alpha+\beta)} \end{pmatrix}, \tag{B.30}$$

$$\det(B_H) = \frac{h^2\sin(\alpha)\sin(\beta)}{\sin(\alpha)\cos(\beta)+\sin(\beta)\cos(\alpha)}, \tag{B.31}$$

$$C_H = \begin{pmatrix} \frac{1}{h^2\sin^2(\beta)} & \frac{\frac{1}{\tan(\beta)}+\frac{1}{\tan(\alpha)}}{h^2\tan(\beta)} \\ \frac{\frac{1}{\tan(\beta)}+\frac{1}{\tan(\alpha)}}{h^2\tan(\beta)} & \frac{\sin^2(\alpha+\beta)}{h^2\sin^2(\alpha)\sin^2(\beta)} \end{pmatrix}, \tag{B.32}$$

$$W = \frac{|\det(B_H)|}{h^2} \begin{pmatrix} 0 & -\frac{\frac{1}{\tan(\beta)}+\frac{1}{\tan(\alpha)}}{\tan(\alpha)} & -\frac{\frac{1}{\tan(\alpha)}+\frac{1}{\tan(\beta)}}{\tan(\beta)} \\ \left(-1+\frac{1}{\tan(\alpha)\tan(\beta)}\right) & \left(-2+\frac{2}{\tan(\alpha)\tan(\beta)}+\frac{2}{\sin^2(\beta)}+\frac{2}{\sin^2(\alpha)}\right) & \left(-1+\frac{1}{\tan(\alpha)\tan(\beta)}\right) \\ -\frac{\frac{1}{\tan(\beta)}+\frac{1}{\tan(\alpha)}}{\tan(\beta)} & -\frac{\frac{1}{\tan(\beta)}+\frac{1}{\tan(\alpha)}}{\tan(\alpha)} & 0 \end{pmatrix}. \tag{B.33}$$

List of Algorithms

List of Figures

List of Tables

Bibliography

[1] N. S. Bakhvalov. On the convergence of a relaxation method with natural constraints on the elliptic operator. USSR Computational Mathematics and Mathematical Physics, 6(5):101–135, 1966.

[2] D. Bast, I. Kulchytska-Ruchka, S. Schops, and O. Rain. Accelerated steady-state torque computation for induction machines using parallel-in-time algorithms. IEEE Transactions on Magnetics, 56(2):1–9, 2020.

[3] A. Bermudez, D. Gomez, M. Pineiro, and P. Salgado. A novel numerical method for accelerating the computation of the steady-state in induction machines. Computers and Mathematics with Applications, 79(2):274–292, 2020.

[4] H. Bodo. Analysis of a fully discrete finite element method for a nonlinear magnetic field problem. SIAM Journal on Numerical Analysis, 31(3):745–759, 1994.

[5] S. Bogdanov. QMGRIT. https://github.com/sourceua/QMGRIT, 2024.

[6] M. Bolten, S. Friedhoff, J. Hahne, and S. Schoeps. Parallel-in-time simulation of an electrical machine using MGRIT. Computing and Visualization in Science, 23(1-4), 2020.

[7] M. Bolten and H. Rittich. Fourier analysis of periodic stencils in multigrid methods. SIAM Journal on Scientific Computing, 40(3):A1642–A1668, 2018.

[8] M. Bostan. Periodic solutions for evolution equations. Electronic Journal of Differential Equations, pages 03–41, 2009.

[9] E. Bozzo and C. D. Fiore. On the use of certain matrix algebras associated with discrete trigonometric transforms in matrix displacement decomposition. SIAM Journal on Matrix Analysis and Applications, 16(1):312–326, 1995.

[10] A. Brandt. Multi-level adaptive solutions to boundary-value problems. Mathematics of Computation, 31(138):333–390, 1977.

[11] T. A. Burton. Stability & Periodic Solutions of Ordinary & Functional Differential Equations. Dover Books on Mathematics. Dover Publications, 2005.

[12] H. Calandra, S. Gratton, J. Langou, X. Pinel, and X. Vasseur. Flexible variants of block restarted gmres methods with application to geophysics. SIAM Journal on Scientific Computing, 34(2):A714–A736, 2012.

[13] D. Calvetti, J. Petersen, and L. Reichel. A parallel implementation of the gmres method. Technical report, Technical Report ICM-9110-6, Institute for Computational Mathematics, Kent, OH, 1991.

[14] A. J. Christlieb, C. B. Macdonald, and B. W. Ong. Parallel high-order integrators. SIAM Journal on Scientific Computing, 32:818–835, 2010.

[15] J. Cortial and C. Farhat. A time-parallel implicit method for accelerating the solution of non-linear structural dynamics problems. International Journal for Numerical Methods in Engineering, 77:451–470, 2009.

[16] R. Courant. Variational methods for the solution of problems of equilibrium and vibrations. Bulletin of the American Mathematical Society, 49(1):1–23, 1943.

[17] J. L. R. d'Alembert. Meditationes de generali ventorum causa, in quibus tentatur solutio problematis ab illustrissima Academia Berolinensi propositi. Chez David, 1747.

[18] F. Danieli and S. MacLachlan. Multigrid reduction in time for non-linear hyperbolic equations. ETNA - Electronic Transactions on Numerical Analysis, 58:43–65, 2022.

[19] H. De Sterck, R. D. Falgout, S. Friedhoff, O. A. Krzysik, and S. P. MacLachlan. Optimizing multigrid reduction-in-time and parareal coarse-grid operators for linear advection. Numerical Linear Algebra with Applications, 28, 2021.

[20] H. De Sterck, S. Friedhoff, A. J. M. Howse, and S. P. MacLachlan. Convergence analysis for parallel-in-time solution of hyperbolic systems. Numerical Linear Algebra with Applications, 27(1):e2271, 2020.

[21] E. De Sturler. A parallel variant of gmres (m). In Proceedings of the 13th IMACS World Congress on Computational and Applied Mathematics. IMACS, Criterion Press, volume 9, pages 682–683, 1991.

[22] V. A. Dobrev, Tz. Kolev, N. A. Petersson, and J. B. Schroder. Two-level convergence theory for multigrid reduction in time (MGRIT). SIAM Journal on Scientific Computing, 39(5):S501–S527, 2017.

[23] C. C. Douglas and J. J. Douglas. A unified convergence theory for abstract multigrid or multilevel algorithms, serial and parallel. SIAM Journal on Numerical Analysis, 30(1):136–158, 1993.

[24] P. Dular and C. Geuzaine. GetDP reference manual: the documentation for GetDP, a general environment for the treatment of discrete problems. http://getdp.info.

[25] P. Dular, C. Geuzaine, F. Henrotte, and W. Legros. A general environment for the treatment of discrete problems and its application to the finite element method. IEEE Transactions on Magnetics, 34(5):3395–3398, 1998.

[26] A. Dutt, L. Greengard, and V. Rokhlin. Spectral deferred correction methods for ordinary differential equations. BIT Numerical Mathematics, 40:241–266, 2000.

[27] M. Emmett and M. Minion. Toward an efficient parallel in time method for partial differential equations. Communications in Applied Mathematics and Computational Science, 7:105 – 132, 2012.

[28] J. Erhel. A parallel gmres version for general sparse matrices. Electronic Transactions on Numerical Analysis, 3:160–176, 1995.

[29] L. Euler. Institutionum calculi differentialis cum eius usu in analysi finitorum ac doctrina serierum. Academiae Imperialis Scientiarum Petropolitanae, 1755.

[30] R. D. Falgout, S. Friedhoff, Tz. V. Kolev, S. P. MacLachlan, and J. B. Schroder. Parallel time integration with multigrid. SIAM Journal on Scientific Computing, 36(6):C635–C661, 2014.

[31] R. D. Falgout, S. Friedhoff, Tz. V. Kolev, S. P. MacLachlan, J. B. Schroder, and S. Vandewalle. Multigrid methods with space–time concurrency. Computing and Visualization in Science, 18(4-5):123–143, 2017.

[32] R. D. Falgout, A. Katz, T. V. Kolev, J. B. Schroder, A. Wissink, and U. M. Yang. Parallel time integration with multigrid reduction for a compressible fluid dynamics application. Technical report, Lawrence Livermore National Laboratory, 2015.

[33] R. D. Falgout, M. Lecouvez, and C. S. Woodward. A parallel-in-time algorithm for variable step multistep methods. Journal of Computational Science, 37, 2019.

[34] R. D. Falgout, T. A. Manteuffel, B. O'Neill, and J. B. Schroder. Multigrid reduction in time for nonlinear parabolic problems: A case study. SIAM Journal on Scientific Computing, 39:S298–S322, 2017.

[35] R. D. Falgout and P. S. Vassilevski. On generalizing the algebraic multigrid framework. SIAM Journal on Numerical Analysis, 42(4):1669–1693, 2004.

[36] C. Farhat, J. Cortial, C. Dastillung, and H. Bavestrello. Time-parallel implicit integrators for the near-real-time prediction of linear structural dynamic responses. International Journal for Numerical Methods in Engineering, 67:697–724, 2006.

[37] R. P. Fedorenko. The speed of convergence of one iterative process. USSR Computational Mathematics and Mathematical Physics, 4(3):227–235, 1964.

[38] TubeExample:Finite Element Method Magnetics — femm.info. https://www.femm.info/wiki/TubeExample. [Accessed 06-03-2024].

[39] J. B. J. Fourier. Théorie Analytique de la Chaleur. Cambridge Library Collection - Mathematics. Cambridge University Press, 2009.

[40] S. R. Franco, C. Rodrigo, F. J. Gaspar, and M. A. V. Pinto. A multigrid waveform relaxation method for solving the poroelasticity equations. Computational and Applied Mathematics, 37(4):4805–4820, 2018.

[41] S. Friedhoff, J. Hahne, I. Kulchytska-Ruchka, and S. Schöps. Exploring parallel-in-time approaches for eddy current problems. In István Faragó, Ferenc Izsák, and Péter L. Simon, editors, Progress in Industrial Mathematics at ECMI 2018, pages 373–379, Cham, 2019. Springer International Publishing.

[42] S. Friedhoff and S. MacLachlan. A generalized predictive analysis tool for multigrid methods. Numerical Linear Algebra with Applications, 22(4):618–647, 2015.

[43] S. Friedhoff and B. S. Southworth. On “optimal” h -independent convergence of parareal and multigrid-reduction-in-time using runge-kutta time integration. Numerical Linear Algebra with Applications, 28(3), 2020.

[44] H. Gahvari, V. Dobrev, R. D. Falgout, T. V. Kolev, J. B. Schroder, M. Schulz, and U. M. Yang. A performance model for allocating the parallelism in a multigrid-in-time solver. In 2016 7th International Workshop on Performance Modeling, Benchmarking and Simulation of High Performance Computer Systems (PMBS), pages 22–31. IEEE, 2016.

[45] M. J. Gander. 50 years of time parallel time integration. In Contributions in Mathematical and Computational Sciences, pages 69–113. Springer International Publishing, 2015.

[46] M. J. Gander, Y.-L. Jiang, B. Song, and H. Zhang. Analysis of two parareal algorithms for time-periodic problems. SIAM Journal on Scientific Computing, 35, 2013.

[47] M. J. Gander, I. Kulchytska-Ruchka, and S. Schöps. A new parareal algorithm for time-periodic problems with discontinuous inputs. In Ronald Haynes, Scott MacLachlan, Xiao-Chuan Cai, Laurence Halpern, Hyea Hyun Kim, Axel Klawonn, and Olof Widlund, editors, Domain Decomposition Methods in Science and Engineering XXV, pages 243–250, Cham, 2020. Springer International Publishing.

[48] M. J Gander and F. Kwok. Numerical analysis of partial differential equations using maple and MATLAB. SIAM, 2018.

[49] M. J. Gander, F. Kwok, and H. Zhang. Multigrid interpretations of the parareal algorithm leading to an overlapping variant and MGRIT. Computing and Visualization in Science, 19(3-4):59–74, 2018.

[50] M. J. Gander and M. Neumueller. Analysis of a new space-time parallel multigrid algorithm for parabolic problems. SIAM Journal on Scientific Computing, 38(4):A2173–A2208, 2016.

[51] F. J. Gaspar, J. L. Gracia, and F. J. Lisbona. Fourier analysis for multigrid methods on triangular grids. SIAM Journal on Scientific Computing, 31(3):2081–2102, 2009.

[52] C. F. Gauss. Theoria motus corporum coelestium in sectionibus conicis solem ambientium. F. Perthes et I.H. Besser, 1809.

[53] S. Gerschgorin. On the limitation of the eigenvalues of a matrix. Bulletin of the Academy of Sciences of the USSR, Section of Mathematical and Natural Sciences, 1931(6):749–754, 1931.

[54] C. Geuzaine. GetDP: a general finite-element solver for the de Rham complex. In PAMM Volume 7 Issue 1. Special Issue: Sixth International Congress on Industrial Applied Mathematics (ICIAM07) and GAMM Annual Meeting, Zürich 2007, volume 7, pages 1010603–1010604. Wiley, 2008.

[55] D. C. Giancoli. Physics for Scientists and Engineers. Physics for Scientists & Engineers with Modern Physics. Prentice Hall, 2000.

[56] L. Giraud, S. Gratton, X. Pinel, and X. Vasseur. Flexible gmres with deflated restarting. SIAM Journal on Scientific Computing, 32(4):1858–1878, 2010.

[57] J. J. C. Gyselinck, L. Vandevelde, and J. A. A. Melkebeek. Multi-slice fe modeling of electrical machines with skewed slots-the skew discretization error. IEEE Transactions on Magnetics, 37(5):3233–3237, 2001.

[58] S. Günther, L. Ruthotto, J. B. Schroder, E. C. Cyr, and N. R. Gauger. Layer-parallel training of deep residual neural networks. SIAM Journal on Mathematics of Data Science, 2:1–23, 2020.

[59] N. Habibi, A. Mesforush, F. J. Gaspar, and C. Rodrigo. Semi-algebraic mode analysis for finite element discretisations of the heat equation. Computational Methods for Differential Equations, 9(1):146–158, 2021.

[60] W. Hackbusch. Multi-grid methods and applications, volume 4. Springer Science & Business Media, 1985.

[61] W. Hackbusch. Iterative Solution of Large Sparse Systems of Equations. Springer, Cham, 2016.

[62] W. Hackbusch and U. Trottenberg, editors. Multigrid Methods III. Birkhaeuser Basel, 1991.

[63] J. Hahne, S. Friedhoff, and M. Bolten. Algorithm 1016: Pymgrit: A python package for the parallel-in-time method mgrit. ACM Transactions on Mathematical Software., 47(2), 2021.

[64] J. Hahne, B. Polenz, I. Kulchytska-Ruchka, S. Friedhoff, S. Ulbrich, and S. Schöps. Parallel-in-time optimization of induction motors. Journal of Mathematics in Industry, 13(1), 2023.

[65] J. Hahne, B. S. Southworth, and S. Friedhoff. Asynchronous truncated multigrid-reduction-in-time. SIAM Journal on Scientific Computing, pages S281–S306, 2022.

[66] Jens Hahne. Parallel-in-Time integration with application to eddy current simulations. PhD thesis, Bergische Universität Wuppertal, Wuppertal, April 2023. Dissertation.

[67] E. Hairer, S. P. Nørsett, and G. Wanner. Solving ordinary differential equations, 1. Nonstiff problems. Springer series in computational mathematics; Solving ordinary differential equations. Springer, Berlin [u.a.], 2. rev. ed., corr. 3. print. edition, 2008.

[68] E. Hairer, S. P. Nørsett, and G. Wanner. Solving Ordinary Differential Equations II: Stiff and Differential-Algebraic Problems. Springer Series in Computational Mathematics. Springer-Verlag Berlin Heidelberg, Berlin, Heidelberg, 2010.

[69] A. Hessenthaler, B. S. Southworth, D. Nordsletten, O. Roehrle, R. D. Falgout, and J. B. Schroder. Multilevel convergence analysis of multigrid-reduction-in-time. SIAM Journal on Scientific Computing, 42(2):A771–A796, 2020.

[70] A. Howse, H. D. Sterck, R. D. Falgout, S. MacLachlan, and J. B. Schroder. Parallel-in-time multigrid with adaptive spatial coarsening for the linear advection and inviscid burgers equations. SIAM Journal on Scientific Computing, 41:A538–A565, 2019.

[71] A. Hrennikoff. Solution of problems of elasticity by the framework method. Journal of Applied Mechanics, 8:A169–A175, 1941.

[72] X. Hu, C. Rodrigo, and F. J. Gaspar. Using hierarchical matrices in the solution of the time-fractional heat equation by multigrid waveform relaxation. Journal of Computational Physics, 416:109540, 2020.

[73] *HYPRE*: High performance preconditioners. https://llnl.gov/casc/hypre, https://github.com/hypre-space/hypre.

[74] E. Isaacson and H. B. Keller. Analysis of Numerical Methods. John Wiley & Sons, 1966.

[75] J. D. Jackson. Classical Electrodynamics. John Wiley & Sons, 3 edition, 1998.

[76] I. Kulchytska-Ruchka and S. Schoeps. Efficient parallel-in-time solution of time-periodic problems using a MultiHarmonic coarse grid correction. SIAM Journal on Scientific Computing, 43(1):C61–C88, 2021.

[77] P. Kumar, C. Rodrigo, F. J. Gaspar, and C. W. Oosterlee. On local fourier analysis of multigrid methods for pdes with jumping and random coefficients. SIAM Journal on Scientific Computing, 41(3):A1385–A1413, 2019.

[78] M. Kyed and J. Sauer. On time-periodic solutions to parabolic boundary value problems. Mathematische Annalen, 374(1):37–65, 2019.

[79] J.-L. Lagrange. Mecanique analytique. Chez la Veuve Desaint, 1788.

[80] U. Langer and O. Steinbach, editors. Space-Time Methods. De Gruyter, 2019.

[81] M. Lecouvez, R. D. Falgout, C. S. Woodward, and P. Top. A parallel multigrid reduction in time method for power systems. In 2016 IEEE Power and Energy Society General Meeting (PESGM), pages 1–5, 2016.

[82] X. Lin, M. K. Ng, and Y. Zhi. A parallel-in-time two-sided preconditioning for all-at-once system from a non-local evolutionary equation with weakly singular kernel. Journal of Computational Physics, 434:110221, 2021.

[83] J.-L. Lions, Y. Maday, and G. Turinici. A "parareal" in time discretization of pde's. Comptes Rendus de l'Académie des Sciences - Series I - Mathematics, 332(7):661–668, 2001.

[84] J. D. Logan and V. Zlotnik. The convection-diffusion equation with periodic boundary conditions. Applied mathematics letters, 8(3):55–61, 1995.

[85] J. L. Massera. The existence of periodic solutions of systems of differential equations. Duke Mathematical Journal, 17(4):457 – 475, 1950.

[86] MATLAB – The Language of Technical Computing. https://matlab.mathworks.com. [Accessed 06-03-2024].

[87] J. C. Maxwell. A dynamical theory of the electromagnetic field. Philosophical Transactions of the Royal Society of London, 155:459–512, 1865.

[88] E. McDonald, J. Pestana, and A. Wathen. Preconditioning and iterative solution of all-at-once systems for evolutionary partial differential equations. SIAM Journal on Scientific Computing, 40(2):A1012–A1033, 2018.

[89] E. Moon and E. C. Cyr. Parallel training of gru networks with a multi-grid solver for long sequences. In International Conference on Learning Representations, 2022.

[90] J. Nievergelt. Parallel methods for integrating ordinary differential equations. Communications ACM, 7:731–733, 1964.

[91] NVIDIA. Amgx: Multi-grid accelerated linear solvers for industrial applications. https://developer.nvidia.com/blog/amgx-multi-grid-accelerated-linear-solvers-industrial-applications. [Accessed 06-03-2024].

[92] B. W. Ong and J. B. Schroder. Applications of time parallelization. Computing and Visualization in Science, 23:1–15, 2020.

[93] G. Pashos, M. E. Kavousanakis, A. N. Spyropoulos, J. A. Palyvos, and A. G. Boudouvis. Simultaneous solution of large-scale linear systems and eigenvalue problems with a parallel gmres method. Journal of Computational and Applied Mathematics, 227(1):196–205, 2009.

[94] Parallel-in-Time — parallel-in-time.org. http://parallel-in-time.org. [Accessed 06-03-2024].

[95] Python.org — python.org. https://www.python.org. [Accessed 06-03-2024].

[96] J. C. Rautio. The long road to maxwell's equations. IEEE Spectrum, 51:36–56, 2014.

[97] M. Renardy and R. C. Rogers. An Introduction to Partial Differential Equations. Texts in Applied Mathematics. Springer New York, 2006.

[98] M. Ries, U. Trottenberg, and G. Winter. A note on mgr methods. Linear Algebra and its Applications, 49:1 – 26, 1983.

[99] C. Rodrigo, F. J. Gaspar, and F. J. Lisbona. Multigrid methods on semi-structured grids. Arch Computat Methods, 19:499–538, 2012.

[100] N. Rouche and J. Mawhin. Ordinary Differential Equations: Stability and Periodic Solutions. Number Bd. 2 in Surveys and References Series. Pitman Advanced Pub. Program, 1980.

[101] J. W. Ruge and K. Stüben. Algebraic multigrid. SIAM, Philadelphia, PA, 1987.

[102] Y. Saad. A flexible inner-outer preconditioned gmres algorithm. SIAM Journal on Scientific Computing, 14(2):461–469, 1993.

[103] Y. Saad. Iterative Methods for Sparse Linear Systems. Springer, New York, 2003.

[104] Y. Saad and M. H. Schultz. Gmres: A generalized minimal residual algorithm for solving non-symmetric linear systems. SIAM Journal on Scientific and Statistical Computing, 7(3):856–869, 1986.

[105] F.-J. Sayas. A gentle introduction to the finite element method. Lecture notes, University of Delaware, 2008.

[106] K. Schmidt, O. Sterz, and R. Hiptmair. Estimating the eddy-current modeling error. IEEE Transactions on Magnetics, 44(6):686–689, 2008.

[107] S. Schoeps, I. Niyonzima, and M. Clemens. Parallel-in-time simulation of eddy current problems using parareal. IEEE Transactions on Magnetics, 54(3):1–4, 2018.

[108] J. B. Schroder. Parallelizing over artificial neural network training runs with multigrid. Technical report, Lawrence Livermore National Laboratory, 2017.

[109] Q. Sheng and R. P. Agarwal. Existence and uniqueness of periodic solutions for higher order hyperbolic partial differential equations. Journal of mathematical analysis and applications, 181(2):392–406, 1994.

[110] M. Sosonktna, D. CS. Allison, and L. T. Watson. Scalability analysis of parallel gmres implementations. Parallel Algorithms and Application, 17(4):263–284, 2002.

[111] B. S. Southworth. Necessary conditions and tight two-level convergence bounds for parareal and multigrid reduction in time. SIAM Journal on Matrix Analysis and Applications, 40(2):564–608, 2019.

[112] C. Steinstraesser, J. Guilherme, P. d. S. Peixoto, and M. Schreiber. Parallel-in-time integration of the shallow water equations on the rotating sphere using parareal and mgrit. Journal of Computational Physics, 496:112591, 2024.

[113] K. Stüben, J. W. Ruge, T. Clees, and S. Gries. Algebraic multigrid: From academia to industry. In Michael Griebel, Anton Schüller, and Marc Alexander Schweitzer, editors, Scientific Computing

and Algorithms in Industrial Simulations: Projects and Products of Fraunhofer SCAI, pages 83–119. Springer International Publishing, Cham, 2017.

[114] K. Stüben and U. Trottenberg. Multigrid methods: Fundamental algorithms, model problem analysis and applications. In Lecture Notes in Mathematics, pages 1–176. Springer Berlin Heidelberg, 1982.

[115] Y. Takahashi, K. Fujiwara, T. Iwashita, and H. Nakashima. Parallel finite-element method based on space-time domain decomposition for magnetic field analysis of electric machines. IEEE Transactions on Magnetics, 55:1–4, 2019.

[116] Y. Takahashi, T. Tokumasu, K. Fujiwara, T. Iwashita, and H. Nakashima. Parallel tp-eec method based on phase conversion for time-periodic nonlinear magnetic field problems. IEEE Transactions on Magnetics, 51, 2015.

[117] G. Teschl. Ordinary differential equations and dynamical systems, volume 140. American Mathematical Soc., 2012.

[118] J. M. F. Trindade and J. C. F. Pereira. Parallel-in-time simulation of two-dimensional, unsteady, incompressible laminar flows. Numerical Heat Transfer, Part B: Fundamentals, 50(1):25–40, 2006.

[119] S. Vandewalle and R. Piessens. On dynamic iteration methods for solving time-periodic differential equations. SIAM Journal on Numerical Analysis, 30(1):286–303, 1993.

[120] O. Vejvoda, editor. Partial differential equations: time-periodic solutions. Springer Netherlands, 1982.

[121] M. Wang. Time-periodic parabolic boundary value problems. In Nonlinear Second Order Parabolic Equations, pages 165–188. CRC Press, 2021.

[122] Wikipedia contributors. Integration by substitution — Wikipedia, the free encyclopedia. https://en.wikipedia.org/w/index.php?title=Integration_by_substitution&oldid=1250641375, 2024. [Accessed 01-12-2024].

[123] S.-L. Wu and T. Zhou. Acceleration of the two-level MGRIT algorithm via the diagonalization technique. SIAM Journal on Scientific Computing, 41(5):A3421–A3448, 2019.

[124] Xbraid/xbraid: Xbraid parallel-in-time solvers — github.com. https://github.com/XBraid/xbraid. [Accessed 06-03-2024].

[125] X. Yue, K. Pan, J. Zhou, Z. Weng, S. Shu, and J. Tang. A multigrid-reduction-in-time solver with a new two-level convergence for unsteady fractional laplacian problems. Computers & Mathematics with Applications, 89:57–67, 2021.